How cavefish gain high body fat to adapt to food scarcity

Shaolei Xiong, M.Sc.

A thesis submitted in partial fulfillment of the requirements of

the Open University of

Degree of Doctor of Philosophy

The Stowers Institute for Medical Research

Kansas City, Missouri USA

an Affiliated Research Center of the

Open University, UK

April 30th, 2021

Abstract

Food availability variation is a major challenge for some animals in their natural environment. A classic example of food scarcity environment are caves, which lack internal food chains based on photosynthesis. Cavefish populations can gain high body fat to deal with food scarcity, but the underlying mechanisms remain unclear. Here, we used Mexican tetra, *Astyanax mexicanus*, to address this question. To this end, I interrogated two perspectives: adipocyte development and lipid metabolism. I showed that cavefish populations store large amounts of fat in different regions throughout the body when fed ad libitum in the lab. After paired feeding, I found Tinaja and Pachón cavefish populations still have more visceral fat than surface fish, while maintaining similar body weight. This is largely because of hypertrophy of adipocytes in cavefish populations. Moreover, I found Pachón cavefish can develop their adipocytes earlier and faster than surface fish, providing a developmental mechanism for high body fat accumulation.

I also found that high body fat is in part due to higher expression of *de novo* lipogenesis genes in cavefish livers compared to surface fish after paired feeding. The fatty acid profiling of the liver also indicated enhanced lipogenesis in cavefish. Moreover, the lipid metabolism regulator, Peroxisome proliferator-activated receptor γ (Pparγ), was upregulated at both transcript and protein levels in cavefish livers. Chromatin immunoprecipitation sequencing (ChIP-seq) showed that Pparγ binds cavefish promoter regions of genes to a higher extent than surface fish. Using pharmacology in Astyanax, I showed that inhibiting Pparγ slowed down the fat accumulation, indicating upregulation Pparγ contributes to fat accumulation. Finally, I identified nonsense mutations in *per2*, a known repressor of Pparγ. Taken together, this study reveals that upregulated Pparγ promotes higher levels of lipogenesis in the liver and contributes to higher body fat of cavefish to adapt to nutrient limited environments.

Dedication

To my family, teachers, and friends

Acknowledgements

First, I would like to thank my supervisor, Dr. Nicolas Rohner, for encouraging and guiding me to finish my graduate study. He is open-minded and always glad to discuss progress and problems on my projects. As progress emerges, no matter how small or exciting, he never hesitates to praise and encourage me, which make me feel great and eager to achieve more. However, when I encounter problems, he patiently listens to me and gives me reasonable advice. When he cannot provide practical suggestions, he always guides me to useful resources. Furthermore, as an excellent presenter, he trains me on making slides and how to tell a coherent story. When I came to United States, my presentation skills were in need of development. Nick taught me how to set up the background of the project, introduce the question, propose a hypothesis, explain data, draw conclusions, and make a coherent transition no next slide. With practice and effort, my presentation skills significantly improved. Moreover, Nick is an efficient writer, and academic writing is my Achilles' heel. Therefore, Nick mentored me by requesting me to write small pieces initially, including abstract and methods, so I can learn to achieve measurable goals. Gradually, I began to write paragraphs for my research report and manuscript. Meanwhile, he helped me to revise them and asked me to pay attention to those changes he made and think about the rationale of those changes. This training on writing improved my writing written communication.

Furthermore, I also want to acknowledge all other Rohner lab members. Alex has tremendous experience in molecular cloning and protein analysis. When I have questions about these topics, he is the first person I consult. Postdocs in Rohner lab, including Drs. Jaya Krishnan, Rob Peuss, Jenna Persons, and Kyle Medley also help me learn some skills. Drs. Jasmin Camacho, Ansa Cobham, Tathagata Biswas, and Sylvain Bertho critically read my thesis and gave valued advice. Another graduate student, Luke Olsen, discussed

metabolic progresses with me, which stimulated me to read and think more about cavefish metabolism.

Moreover, I want to thank my committee meeting members, including Drs. Sarah Zanders, Tatiana Piotrowski, John Thyfault, and Matt Gibson. They always patiently listened to my progress in committee meetings, asked critical questions, and provided insightful advice about my projects. They also encouraged me to think deeper about my project and improve my skill sets to be a scientist.

I want to thank Leanne Wiedemann and Lisa Hodges of the Open University program, who supported and organized the program for OU students. I also thank my third-party monitor, Dr. Ron Yu for his discussion and advice.

I also thank all the core facility members who collaborated with me. The cavefish facility members, including Zakibe Zachary, Alba Aparicio Fernandez, Jessica Skyfield, Andrew Ingalls, David Jewell, Franchesca Hutton-Lau, Molly Miller, Elizabeth Fritz, help the Rohner lab maintain all fish stocks, which make research more productive. I want to especially thank Yongfu Wang, Nancy Thomas, Dai Tsuchiya, Seth Malloy, and Karen J Smith of histology core. They trained me how to section samples and how to do histological staining. Some of them also collaborated with me directly. Moreover, I appreciate Sean McKinney, Zulin Yu, Richard Alexander, Cindy Maddera, Brian Slaughter, and Steven Hoffman from the microscopy facility. They helped me image samples and trained me to use different microscopes and FIJI to process images. I also want to acknowledge the help from Rhonda Egidy, Anoja Perera, Amanda Lawlor, and Michael Peterson of the molecular biology facility. They helped me build the library for RNA-seq and ChIP-seq. Furthermore, I want to thank Wei Wang, Robert Schnittker, Augusto Ortega Granillo, and Jim Jenkin of the Sánchez Alvarado lab. I also appreciate the assistance from Alexis Murray, Olga Kenzior, and Chongbei Zhao of the Stowers tissue

culture support facility. Finally, I also appreciate the analysis of RNA-seq and ChIP-seq data by Cynthia Chen and Ning Zhang of computational biology core.

Lastly, I also want to thank my family, who support my study and life. My friends, including Wei Wang, Yan Yan, Kai Zhang, Yanfeng He, Shuonan He, Qiushuang Wu, Minling Hu, and Ann Liu, deserve special thanks. They are always glad to discuss about my projects and unconditionally support me.

Table of Contents

Table of Abbreviations

Abbreviation	Full name
acca	acetyl-CoA carboxylase alpha
acly	ATP-citrate lyase
AGPAT	1-acylglycerol-3-phosphate O-acyltransferase
AMPK	adenosine monophosphate-activated protein kinase
AP2	adipocyte protein 2
ATF2	activating transcription factor 2
ATP	adenosine triphosphate
BAT	brown adipose tissue
BMI	body mass index
BMP2	bone morphogenetic protein 2
bp	base pair
BrdU	bromodeoxyuridine
C/EBPα	CCAAT/enhancer-binding protein α
cAMP	adenosine 3’,5-cyclic monophosphate
CD36	cluster of differentiation 36
cDNA	complementary deoxyribonucleic acid
ChIP-seq	Chromatin immunoprecipitation sequencing

ChoRE	carbohydrate response elements
chrebp	carbohydrate response element binding protein
CLSs	crown-like structures
CNV	copy number variation
cpt1	carnitine palmitoyltransferase I
CREs	cis-regulatory elements
DE	differentially expressed
DGAT	diacylglycerol acyltransferase
DNL	*de novo* lipogenesis
dpf	days post fertilization
ELOVL6	Elongation of very long chain fatty acids family 6
ER	endoplasmic reticulum
fabp10a	fatty acid binding protein 10a
fabp11a	fatty acid binding protein 11a
FAO	fatty acid oxidation
FAs	fatty acids
fasn	fatty acid synthase
FATPs	fatty acids transport proteins
fgf21	fibroblast growth factor 21

fto	fat mass and obesity-associated protein
G6Pase	Glucose 6-phosphatase
G6PD	glucose-6-phosphate dehydrogenase
GFP	green fluorescent protein
GK	Glucokinase
gpam	glycerol-3-phosphate acyltransferase, mitochondrial
GWAS	Genome-wide association study
HDL	high-density lipoproteins
HFD	high fat diet
IL-1α	interleukin-1 alpha
IL-6	interleukin-6
ilgf1	insulin-like growth factor 1
IP injection	intraperitoneal injection
Ldh-B	lactate dehydrogenase-B
LDs	lipid droplets
LPK	liver pyruvate kinase
MAGs	monoacylglycerols
MC4R	melanocortin-4 receptor
ME	malic enzyme

mGPAT	Mitochondrial glycerol-3-phosphate acyltransferase
MUFAs	monounsaturated fatty acids
Myf5	myogenic factor 5
NADPH	nicotinamide adenine dinucleotide phosphate
ob	obese gene
OCT compound	optimal cutting temperature compound
PAP	phosphatidade phosphatase
Bmp4	bone morphogenetic protein 4
PBS	phosphate-buffered saline
PBST	phosphate-buffered saline Triton
Pdgfr-α+	platelet-derived growth factor receptor-alpha+
PEPCK	Phosphoenolpyruvate carboxykinase
per2	Period circadian clock 2
pfa	Paraformaldehyde
PGC-1α	peroxisome proliferator-activated receptor-gamma coactivator-1 alpha
PGD	6-phosphogluconate dehydrogenase
PKF1	phosphofructokinase 1
PKF2	phosphofructokinase 2

pomc	pro-opiomelanocortin
PPARα	peroxisome proliferator-activated receptor α
PPARβ	Peroxisome proliferator-activated receptor β
PPARγ	peroxisome proliferator-activated receptor γ
PPARδ	Peroxisome proliferator-activated receptor δ
PUFAs	Polyunsaturated fatty acids
pvdf	Polyvinylidene fluoride
QTL-mapping	quantitative trait locus mapping
RNA	ribonucleic acid
RPM	reads per million
RT	room temperature
RT-qPCR	Reverse transcription quantitative polymerase chain reaction
SAT	subcutaneous adipose tissue
scd1	stearoyl-CoA desaturase 1
scRNA-seq	single-cell RNA sequencing
SRE	sterol regulatory element
srebp1	sterol response element binding protein 1
T2D	type 2 diabetes
TAG	Triglyceride

TCA	tricarboxylic acid
tfap2b	transcription factor AP-2 beta
TNF-α	tumor necrosis factor alpha
TPM	Transcripts Per Kilobase Million
UCP1	uncoupling protein-1
UCP2	uncoupling protein-2
VAT	visceral adipose tissue
VLDL	very low-density lipoproteins
WAT	white adipose tissue
WT	wide type

Table of Figures

Table of tables

Chapter 1. Introduction

1.1 How animals adapt to challenging environments

Animals adapt to challenging environments by changing their morphology, behavior, and physiology. Studying organisms in these environments can help us understand underlying mechanisms. For example, the hot desert climate is a challenging environment for animals. High temperature is stressful for many animals since it leads to dehydration, appetite decrease, macro-molecule denaturation, and even heat stroke (Bouchama and Knochel, 2002; Zheng et al., 2019). Hence, animals in the desert have adapted behavioral patterns to avoid overheating (Caldwell, 1999). The easiest way is to avoid activities in the day, that is why many animals in the desert are nocturnal or crepuscular (Feldhamer, 2007). Burrowing is another useful mechanism for some desert animals, including rodents and rabbits (Feldhamer, 2007). These animals can stay in their burrow during the daytime to avoid exposure to sunlight. Moreover, animals in desert use different strategies to keep themselves cool. For example, desert foxes and rabbits usually have extraordinarily large ears which have thin skin and many blood vessels to facilitate heat dissipation (Hinds, 1973).

Water is a major limiting factor which impacts biodiversity on the earth. Generally, high precipitation or surface water can allow species to thrive when other abiotic conditions, including sunlight and temperature, are appropriate (Yan et al., 2015). Low water supply can be a serious problem for many animals. However, some desert animals manage the challenges by reducing water loss and enhancing water absorption from food. The kangaroo rat, a desert rodent species, has no sweat glands and lose little water through their skin. It also has a powerful nasal system which maintains water from

the exhaled air (Tracy and Walsberg, 2000). Furthermore, a kangaroo rat can survive independent of free water by utilizing the metabolized water from high carbohydrate seeds (Frank, 1988). The kidney and gut of kangaroo rats absorb water so efficiently that their urine is twice as concentrated as sea water and their feces are very dry (Beuchat, 1990; Urity et al., 2012).

Low temperature is another hostile environment, such as at the polar regions of the planet. For animals that can thrive there, one common adaptation is a high thermoregulation capability. Polar bears, for example, maintain their body temperature around 37 degree Celsius (°C) even when the surrounding temperature is below -40 °C. Polar bears can effectively prevent heat loss with the combination of a thick layer of fur, tough hide, and insulating fat layer (up to 11cm) under their skin. The fur of polar bears consists of two layers: 1) the short, dense inner layer near the skin; 2) the long, hallow guard hair (Uspenskii, 1977). The short and dense inner layer fur slowdowns heat dissipation, meanwhile the guard hair is effective in absorbing the heat emitted from the body. Moreover, the transparent guard hair also allow the dark skin to efficiently absorb warmth from sunlight (Dawson et al., 2014). Lastly, the thick subcutaneous fat of polar bears insulates their body from heat loss and maintains core body temperature.

Low oxygen is another stressful environment for most animals, and only a few animals can deal with it. The bar-head goose is famous for its capability to adapt to hypoxia. This bird species migrates biannually across Himalayan mountain regions, which have the altitude up to 7000 meters and extremely low oxygen level (Hawkes et al., 2013). They migrate to India in the winter and return to China and Mongolia for breeding in the spring. During the flight in the hypoxia condition, they reduce their metabolic rate and increase breathing (Scott and Milsom, 2007). Meanwhile, they maintain oxygen in their arterial blood and lower their venous oxygen (Meir et al., 2019). They also ride “aerial

roller coasters" to take advantage of drafting currents and wind patterns to conserve energy during trans Himalayan migration (Bishop et al., 2015).

1.2 Molecular mechanisms for animal adaptation

Although multiple studies have characterized how animals change their morphology, behaviors, and physiology to adapt to extreme environments, the underlying molecular mechanisms are less known. More and more investigations are designed to reveal those mechanisms, including the genetic basis of those mechanisms. Genetic variations exist between different populations and/or species, which lead to variation in traits and facilitate animals to adapt to extreme environments. These genetic variations include protein coding changes, cis-regulatory element variation, and gene copy number variation.

Protein coding changes are one form of genetic variation that allows animals to adapt to challenging environments. For example, in addition to physical and behavior changes, bar-headed geese have higher oxygen affinity for their hemoglobin compared to that of their low attitude relatives. Comparison of the hemoglobin peptide reveals that there is a coding mutation, Pro119Ala, in bar-headed goose compared to graylag goose, which live in the Indian plains all year round (Jessen et al., 1991). This mutation raises the oxygen affinity of bar-headed goose by attenuating the alpha beta interface (Jessen et al., 1991; Liu et al., 2001; Perutz, 1983).

The evolution of cis-regulatory elements (CREs), mainly promoters and enhancers, is another well-studied mechanism used by animals to adapt to challenging environment. With the changes in cis-regulatory elements, the corresponding genes modulate their expression level, which allows animals to deal with environmental stress.

For example, a small killifish, *Fundulus heteroclitus*, inhabits the east coast in North America, from Newfoundland to Florida. The fish populations along the coast exhibit different tolerances to thermal stress, with northern populations being more tolerant to low temperature and southern populations being more tolerant to high temperature (DiMichele et al., 1991; DiMichele and Powers, 1982). The expression level of lactate dehydrogenase-B (*Ldh-B*) in the liver of the fish is positively correlated with the latitude (Crawford and Powers, 1989), which is thought to be an adaptation to environmental temperature (Pierce and Crawford, 1997). Furthermore, it has been shown that there is a stress response element located approximately 500 base pair (bp) upstream of the transcription start site of *Ldh-B.* In the stress-responsive element, the northern population has one nucleotide variation compared to the southern population, which is the ancestral allele (Schulte et al., 2000). Functional tests further verified the single nucleotide change increases the transcription level of *Ldh-B*, which helps the northern populations adapt to the cold environment (Schulte et al., 2000).

Gene copy number variation (CNV), resulting from gene duplication and loss, is another mechanism for animals to adapt to challenging environment. Most animals need light to communicate with other organisms and the surrounding environment. However, some animals live in the deep sea, which is a dark environment. Some of those deep-sea animals use bioluminescence for vision and/or communication, but others have lost their eyes. A deep-sea fish, spinyfins, has excellent vision. Musilova and colleagues investigated 101 fish genomes and found the silver spinyfin (*Diretmus argenteus*) have the highest number of visual opsin gene copy in vertebrates (Musilova et al., 2019). This fish species has 2 core opsins and 38 rod opsins, which are the products of gene duplication. These rod opsins diversified during evolution and there are up to 14 rod opsins expressed in spinyfins. With the 14 rod opsins, spinyfins have the ability to detect the range of daylight and

bioluminescence spectrum present in the deep sea. Therefore, they have keen sight in the perpetual darkness.

1.3 Food availability and adipose tissue

Food availability variation can be challenging for animals in nature. Animals tend to consume more than they need when food is available. Once they consume large amount of food, the excess nutrition will be digested and absorbed through the gastrointestinal track. The energy is stored in the form of glycogen and fat. Fat is mainly stored in adipose tissue for long term use and is a very conserved way for animals to store fat to deal with variation in food availablity in the wild. For example, brown bears have increased appetite in the summer and fall, which leads them to consume dozens of kilograms of food per day. They have been documented to gain up to 4 kg of body fat each day in the fall before hibernation (Kingsley et al., 1983). Even invertebrates, including many insect larvae, consume high level of food to accumulate high body fat. It is critical, as the high body fat can ensure their normal development and growth during pupa stage (Arrese and Soulages, 2010).

The main cell type of adipose tissue is adipocytes in vertebrates. Within adipocytes, lipids are stored in lipid droplets (LDs), which are organelles with a lipid ester core and phospholipid monolayer surface (Tauchi-Sato et al., 2002). LDs have sphere structures. Their diameters vary from 0.1-5 μm in nonadipocyte cell types, but they can reach up to 100 μm in adipocytes (Fujimoto and Parton, 2011). The surface of LDs are phospholipids, including phospatidylethanolamine, phosphatidylcholine, phosphatidylinositol (Bartz et al., 2007; Leber et al., 1994). The core of LDs are lipid esters, which are mainly composed of triglycerides (TGs) and sterol esters. Proteins can also exist both on the surface as well as in the core of LDs (Robenek et al., 2005).

Adipose tissue can be classified into different types based on their characteristics in vertebrates. Regarding anatomical distribution, the most common adipose tissues are subcutaneous adipose tissue and visceral adipose tissue. Subcutaneous adipose tissue locates under the skin, while visceral adipose tissue distrubutes near the internal organs. In mammalians, adipose tissue also exists as retro-orbital adipose tissue, epicardial adipose tissue, mammary adipose tissue, joint adipose tissue, mesenteric adipose tissue, dermal adipose tissue, and bone marrow adipose tissue (Zwick et al., 2018). In fish, adipose tissues can be found all over the body from the snout to the tail fin. They are classfied as internal adipose tissue (visceral adipose tissue and non-visceral adipose tissue) and subcutanceous adipose tissue (cranial adipose, truncal adipose tissue, and appendicular adipose tissue) based on relative locations (Minchin and Rawls, 2017b). In mammals, there is additional subdivision based on color: white adipose tissue (WAT) and brown adipose tissue (BAT). Recent evidence shows a third type of adipose tissue exits in adult human, which is termed beige adipose tissue. Beige adipoe tissue has characteristics of both white adipose tisse and brown adipose tissue (Wang and Seale, 2016).

WAT distributes throughout the body in vertebrates, which have sufficient nutrient supply. One major function of WAT is to store excess energy in form of triglycerides. Therefore, WAT is an energy sink. When nutrients are deprived, the triglycerides in the WAT can be mobilized for oxidation to provide energy for the organism. Taken together, WAT works as an energy buffer. Whereas BAT only exists in mammalians, including newborns and BAT amount decrease in adults. In human adults, BAT locates near axillary, cervical, mediastinal and upper abdominal regions (Wehrli et al., 2007). BAT mainly dissipate heat to maintain the temperature of those vital organs. Mechanistically, the uncoupling protein-1 (UCP1) in the mitochondria stimulate uncoupled respiration and heat generation in BAT. It is also important for survival of mammalians in cold environment and for arousal in hibernators.

In addition, adipose tissue is also a vital endocrine organ. Adipocytes can secrete several endocrine hormones, meanwhile other non-adipocytes in adipose tissue can also release endocrine factors (Fain et al., 2004). These secreted hormones and proteins often regulate metabolism. The proteins secreted by WAT are adipokines. Adipokines mainly include leptin, adiponectin, tumor necrosis factor alpha (TNF-α), and interleukin-6 (IL-6) (Kershaw and Flier, 2004).

An important hormone released from WAT is leptin. When the gene coding leptin, known as obese gene (*ob*), was mutated in mice, mutant mice showed profound obesity and type II diabetes, suggesting the gene was crucial in regulating energy homeostasis (Ingalls et al., 1950). In 1994, the gene was cloned by Friedman and his colleagues (Zhang et al., 1994). Leptin is a 16 kDa peptide in mammals, which is transcribed and secreted by white adipose tissue. One year later, the receptor gene of leptin, OB-R, was also identified (Tartaglia et al., 1995). Through the circulating system, leptin can reach the hypothalamus and bind with its receptor. Then, it stimulates pro-opiomelanocortin (*pomc*) gene expression in the Arc of hypothalamus, which activates melanocortin signaling mediated by the melanocortin-4 receptor (MC4R). Eventually, it suppresses appetite and regulates energy homeostasis (Shimizu et al., 2007). The disruption of the pathway leads to increased appetite and extreme obesity (Clement et al., 1998; Vaisse et al., 1998; Yeo et al., 1998).

The circulating leptin level reflects the energy sufficiency and positively correlates with adipose tissue mass. However, for some obese patients or disease animal models, they do not decrease their food intake even when their plasma leptin level is very high. This phenomenon is termed leptin resistance (Myers et al., 2008). The proposed mechanisms mainly include changes in the transport of leptin across the blood brain barrier, variation in cellular long form of the leptin receptor signaling, and perturbations in developmental programming (Bouret and Simerly, 2006; Caro et al., 1996; Munzberg et al., 2005).

Adiponectin is another important cytokine, which is secreted by WAT. It is a ~250 amino acid peptide in mammals and is abundant compared to other hormones in the plasma, with concentration around 5-10 μg/mL. In normal adults, women have higher circulating adiponectin than men. In obese humans, an inverse correlation exists between circulating adiponectin and body mass index (Ukkola and Santaniemi, 2002). Moreover, weight loss increases circulating adiponectin concentration profoundly (Coppola et al., 2009).

Adiponectin is mainly involved in glucose metabolism and fatty acid oxidation. Adiponectin molecules can bind together to form multimeric forms of adiponectin, including trimer, hexamer, and even dodecamer. High-molecular weight forms may be the most active in regulating glucose metabolism (Oh et al., 2007) and it is linked to lower risk of diabetes (Zhu et al., 2010). In addition, adiponectin enhances insulin sensitivity by suppressing hepatic glucose production and promoting fatty acid oxidation in the skeletal muscle (Lihn et al., 2005). In muscle, adiponectin activates Peroxisome proliferator-activated receptor α (Pparα), therefore leading to upregulation of its target genes, including cluster of differentiation 36 (CD36), acyl-coenzyme A oxidase, and uncoupling protein 2 (UCP2) (Yamauchi et al., 2001). Those upregulated target genes enhance beta-oxidation. On the other hand, adiponectin also activates adenosine monophosphate-activated protein kinase (AMPK), which stimulates glucose uptake and fatty acid oxidation (Tomas et al., 2002). In the liver, adiponectin also enhances fatty acid oxidation, analogous to its activity in muscle. In addition, activated AMPK also reduces gluconeogenesis through suppressing phosphoenolpyruvate carboxykinase (PEPCK) and glucose 6-phosphatase (G6Pase) (Kadowaki and Yamauchi, 2005; Yamauchi et al., 2002).

1.4 Adipocyte development

1.4.1 Adipogenesis and gene regulation

Adipocytes are the main cell types of adipose tissue. The process of forming lipid-loaded mature adipocytes from stem cells is termed adipogenesis (Ghaben and Scherer, 2019; Gregoire et al., 1998). In mammals, adipocytes primarily derive from mesenchymal stem cells, which differentiate into pre-adipocytes that eventually develop into adipocytes (Berry et al., 2013). However, some adipocytes also derive from hematopoietic stem cells from the bone marrow (Crossno et al., 2006; Majka et al., 2011). Different adipose tissue types have different developmental chronology. In the human fetus, cheek adipocytes begin to develop at around 14 to 16 weeks (Poissonnet et al., 1983). The gluteal fat tissue, however, begins development 1 to 4 weeks later (Burdi et al., 1985). New adipocytes form throughout life and continue in adults at substantial rate (Spalding et al., 2008). In humans, subcutaneous adipose tissue (SAT) begin to emerge from week 14 to week 24 of fetus development (Poissonnet et al., 1984). Unlike SAT, the developmental timing of visceral adipose tissue (VAT) is less clear. It has been reported that VAT rarely forms during gestation and the size of VAT remains relatively small until adolescence (Fox et al., 1993; Siegel et al., 2007).

Adipogenesis can be briefly divided into two steps: adipocyte commitment and adipocyte differentiation (Ghaben and Scherer, 2019). The first step is that multipotent precursor cells restrict their fate into adipocyte lineage (preadipocyte) rather than developing into other cell types. Multiple lines of evidence indicate that certain bone morphogenetic proteins (BMP2 and BMP4) are sufficient to stimulate adipocyte commitment in cultured fibroblasts (Bowers et al., 2006; Huang et al., 2009; Wang et al., 1993). Then, a second transcription cascade drives the adipocyte differentiation. The most important gene involved in this step is a nuclear hormone receptor, Pparγ. Pparγ is

indispensable for adipocyte differentiation *in vivo* (Barak et al., 1999; Rosen et al., 1999) and in *vitro* (Tontonoz et al., 1994). Specifically, ectopic expression of Pparγ is sufficient to induce 3T3-L1 cells to differentiate into adipocytes in vitro (Tontonoz et al., 1994). Moreover, Rosen and colleagues injected Pparγ$^{-/-}$ embryonic stem cells into wild type (WT) blastocytes and generated chimeric mice by transplanting the blastocytes into WT mice. Their findings show that Pparγ null cells had little or no contribution to the adipose tissue (Rosen et al., 1999).

Pparγ regulates several downstream target genes, some of which are specifically expressed in the adipocyte cell lineage. One of the most important downstream target gene of Pparγ is CCAAT/enhancer-binding protein *α* (*C/EBPα*). Intriguingly, C/EBPα also induces *pparγ* expression. Together, they form a positive feedback regulatory loop. These two factors enhance each other's expression and maintain the differentiated state of adipocytes (Rosen et al., 2002), as they work synergistically and share 90% of genome-wide binding sites. Cooperating with C/EBP family proteins, Pparγ stimulates the transcription of genes, which are crucial for mature adipocytes. Those genes include adipocyte protein 2 (AP2), insulin receptor, and adiponectin (Lefterova et al., 2008). Therefore, adipogenesis is a tightly regulated cascade of gene transcription.

Adipose tissue is made of multiple cell types and plays a central role in energy metabolism, but the precise cell type, cell hierarchy, and cell crosstalk are largely unknown. Recently, with the advent of single-cell ribonucleic acid sequencing (scRNA-seq) (Kolodziejczyk et al., 2015; Tang et al., 2009), it becomes possible to investigate these questions. For example, the Deplancke group used scRNA-seq to reveal the cell types in mouse fat tissue. They found various cell populations of adipose stem and precursor cells in stromal vascular fraction of mouse subcutaneous fat. Intriguingly, they identified one cell type, which inhibits adipogenesis. This cell type can be distinguished from other cell populations by a cell surface marker, CD142. Functional tests showed that this cell type

can suppress adipogenesis both *in vivo* and *in vitro* in a paracrine manner. Furthermore, the cell type is functionally conserved in humans (Schwalie et al., 2018).

Recently, zebrafish has been developed into a useful model to study human obesity and other metabolism disorders (Seth et al., 2013). Zebrafish have many advantages, including optical transparency at young age, easy to raise in the lab, and large number of offspring. It has been reported that zebrafish begin to develop their visceral adipocytes at the age of 8 days post fertilization (dpf). The visceral adipose tissue always appears in the region between the swim bladder and intestine, which is the first location to show adipogenesis in zebrafish. Moreover, adipogenesis in zebrafish is also nutrition dependent (Flynn et al., 2009). Without feeding, adipogenesis does not happen in zebrafish. Furthermore, a high fat diet (HFD) can promote adipogenesis in zebrafish (den Broeder et al., 2017), suggesting that dietary lipids can somehow stimulate adipocyte development. In zebrafish, Flynn and colleagues proposed two possible models to explain the origin of visceral adipocytes. In the first model, they propose that fatty acid binding protein 11a (fabp11a)-negative cells near the pancreas or stroma turn into fabp11a-positive cells after feeding and represent visceral preadipocytes. Then, the preadipocytes differentiate into mature adipocytes. In an alternative model, fabp-11a-positive precursor cells, located in the caudal hematopoietic tissue, migrate to the region near the pancreas as a consequence to feeding, and then develop into mature adipocytes (Flynn et al., 2009). Once adipogenesis begins, the adipose tissue expands to the body cavity (Flynn et al., 2009).

1.4.2 Adipocyte number and size

Adipose tissue expansion can be achieved by hyperplasia (increased adipocyte number), hypertrophy (enlarged cell size), and/or both. In the human fetus, the SAT expands mainly through hyperplasia (Poissonnet et al., 1984). In the first year after birth

the adipocyte number keeps increasing. Then, the total number of adipocytes roughly remains constant until adolescence, when the adipose tissue will again undergo hyperplasia (Knittle et al., 1979). Adipose tissue hyperplasia consists of proliferation of adipocytes and formation of new blood vessels. During hyperplasia, pro-inflammatory cytokines decrease, immune cell recruitment to adipose tissue diminishes, and insulin sensitivity increases, all of which are beneficial metabolic phenomena (Choe et al., 2016). Therefore, hyperplasia is a healthy way to store excessive energy (Figure 1.1).

When energy intake exceeds energy expenditure and hyperplasia cannot deal with the situation, hypertrophy is initiated. That is because adipocytes have an upper volume limit. Hypertrophy is also a solution to store extra energy. In the process of enlarging size, adipocytes size is positively correlated with the expression levels of pro-inflammatory adipokines, including IL-6 and TNF-α (Skurk et al., 2007). Excessive adipocyte hypotrophy is usually associated with obesity and type-II diabetes. Meanwhile, enlarged adipocytes also release more free fatty acids, which may lead to decrease of insulin sensitivity. Dramatical enlargement of existing adipocytes and limited angiogenesis leads to hypoxia (Sun et al., 2011). Then, immune cells, like macrophages, will be recruited into hypertrophic adipose tissue. In some obese individuals, macrophages have been shown to aggregate and form crown-like structures (CLSs) surrounding necrotic adipocytes (Russo and Lumeng, 2018).

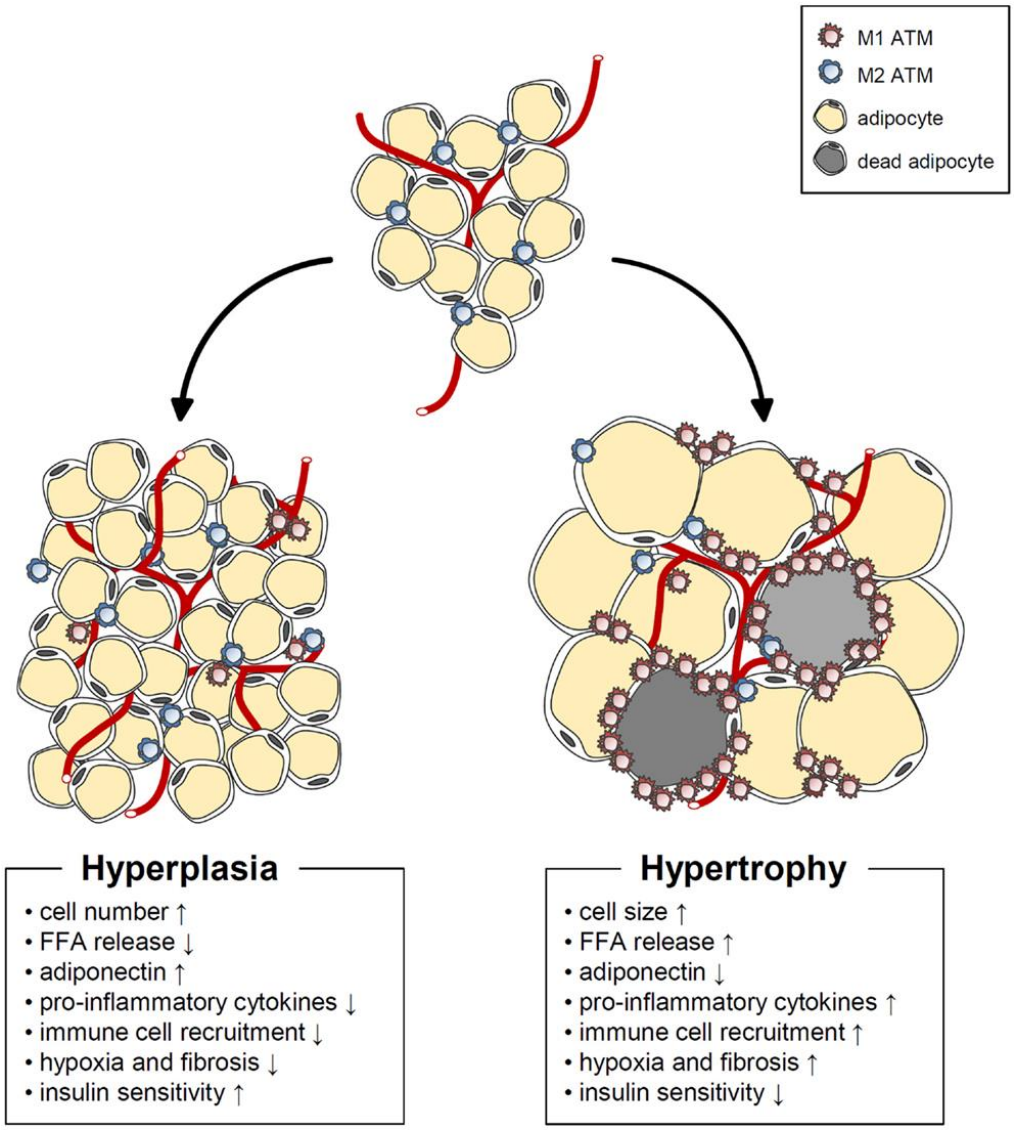

Figure 1.1 Characteristics of hypertrophic and hyperplastic adipocytes (Choe et al., 2016).

Adipose tissue expansion occurs by two different mechanisms. Hypertrophic adipose expansion through increased adipocyte size is associated with harmful phenomena as increased basal fatty acids release, pro-inflammatory cytokine release, immune cell recruitment, hypoxia, fibrosis, decreased adiponectin, and impaired insulin sensitivity. On the other hand, hyperplasic adipose expansion though increased adipocyte number is linked to beneficial phenomena, such as increased adiponectin, decreased basal fatty acids release, pro-inflammatory cytokine release, immune cell recruitment, hypoxia, fibrosis, and improved insulin sensitivity.

1.5 Cave and Astyanax mexicanus

1.5.1 Cave environment

A cave is a peculiar environment. First, caves are usually perpetual dark. The light/dark cycle is an important signal and has huge impact on circadian rhythm. This includes feeding behaviors, sleeping, and locomotion. Since most cave animals have poor vision or are even blind, they must depend on other senses and show different feeding behaviors. Meanwhile, they also have different locomotion compared to animals live out of caves. For animals live in natural light/dark cycle, they usually have obvious sleeping rhythm based on the light signal. However, for cave animals, their sleep rhythm is weakened.

Second, caves are usually food limited. There are no plants that survive in caves because of lacking sunlight, except the roots of some plants may grow into caves. Therefore, the food chain in the cave is quite limited. There are only a few animals that can survive the environment, including bats, some cave morphotypes of reptiles, amphibians, fish and invertebrates. Even parasites species and number are less than those in the fresh water outside (Peuss et al., 2020). Hence, the diversity of animals in the cave is far smaller than outside of the cave (Langecker, 2000).

Some animals forage outside of the cave and only stay in the cave for certain periods of the day. For example, bats forage out of the cave and fly back to the cave to rest. However, other animals live in the cave for their whole life but they still depend on food from the outside. For example, flooding may bring organic debris into the cave. Moreover, bat droppings can provide food for other animals. Overall, food sources are rare and nutrient limited, hence, caves are considered food-limited environments (Wilkens, 2000).

1.5.2 Astyanax mexicanus

Astyanax mexicanus, a freshwater fish, is native to the central and eastern parts of Mexico and southern parts of Texas. This organism has gained popularity in evolution and development studies because of striking differences between surface fish and cavefish populations (Figure 1.2). The former has fully-grown eyes and normal pigmentation, which is typical of river-dwelling fish. However, the cavefish have lost or reduced pigmentation (Gross et al., 2009; Protas et al., 2006) and degenerated eyes (Jeffery et al., 2003). Apart from these obvious morphological phenotypic variations, the two fish populations also display different social behaviors (Kowalko et al., 2013b), feeding postures (Kowalko et al., 2013a), sensitivity to vibrations (Yoshizawa et al., 2012), and olfactory capabilities (Protas et al., 2008). Furthermore, they differ in both size and number of neuromasts (Yoshizawa et al., 2012) and taste buds (Protas et al., 2007).

In addition to morphology and behaviors, cavefish populations also show differences in physiology compared to surface fish. For example, cavefish sleep much less than surface fish (Duboue et al., 2011) and enhanced Hypocretin/Orexin (HCRT) signaling underlies the evolution of sleep loss (Jaggard et al., 2018). Furthermore, Pachón cavefish lost the capability for heart regeneration, while surface fish maintain this ability (Stockdale et al., 2018). Moreover, Pachón cavefish have a more sensitive immune system compare to surface fish due to T-cell populations changes (Peuss et al., 2020).

Despite having the diverse differences, the two populations remain interfertile with each other (Sadoglu, 1957), which enables genetic studies. The fact that these fish can be housed and maintained easily in a lab environment makes functional and genomic studies feasible (Jeffery et al., 2003). Moreover, there are over 30 different cavefish populations in the wild, many of which are independently derived. Among them, three cavefish

populations, including Pachón, Tinaja, and Molino, are the most frequently used for lab research involving genetic, developmental, and evolutionary studies.

Astyanax mexicanus become sexual maturity around 1 year in the lab. They are highly productive. A single pair parental fish can generate up to 300 fertilized eggs. Those eggs are transparent, which facilitate the transgenic injection. Moreover, we can also easily generate hybrid progenies between surface fish and cavefish. Given the surface fish and cavefish have some dramatical phenotypical difference, we can use the hybrid progenies to do QTL-mapping to reveal the genetic basis of those traits. Taken together, *Astyanax mexicanus* is an excellent model to study genetics, development, and evolution.

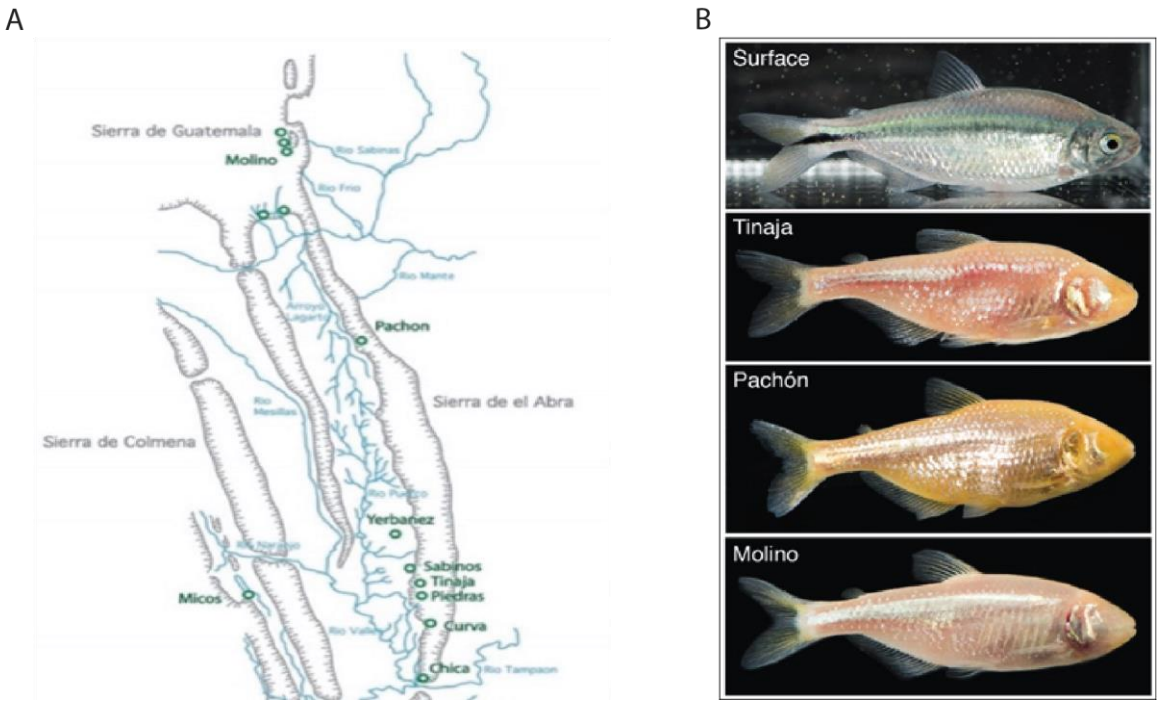

Figure 1.2 Geographical distribution of *Astyanax mexicanus* populations in Mexico.

A) The green circles represent the location of the cavefish populations in Mexico. B) The examples of surface fish (top) and cavefish populations commonly used in the lab (Tinaja, Pachón, and Molino respectively).

1.6 Metabolic adaptation of Mexican cavefish populations

When raised in the lab, cavefish populations can store higher body fat compared to surface fish (Aspiras et al., 2015; Hüppop, 2001). For some cavefish populations, they show higher appetite than their surface counterpart. That is why they can consume more food than surface fish when food is available. With enhanced appetite, they can obtain high body fat to be more starvation resistant than surface fish. Aspiras and colleagues further pinpointed a coding mutation in *mc4r* gene, the cause for the increased appetite in some cavefish populations, including Tinaja and Molino (Aspiras et al., 2015). However, some cavefish populations do not have this mutation, yet, they still have higher body fat than surface fish, indicating appetite-independent mechanisms exist.

To interrogate alternative mechanisms which help cavefish gain high body fat, the Tabin lab hypothesized that some cavefish populations have higher nutrient absorption efficiency than surface fish. They found that Pachón cavefish exhibit bi-directional churning mobility in the stomach region, but surface fish do not. Furthermore, live food transit from stomach to midgut in Pachón cavefish happens more slowly than that of surface fish. This gastrointestinal motility may enhance nutrient absorption in Pachón cavefish (Riddle et al., 2018b).

Furthermore, Riddle and colleagues found that some cavefish populations show dysregulated blood glucose (Riddle et al., 2018a). Specifically, Pachón, Tinaja, and Molino have higher postprandial glucose levels than surface fish. After 21 days fasting, both Pachón and Tinaja store their blood glucose level to a similar level as that of surface fish (around 45 mg/dL), but the blood glucose level of Molino is still up to 100 mg/dL. Furthermore, Surface fish can restore the blood glucose back to base line level in 13.5 hours after glucose intraperitoneal injection (IP injection). However, all the three cavefish populations need 24 hours to achieve this shift. Moreover, both Pachón and Tinaja show

insulin resistance, which is caused by P211L mutation in the insulin receptor. When this mutation is introduced into zebrafish, they also show insulin resistant and gain weight faster than wild type fish. Therefore, the authors proposed that this mutation in the insulin receptor is advantageous for cavefish to deal with food scarcity in the cave environment.

Moreover, it has been shown that cavefish populations, especially Molino cavefish, are naturally hyperglycemic (Riddle et al., 2018a). However, the cause was still unknown. Recently, a loss-of-function mutation, R42H, in the *hk2* gene has been identified in Molino cavefish by Shimobayashi and colleagues (Shimobayashi, 2019). The mutated site is highly conserved among vertebrates and the mutated histidine is predicted to destabilize the HK2 protein conformation. Indeed, the mutated HK2 enzyme reduced its hexokinase activity to about half of the wild type. Furthermore, the homozygous R42H mutated *hk2* mice have lower number than 25% of all offspring, implying the mutated *hk2* gene has deleterious effect. Taken together, the R42H, a loss-of-function, contributes to hyperglycemia in Molino cavefish.

1.7 Lipid metabolism

1.7.1 Lipid absorption

Understanding lipid metabolism is helpful to know how cavefish gain high body fat to adapt to food scarcity. Therefore, I will introduce the three major aspects of lipid metabolism in animals: lipid absorption, lipogenesis, and fatty acid oxidation.

Lipids are one of the major micronutrition molecules for animals. Some of them can be digested and absorbed by animals, which are utilized as cell structural molecules, signaling molecules, or energy resource (Fahy et al., 2009). The digestion of dietary fat begins in the oral cavity mediated by lingual lipases, which are secreted by the tongue.

Both lingual and gastric enzymes promote further digestion in the stomach, where the emulsification of dietary fat begins. Then, the emulsified lipids enter the gut and are mixed with bile acids and pancreatic lipase. The hydrolysis of lipids is highly efficient in the intestine, where lipid absorption mainly takes place.

Among all the cell types in intestine, enterocytes are the most abundant and primarily used for nutrient absorption (Iqbal and Hussain, 2009). Enterocytes use diffusion and protein-mediated transport mechanisms to take up monoacylglycerols (MAGs) and fatty acids (FAs) (Abumrad and Davidson, 2012; Pan and Hussain, 2012). Diffusion across cell membrane occurs when concentrations are higher than those inside the cell (Strauss, 1966). However, when extracellular concentrations are lower, protein-mediated uptake mechanisms might become more important (Stremmel, 1988; Stremmel et al., 1985). Several proteins including CD36 and various fatty acids transport proteins (FATPs) have been shown to be involved in this process (Abumrad et al., 1998; Schaffer and Lodish, 1994).

Once inside the enterocyte, the products of triglyceride hydrolysis need to cross cytoplasm to reach the endoplasmic reticulum (ER), where they will be used to synthesize TAG. Packing with cholesterol, phospholipids, and apolipoproteins, the synthesized TAG can form lipoproteins, which mainly include chylomicrons, very low-density lipoproteins (VLDL), and high-density lipoproteins (HDL) (Goodman, 2010).

1.7.2 Lipogenesis

Another source of lipids for animals is to derive fat from non-lipid molecules. In animals, glucose and amino acids can be converted into acetyl-CoA to be used to synthesize fatty acids and triglycerides. This process is termed *de novo* lipogenesis (DNL)

(Wang et al., 2015). DNL mainly happens in the liver, adipose tissue, and mammary glands of lactating mammals. In humans and birds, the liver is considered as the major site for lipogenesis (Gondret et al., 2001; Mourot et al., 2000). In contrast, the dominant site for lipogenesis is adipose tissue in ruminants and pigs (Ingle et al., 1972). Meanwhile, both liver and adipose tissue are critical for lipogenesis in rodents (Nafikov and Beitz, 2007). Three key enzyme genes are involved in DNL: adenosine triphosphate-citrate lyase (*acly)*, acetyl-CoA carboxylase alpha (*acca)*, and fatty acid synthase (*fasn)*. Fatty acids can undergo desaturation (Brock et al., 2007), elongation (Horikawa et al., 2008), and esterification (Elliott et al., 1999) to synthesize triglyceride, which is the most common fat as energy storage in animals (see Figure 1.3 from (Wang et al., 2015)).

The nutritional state heavily affects lipogenesis in mammals. A diet rich in carbohydrates stimulates lipogenesis in both liver and adipose tissue in human and rodents. In carbohydrate-rich diets, the blood glucose levels increase and stimulate insulin release. The insulin signaling pathway stimulates liver cells and adipocytes to uptake glucose for lipogenesis via recruitment of glucose transporter on the cell membrane. In addition, insulin also activates lipogenic genes, including sterol response element binding protein 1 (*srebp1* a.k.a *srebf1*) (Tian et al., 2016). In contrast, fasting reduces lipogenesis in adipose tissue and inhibits lipogenesis in the liver.

Lipogenesis is regulated at multiple aspects, including the transcriptional level, translational level, and posttranslational level. At the transcriptional level, several transcription factors have been reported to regulate lipogenesis process. Among them, *srebp1* and carbohydrate response element binding protein (*chrebp* a.k.a *mlxip*) are important transcriptional regulators of lipogenesis and triglyceride biosynthesis in the liver (Xu et al., 2013). Activated SREBP1-c binds to sterol regulatory element (SRE) sequences found in the promoter of its target genes, including *acly*, *acc*, *fasn*, and glycerol-3-phosphate acyltransferase, mitochondrial (*gpam*) (Horton et al., 1998; Horton et al., 2003;

Liang et al., 2002). These target genes are then upregulated at the transcriptional level, to increase fatty acid and triglyceride biosynthesis. Similarly, ChREBP binds to carbohydrate response elements (ChoRE) in the promoter of genes, which are involved in glycolysis, gluconeogenesis, and lipogenesis (Yamashita et al., 2001). ChREBP promotes lipogenesis through upregulating *acc*, *fasn*, and stearoyl-CoA desaturase 1 (*scd*1) (Iizuka et al., 2004).

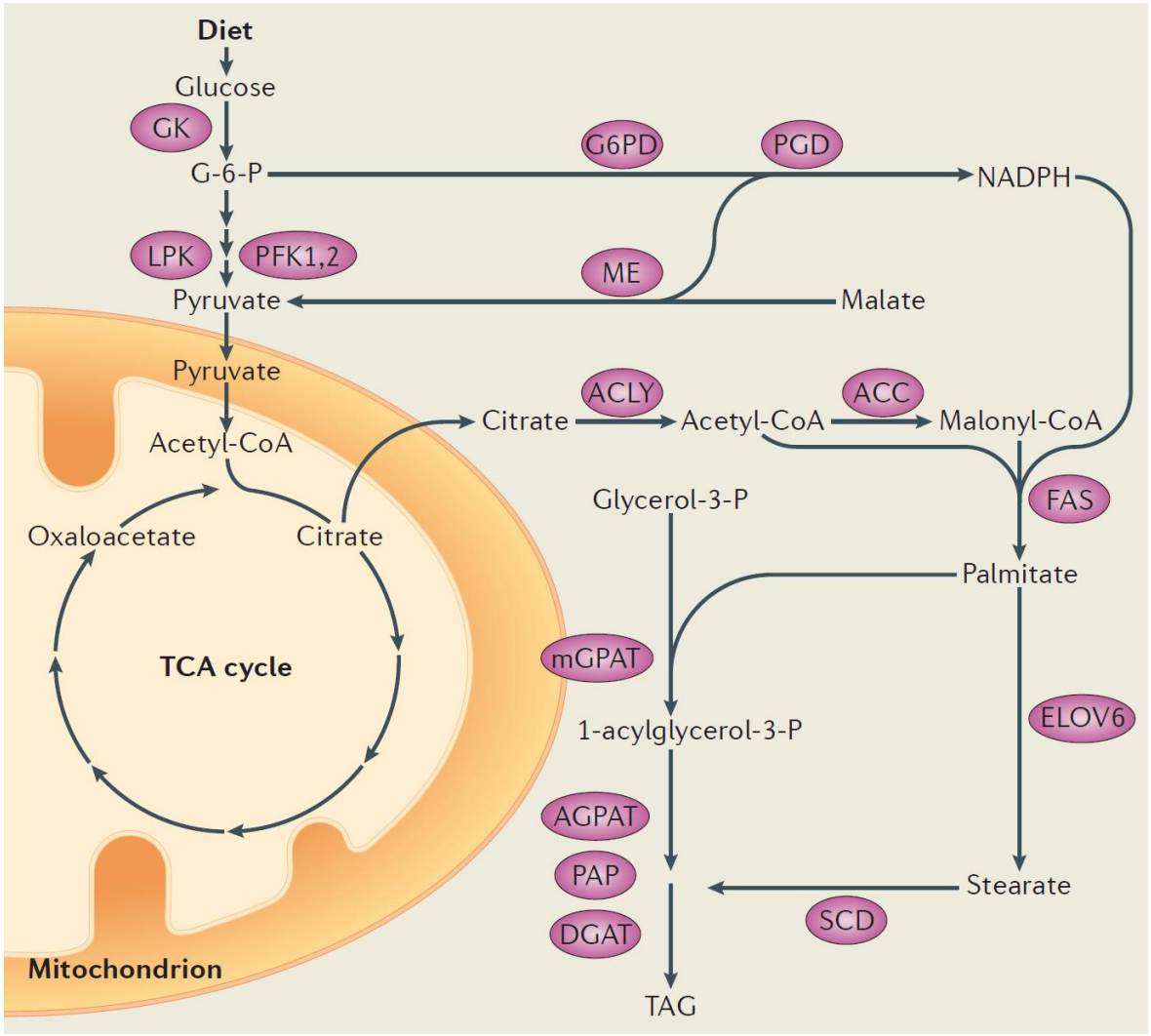

Figure 1.3 Metabolic pathways for fatty acid and triglyceride synthesis (Wang et al., 2015).

Glucose taken up by the cell is converted to pyruvate through glycolysis. Pyruvate is further converted into acetyl-CoA and enters the tricarboxylic acid (TCA) cycle (which is also known as the Krebs cycle for energy production). Excess acetyl-CoA converted to citrate can exit the mitochondria and becomes the substrate for lipogenic enzymes. Enzymes involved in FA and TAG synthesis include Glycolytic enzymes, such as glucokinase (GK), phosphofructokinase 1 (PKF1) and phosphofructokinase 2 (PKF2), and liver pyruvate kinase (LPK), which provide the carbon source for fatty acid and TAG synthesis.

Enzymes for the fatty acid synthetic pathway include Adenosine triphosphate -citrate lyase (ACLY), acetyl-CoA carboxylase (ACC), fatty acid synthase (FAS), elongation of very long chain fatty acids family 6 (ELOVL6) and stearoyl-CoA desaturase (SCD). Enzymes to produce nicotinamide adenine dinucleotide phosphate (NADPH) used in fatty acid synthesis contain the oxidative branch of the pentose-phosphate pathway, such as glucose-6-phosphate dehydrogenase (G6PD) and 6-phosphogluconate dehydrogenase (PGD), as well as malic enzyme (ME). Mitochondrial glycerol-3-phosphate acyltransferase (mGPAT), 1-acylglycerol-3-phosphate O-acyltransferase (AGPAT), phosphatidade phosphatase (PAP) and diacylglycerol acyltransferase (DGAT) are enzymes involved in esterification for TAG production.

1.7.3 Lipolysis and fatty acid oxidation

Since lipid metabolism is usually under a state of homeostasis, the degradation and usage of lipid is also important for animals. Triglycerides can be hydrolyzed into glycerol and fatty acid, which is termed lipolysis (Zechner et al., 2005). It is mediated by lipase and hydrolases (Schwartz and Jungas, 1971; Soni et al., 2004; Zimmermann et al., 2004). It is usually utilized to mobilize the stored energy, fat, during fasting or exercise. This process is induced by some hormones, including glucagon and adrenaline (Duncan et al., 2007). The fatty acids are released into the circulatory system and transported into cells through fatty acid transporters on cell membranes (Schwenk et al., 2010). Then, fatty acids will be modified into acyl-CoA and transported into mitochondria for oxidation. The carnitine shuttle on mitochondria membranes is responsible for the transportation (Kerner and Hoppel, 2000). This is the essential step for fatty acid oxidation, mediated by carnitine palmitoyltransferase I (*cpt1*) (Kerner and Hoppel, 2000). After fatty acyl-CoA is imported into mitochondrial matrix, fatty acid oxidation (FAO) begins. The long carbon chain of the fatty acids (in the form of acyl-CoA) undergoes a series of cutting two-carbon units, which combines with co-enzyme A to form acetyl-CoA. Acetyl-CoA will be used in citric acid cycle to generate adenosine triphosphate (ATP), CO_2 and H_2O. It provides energy source for heart, skeleton muscle, liver, and kidney (Houten et al., 2016). In addition to energy, fatty acid oxidation also generates many intermediate metabolites, which can be used as substrate to synthesize other important biological molecules.

FAO is regulated by both transcriptional and posttranscriptional mechanisms (Houten et al., 2016). PPARα controls many genes involved in FAO in the mouse liver (Lee et al., 1995), which plays a crucial role in the adaptation to starvation (Kersten et al., 1999; Leone et al., 1999). Similarly, PPARα, along with Peroxisome proliferator-activated receptor β (PPARβ) and Peroxisome proliferator-activated receptor δ (PPARδ), plays a role

in the expression of FAO enzymes in skeletal muscle and the heart (Muoio et al., 2002; Neels and Grimaldi, 2014). An important posttranscriptional regulatory step in FAO is the inhibition of CPT1 by malonyl-CoA (McGarry et al., 1977), which is the intermediate product of DNL. Hence, DNL can inhibit FAO to facilitate lipid synthesis and storage.

Chapter 2. Adipose tissue and adipogenesis in *Astyanax*

2.1 Introduction

Animals change their morphology, behavior, and physiology to adapt to challenging environments. Numerous studies have investigated the basis of morphological adaptations while few have focused on changes to behavior or physiology. To survive periods when food is limited or absent, many organisms have evolved a range of physiological strategies, such as hibernation, diapause, torpor, and estivation (Staples, 2016). Such strategies are often associated with increased fat gain and help these animals sustain through prolonged periods of deprivation to a time of greater nutrient abundance (Chippindale et al., 1996; Staples, 2016).

Astyanax mexicanus is an ideal species to study the genetic and developmental basis of metabolic adaptations. This Tetra species consists of cave-dwelling forms that are endemic to a few dozen caves in the Sierra de El Abra in the states of San Luis Potosí and Tamaulipas in central Mexico and river-dwelling populations that can be found on a broader range from North to Central America. The cave and surface morphs diverged approximately 20–200k years ago (Herman et al., 2018). Despite their divergence, surface and cave populations are able to generate fertile offspring both in the wild and in the laboratory, therefore, they are considered populations of the same species, *A. mexicanus* (Bradic et al., 2013). Of great importance is the availability of different, independently derived cavefish populations that can inform about the repeatability of evolution (Bradic et al., 2013; Coghill et al., 2014).

Cave-dwelling animals have to withstand long periods of nutrient limitation, as photosynthesis-driven primary producers are absent within the caves (Wilkens, 2000).

Hence, cave food chains are dependent on energy input from external sources, such as seasonal floods and/or bat droppings. To thrive under such harsh and unpredictable conditions, cave animals must evolve unique metabolic strategies that are currently not well understood. The cavefish populations of *Astyanax mexicanus* have evolved a suite of metabolic adaptations to survive in these nutrient limited cave environments. For example, cavefish display significantly increased levels of white adipose tissue compared to surface fish (Aspiras et al., 2015; Hüppop, 2001). In some cave populations, such as Tinaja, parts of this phenotype can be attributed to a mutation in the melanocortin 4 receptor (MC4R) which elicits hyperphagia (Aspiras et al., 2015). In addition, Tinaja and other populations have developed insulin resistance as an extra mechanism that helps them grow faster (Riddle et al., 2018a). Here, I show that most cavefish populations display elevated levels of visceral adipose tissue due to extreme hypertrophy of adipocyte. Moreover, Pachón cavefish also develop visceral adipocytes earlier and faster than surface fish.

2.2 Material and methods

2.2.1 Experimental animals

In this thesis research, I used surface fish (Mexican surface fish) and three cavefish populations, including Pachón cavefish, Tinaja cavefish, and Molino cavefish. The fish husbandry and breeding were done by the cavefish facility of the Stowers Institute. For all fish populations, embryos were collected and cultured in E2 embryo media containing methylene blue at 28 °C. When they were 6 dpf, 25 fry were housed in one 3 L tank on the circulating system. The fry were fed twice per day with live artemia. At the age of two months, fish were housed at a density of 2 fish per liter and fed ad libitum with artemia, frozen mysis shrimp, and Gemma (Skretting, USA) three times per day. The nutritional composition of Gemma according to the manufacturer is Protein 59%; Lipids 14%; Fiber 0.2%; Ash 14%; Phosphorus 1.3%; Calcium 1.5%; Sodium 0.7%; Vitamin A 23000 IU/kg; Vitamin D3 2800 IU/kg; Vitamin C 1000 mg/kg; Vitamin E 400 mg/kg. All populations were exposed to the same parameters: Light cycle (L/D): 14/10; Conductivity: 750–800 μS/cm; Temperature: 23 °C; pH: 7.6 (Elipot et al., 2014).

2.2.2 Visceral fat analysis

Fish between 9 and 10-months old, and of similar size, were selected and euthanized with 500 mg/L MS222. The wet weight and standard body length were measured. Then, I dissected the visceral adipose tissue (VAT) from the abdominal cavity according to the classification in (Gupta and Mullins, 2010; Minchin and Rawls, 2017b). In short, I manually removed the intestinal sack of the fish and carefully isolated fat tissue

located around the stomach and gut. I determined the wet weight of the VAT with a Mettler Toledo (XS105 Dual range) balance.

2.2.3 H & E staining

The VAT was isolated from the abdominal cavity and fixed in 4% paraformaldehyde for 18 h at 4 °C. Then I sent samples to Histology facility. They embedded in JB-4 Embedding solution (Electron Microscopy Sciences, 14270-00) while following kit instructions for dehydration, infiltration and embedding. After sectioning at 5 µm, the slides were dried for 1 h in a 60 °C oven and stained slides with hematoxylin for 3 min. This was followed by rinsing the slides in PBS, and semi-dried slides were stained with eosin (3% made in desalted water) for 1 min. Slides were then washed with desalted water and air dried. Images were obtained using a Zeiss Axioplan2 upright microscope and analyzed with Adobe Photoshop CC (Version 19.1.0) by Rob, a former postdoc in the Rohner lab.

2.2.4 Fish growth monitor

Five similar sized sibling fish from each population (Surface fish, Pachón cavefish, and Tinaja cavefish) were selected for the paired feeding assay and housed each population in one 10 L tank. Three biological replicates (three tanks per population) were performed for each fish populations. Fish were fed with Gemma twice a day (~9 am in the morning and ~ 3pm in the afternoon). The amount of food was decided based on trial experiments in which I determined how much surface fish can eat within one feeding. Then, I provided equal amounts of food to all populations. During this experiment, I measured the standard body length and wet body weight of each fish every two weeks. Additionally, the amount

of food (Gemma) was gradually increased from 15 mg to 80 mg per feed per tank as the fish were growing up and were able to ingest more food.

2.2.5 Nile red staining

Nile red staining was performed as described in (Flynn et al., 2009). Briefly, Nile red (Invitrogen, N-1142) stock solution was made by dissolving in acetone with a concentration of 1.25 mg/mL and stored in the dark at −20 °C. Then, I diluted the stocking solution with fish system water to a final working concentration of 1 μg/mL. Next, fish were euthanized with 500 mg/L MS222 and immersed in 12-well cell culture plates (Corning, CLS3513) containing 2 mL diluted Nile red solution per well in the dark for 30 min. After the whole mount staining, I washed the fry with PBS before imaging.

2.2.6 Fry feeding assay

The live artemia were collected and 400 μL artemia solution transferred into a pre-weighted Spin-X centrifuge tube filter (Costar, 27018000). Then, I centrifuge the filter tube loaded with artemia solution at 12,000 g for 5 min. The total weight of filter and artemia were determined and the wet weight of artemia can be calculated by subtracting the net filter weight. I diluted the artemia with fish system water and mixed the solution evenly before feeding them to fry. The feeding amount of artemia (40 mg and 80 mg) can be converted into feeding artemia solution volume based the wet artemia weight and total fish system water volume. The larvae were fed twice per day (morning feeding and afternoon feeding).

2.2.7 Microscopy

Images for visceral adipocyte diameter analysis were taken by my collaborator, Rob, on Axioplane2 (Zeiss) microscope with an Infinity3 (Lumenera) camera. Images were exported to Adobe Photoshop CC (Version 19.1.0) and the scale was adjusted to the magnification (1 Pixel = 0.9110 µm) that was used to acquire the image. Area and diameter were measured using the measurement tool and data was exported to a text file for statistical analysis.

For fry Nile red staining, I took the images on M205 C (Leica) dissecting microscope with an DFC7000 T (Leica) camera using a 9.79× magnification under green fluorescent protein (GFP) channel (Excitation = 470 nm, Emission = 525 nm). Wand tool in ImageJ was used to define the edge of adipose tissue, the area was measured using "Measure" under the "Analyze" menu, and data was exported to a text file for statistical analysis.

2.3 Results

2.3.1 Visceral adipose tissue comparison between fish populations fed ad libitum

First, I compared VAT from similar sized surface fish and three independently derived cavefish populations (Pachón, Tinaja, and Molino) that were fed ad libitum in the laboratory for around 9–10 months. I dissected the visceral fat from the abdominal cavity and determined its wet weight. In line with previous study (Aspiras et al., 2015), I found that Tinaja and Pachón populations display significantly more visceral fat than surface fish (Figure 2.1A, B). To test if this increase in fat mass is due to hypertrophy of the visceral adipocytes, I performed H&E staining on visceral adipose tissue section. I detected massive hypertrophy in Tinaja and Pachón cavefish adipocyte compared to surface fish. I observed a median adipocyte diameter of 220.63 μm in Pachón and 230.13 μm in Tinaja vs 66.34 μm in surface (Figure 2.1A, C). Surprisingly, while the median adipocyte diameter in Molino fish is significantly larger compared to surface fish, the fish showed only slightly increased VAT levels, which were not significantly different from the surface fish (Figure 2.1A, B). Tinaja cavefish display hyperphagia compared to surface fish, which has been suggested to lead to increased fat depot acquisition and contribute to starvation resistance (Aspiras et al., 2015). However, cavefish from the Pachón population show similar starvation resistance and increased fat content to Tinaja cavefish, but are not known to overeat, both as larvae and as adult fish (Alie et al., 2018; Aspiras et al., 2015). This suggests that appetite-independent mechanisms exist in the cavefish populations.

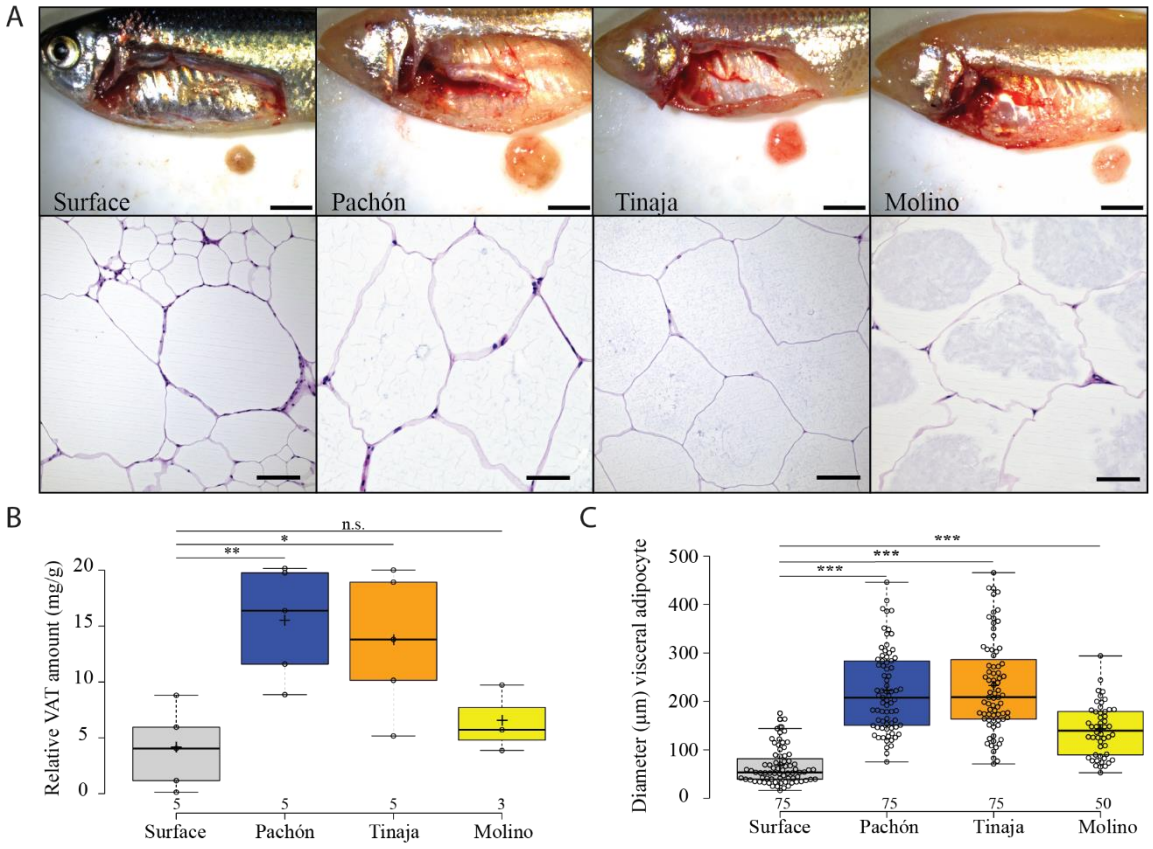

Figure 2.1 Relative VAT amount and adipocyte size comparison of surface and cave populations of *A. mexicanus*.

A) Dissection of VAT tissue from surface, Pachón, Tinaja and Molino fish and their corresponding H&E staining of the VAT tissue. B) VAT tissue wet weight from surface (grey), Pachón (blue), Tinaja (orange), and Molino (yellow) was measured and plotted relatively to the wet body weight (mg/g) for each population (n = 5,5,5,3 respectively). C) Visceral adipocyte size comparison between fish populations (n of analyzed adipocyte number for each population is shown in plot). Indicated significances are the result of Wilcoxon test. Significant differences are shown as *($p \leqslant 0.05$), ** ($p \leqslant 0.01$) or ***($p \leqslant 0.001$) and n.s. indicating not significantly different from control (surface population). Scale bar in A) is 5 mm for dissected fish and 200 µm for visceral adipocytes.

2.3.2 Visceral adipose tissue comparison between paired feeding fish

To test whether the increased fat content can be entirely explained by the increased appetite in the Tinaja cavefish, I raised fish by paired feeding. I achieved this by feeding a limited amount of regular Gemma diet so that surface fish and cavefish eat the entire amount of food per feeding. Such studies have been used in mice to study the influence of metabolism on various processes like circadian rhythm, adiposity, etc. (Harrison et al., 1984; Kuroda et al., 2012). I raised Tinaja cavefish and surface fish from the age of two months for an additional six months on this consistent diet. Throughout the whole paired feeding process, I monitored the standard body length and wet weight of individual fish (Figure 2.2A). I detected no overall significant difference in body weight change between Tinaja cavefish and surface fish ($p=0.8873$, using R packages lme4 and lmerTest linear mixed models). Next, I determined the amount of visceral fat in the fish and found Tinaja cavefish display significantly increased levels of visceral fat content compared to surface fish (median wet visceral fat weight of 32.76 mg per g wet body weight in Tinaja vs. median visceral fat weight of 3.72 mg per g wet body weight in surface, $p=0.004$, one-way ANOVA) (see Figure 2.2C, D). This strongly suggests that there are additional appetite-independent mechanisms driving fat acquisition in the Tinaja population. I hypothesized that such mechanisms would be even more pronounced in Pachón cavefish as this population cannot rely on hyperphagia as a mechanism to gain fat. To test this hypothesis, I repeated the experiment with Pachón cavefish. As for the Tinaja experiment, I also measured standard body length and wet weight of individual fish at two-week intervals (Figure 2.2B, Figure 2.4A). For the Pachón vs. surface comparison, I found Pachón cavefish to have higher increased VAT levels compared to surface fish and Tinaja cavefish (median visceral fat wet weight of 39.29 mg per g wet bodyweight in Pachón vs. a median visceral fat wet weight of 2.92 mg per g wet bodyweight in surface, $p \leqslant 0.001$, Wilcoxon

test) (see Figure 2.2C, E). This suggests that while both cavefish populations can develop increased visceral fat depots in the absence of overeating, Pachón cavefish may have acquired additional developmental and/or physiological differences that allow them to acquire more fat with the same amount of food.

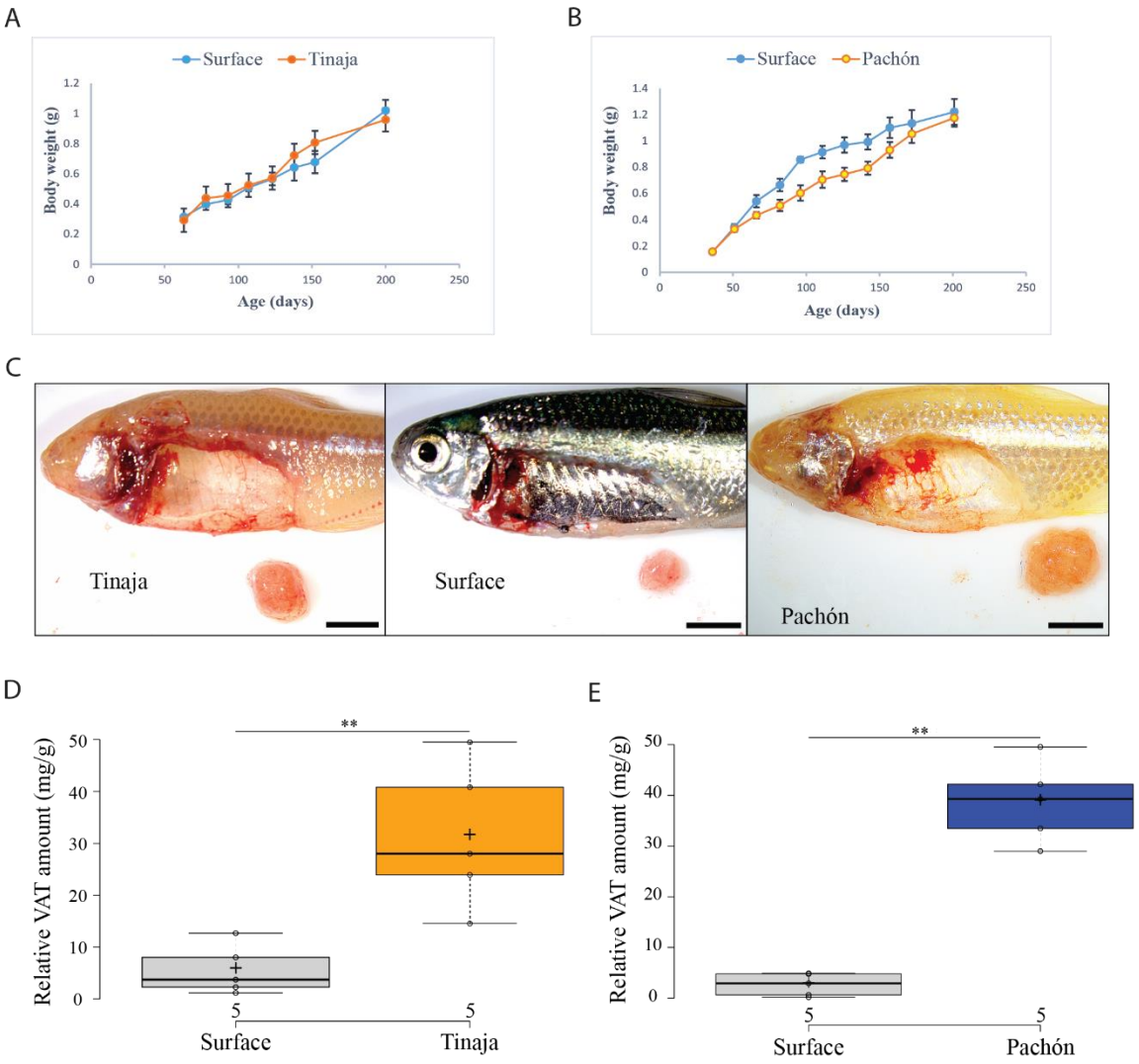

Figure 2.2 Weight gain and VAT development of *A. mexicanus* on paired feeding.

A) Wet body weight/length of surface fish (grey line) and Tinaja cavefish (orange line) and B) surface fish (grey line) and Pachón cavefish (blue line) are the result of two independent experiments where respective populations were raised under a controlled diet regime for 150 days (n = 15 fish for each population). Significant differences of the growth rate between surface and the respective cave population were determined using linear mixed model for analysis. C) After six months on a controlled diet, fish from A) and B) were dissected, and VAT was removed as described before. Relative VAT amount (wet VAT weight relative to wet body weight (mg/g)) of n = 5 fish for each population was analyzed for D) Tinaja cavefish (orange plot) and respective surface fish (grey); and for E) Pachón

cavefish (blue plot) and respective surface fish (grey plot) population. Significant differences between surface fish and the respective cave population were determined using Wilcoxon test. Significant differences are shown as ** ($p \leqslant 0.01$) or ***($p \leqslant 0.001$). Scale bar in C) is 5 mm.

2.3.3 Adipogenesis dynamics comparison between fish populations

Previous studies have suggested changes to energy expenditure allow adult cavefish to be thriftier than surface fish (Moran et al., 2014, 2015), however no detailed early larval studies of fat development have been performed in cavefish. To understand whether there are differences between Pachón cavefish and surface fish adipogenesis, I compared adipocyte development between surface fish and Pachón cavefish born on the same day from similarly sized and aged parents. A previous study show that visceral fat development in zebrafish starts between 8 dpf and 12 dpf depending on the age and size of the fish (Minchin and Rawls, 2017a). Early adipocytes can be visualized using the lipophilic stain Nile red (Flynn et al., 2009; Greenspan et al., 1985). I performed Nile red staining in the surface and Pachón populations from 8 dpf to 12 dpf and observed that while surface fish begin adipogenesis at 11 or 12 dpf (Figure 2.3.1A), Pachón cavefish start developing adipocytes as early as 8 dpf (Figure 2.3.1A, B). Furthermore, at 12 dpf, the Pachón cavefish display significantly more adipocytes than the surface fish. I quantified this by measuring the area of fluorescent positive cells (median value: 1,03,527.13 μm^2 in Pachón vs. 6270.87 μm^2 in surface, $p<0.001$, Wilcoxon test) (Figure 2.3.1C). Next, I tested whether earlier adipogenesis is unique to Pachón cavefish or if it applies also to other cavefish populations. I found that the development of adipocyte dynamics in Tinaja larvae were very similar to that of surface fish (Figure 2.3.1A, B) and that the area of positive Nile red staining (i.e., visceral fat) is not different from surface fish (median value: 8973.77 μm^2 in Tinaja vs. 6270.87 μm^2 in surface fish, $p=0.2426$, Wilcoxon test) (Figure 2.3.1C). Remarkably, Molino cavefish do not develop visible adipocytes even as late as 12 dpf (Figure 2.3.1A). I noticed, however, some variability in the individual tested fish. To get a better understand of the variation between different fish, I repeated the experiment with 12 individual fish from Tinaja, Pachón and surface fish, which were born on the same day and

fed the same amount. I determined the onset of visceral fat development in each individual fish daily. Similarly, I found that at 8 dpf, five out of twelve Pachón cavefish developed visible adipocytes. However, surface fish and Tinaja cavefish reached this level only by 11 dpf.

To test whether Pachón cavefish develop their visceral adipocyte faster than surface fish, I monitored the area of visceral adipose tissue growth dynamics through Nile red staining. Based on the dynamics of adipose tissue area, I found that adipose tissue expansion was much faster in Pachón cavefish than surface fish (Figure 2.3.1D). There were more adipocytes in Pachón cavefish than surface at 10 dpf (Figure 2.3.1E). Therefore, Pachón cavefish can be ready to store fat at an earlier age than surface fish. This is an alternative mechanism for Pachón cavefish to survive in food scarcity environment. To sum up, Pachón cavefish develop their adipose tissue earlier and faster than surface fish and some other cavefish when they are fry.

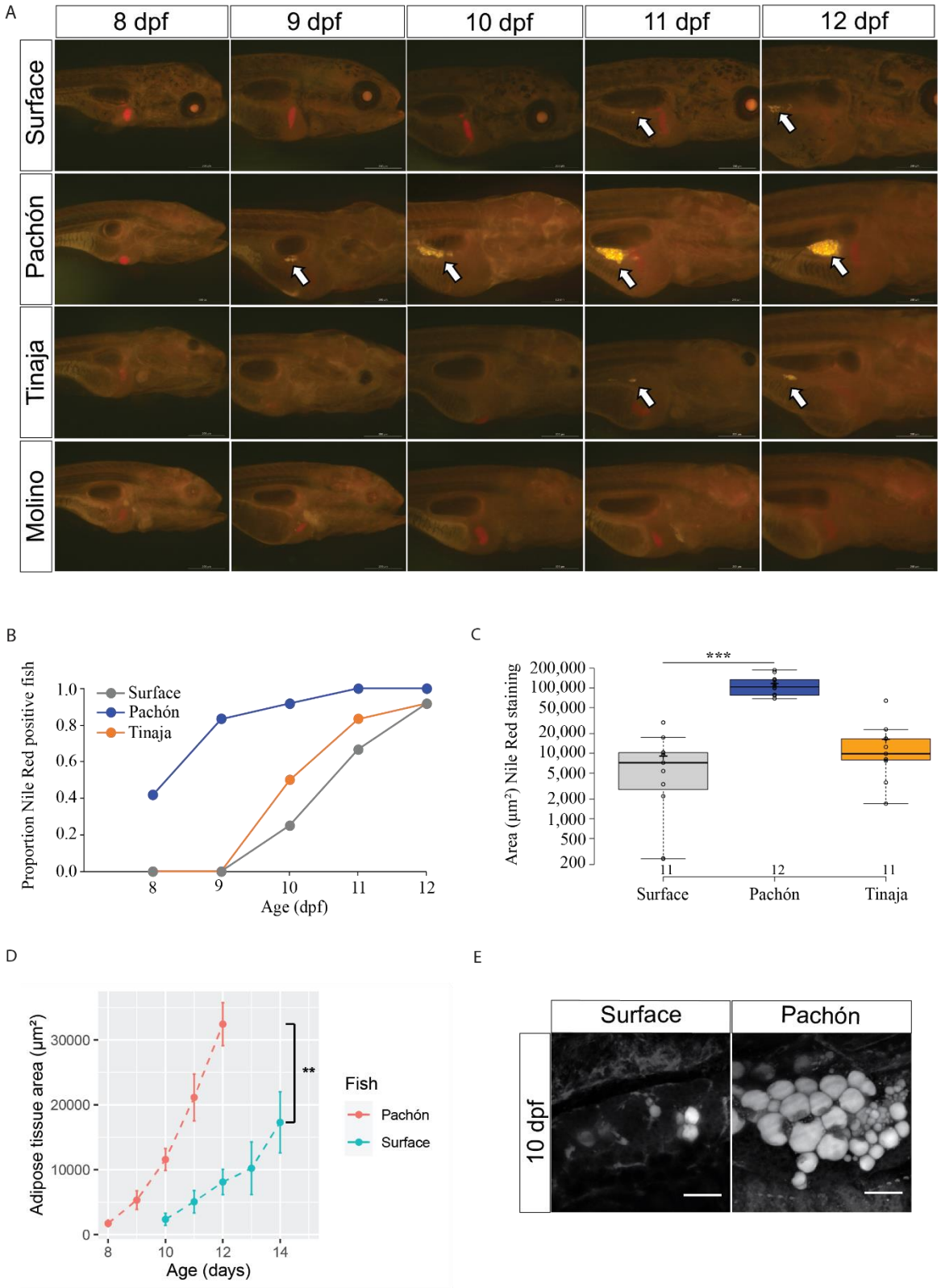

Figure 2.3.1. Early visceral adipocyte development in *A. mexicanus* populations.

A) Nile red staining of developing fry from indicated *A. mexicanus* populations at given developmental stages. Images were taken as described in Methods with an excitation of

470 nm and emission 525 nm. White arrows indicate cells positive for Nile red staining. B) Proportion of fish (total $n = 12$ for each population and timepoint) positive for Nile red staining for surface (grey line), Pachón (blue line) and Tinaja (orange line) populations at given developmental stages (dpf). C) Area of positive Nile red staining in μm^2 plotted on log-scale for surface (grey), Pachón (blue), and Tinaja (orange) populations at 12 dpf. Sample size for each population is indicated in plot. Positive Nile red staining was measured using Photoshop CC (Adobe, Version 19.1.0). Indicated significances are the results of Wilcoxon test, significant differences were shown as ** ($p < 0.01$) or ***($p < 0.001$) and n.s. indicating not significantly different from surface fish. Adipose tissue size change dynamics during 8-14 dpf for surface fish and Pachón cavefish. Significance was calculated with anova lm function. E) Adipose tissues examples of 10 dpf surface and Pachón cavefish. Scale bar in A) is 500 µm and in E) is 50 µm.

To understand if the early adipogenesis in the Pachón cavefish is influenced by growth or developmental differences of Pachón fish, I staged the development of the fish using standard body length (Figure 2.3.2A), the height at anterior anal fin (Figure 2.3.2B) and the flexion angle of the notochord (Figure 2.3.2C), the number of swim bladder lobes (Figure 2.3.2D) (Parichy et al., 2009). For all parameters Pachón developed slightly slower than surface fish, suggesting a potential tradeoff between growth and adipocyte development. To test to what extent this is true, I staged developmental parameters in Tinaja cavefish and found that the Tinaja population displays a similar developmental rate as Pachón but without the early adipogenesis phenotype (Figure 2.3.2). This indicates that slower growth is a general cave phenotype while early adipogenesis is specific to non-hyperphagic Pachón cavefish.

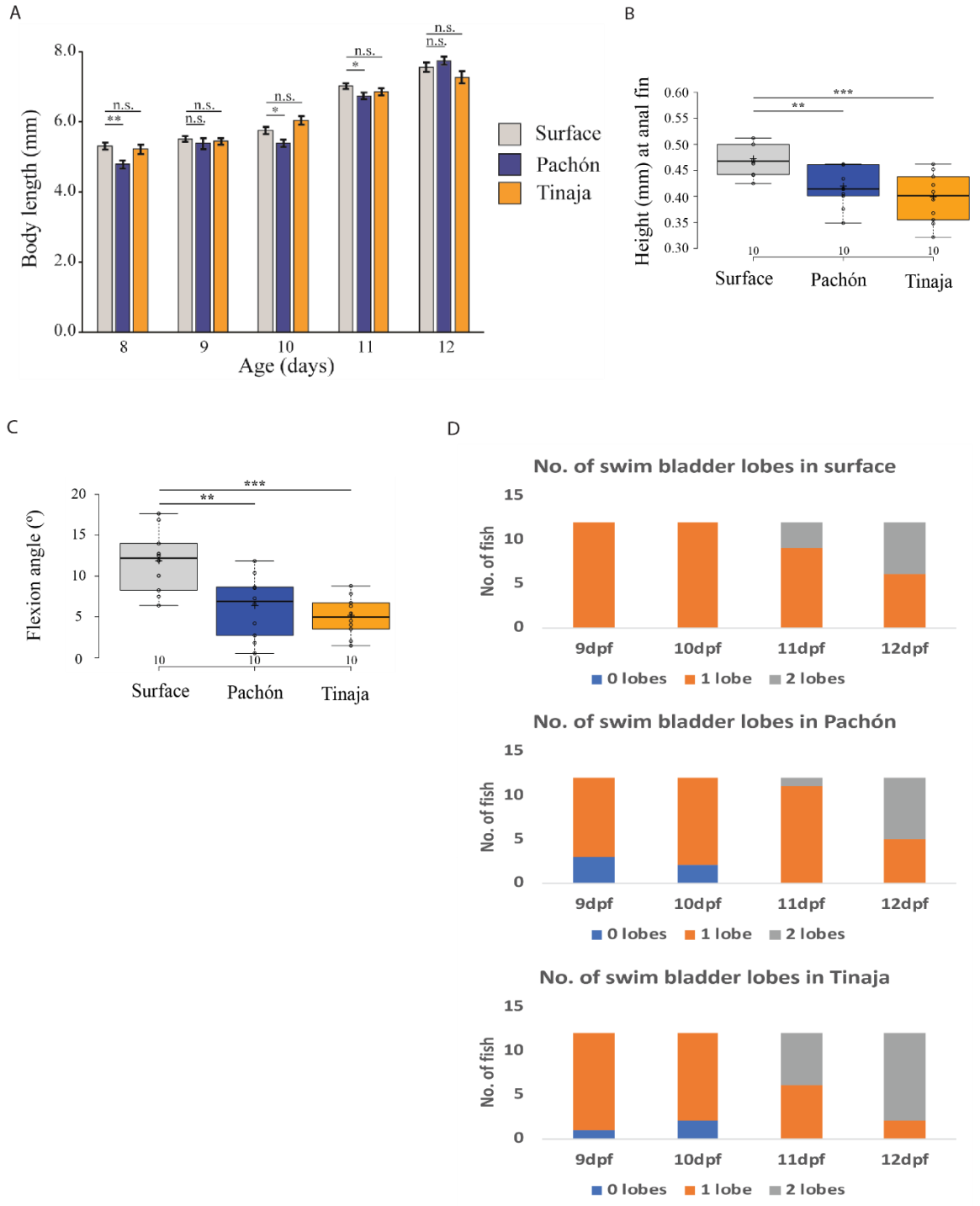

Figure 2.3.2 General developmental comparison between fish populations.

A) The standard body length comparison between surface fish, Pachón cavefish, and Tinaja cavefish at 8-12 dpf. B) Height at anterior anal fin (mm) at 12 dpf in three fish populations. C) Flexion angle of the notochord (°) at 12 dpf in three fish populations. D) The number of swim bladder lobes development dynamics between 9-12 dpf. Significant

differences were calculated with Wilcoxon test and shown as ** ($p \leqslant 0.01$) or ***($p \leqslant 0.001$) and n.s. indicating not significantly different from surface fish.

Another possible explanation for this could be that Pachón cavefish start feeding at an earlier timepoint than the other populations. To test the idea, I monitored food intake after feeding starts (i.e., at 6 dpf) and confirmed that both surface and Pachón populations start feeding within the first two hours of food being available (Figure 2.3.3A). To test the effect of light on adipocyte development, I raised surface fish and Pachón cavefish in complete darkness and quantified visceral fat development using Nile red. Pachón cavefish raised in the dark showed the same early adipogenesis phenotype as Pachón cavefish raised in the light (Figure. 2.3.3B). The onset of visceral adipocyte development is in line with the fat accumulation efficiency in the different A. mexicanus populations. To examine whether the difference in visceral adipocyte development persists into later developmental stages, I stained juvenile fish (32 dpf) with Nile red and detected considerably higher amounts of fat tissue at intermediate stages (Figure 2.3.3C). These results indicate that earlier adipogenesis could provide Pachón with an advantage to acquire fat faster and thus could be an additional mechanism, which facilitates increased fat accumulation in Pachón cavefish.

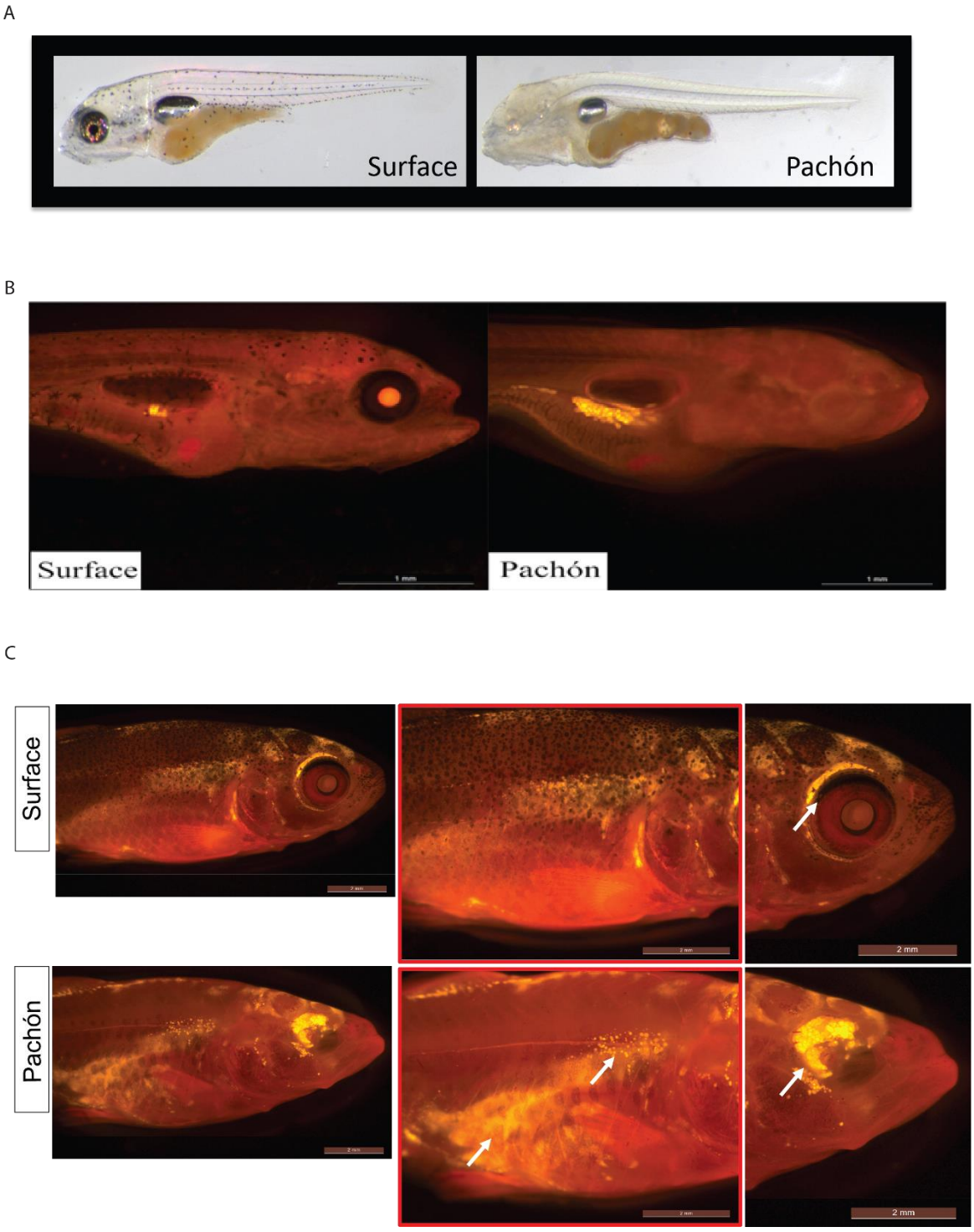

Figure 2.3.3 The effect of feeding time and light on adipogenesis.

A) Both surface fish and Pachón cavefish began eating food within 2 hours of food being provided to them on the sixth day post fertilization. The pictures show 6 dpf fish with artemia in their gut. B) Nile red staining of 12 dpf fish raised in the dark. Pachón accumulate visceral fat earlier than surface fish. C) Adipocytes distribution in Surface fish

and Pachón fish at 32 days post fertilization, indicating that the trend of excess fat in Pachón cavefish that starts as early as 8 dpf continues further into later developmental stages. Scale bar in B) is 1 mm and in C) is 2 mm.

2.3.4 The effect of feeding amount on adipogenesis

To explore the factors that affect this observed difference in adipogenesis between surface fish and Pachón cavefish, I tested the effect of feeding on adipogenesis in fish fry. Without feeding, both populations do not initiate adipogenesis at 9 dpf (Figure 2.4A, B). However, with 40 mg Artemia feeding, 23 out of 27 (85.19%) Pachón cavefish showed adipocyte development (Figure 2.4A, B), indicating that feeding is necessary for adipocyte formation. Meanwhile, 9 dpf surface fish still do not develop adipocytes under this feeding regime, which is consistent with the result in the last section (section 2.3.3). Then, I tested whether more Artemia feeding can accelerate adipogenesis by feeding 80 mg Artemia to both fish populations. Intriguingly, 6 out 22 (27.3%) surface fish began adipogenesis (Figure 2.4A, B) and all 27 Pachón cavefish had adipocytes at 9 dpf (Figure 2.4A, B). Furthermore, I measured the size of adipose tissue of these fish under different feeding regime and found that Pachón cavefish had bigger adipose tissue than surface fish under feeding (Figure 2.4C).

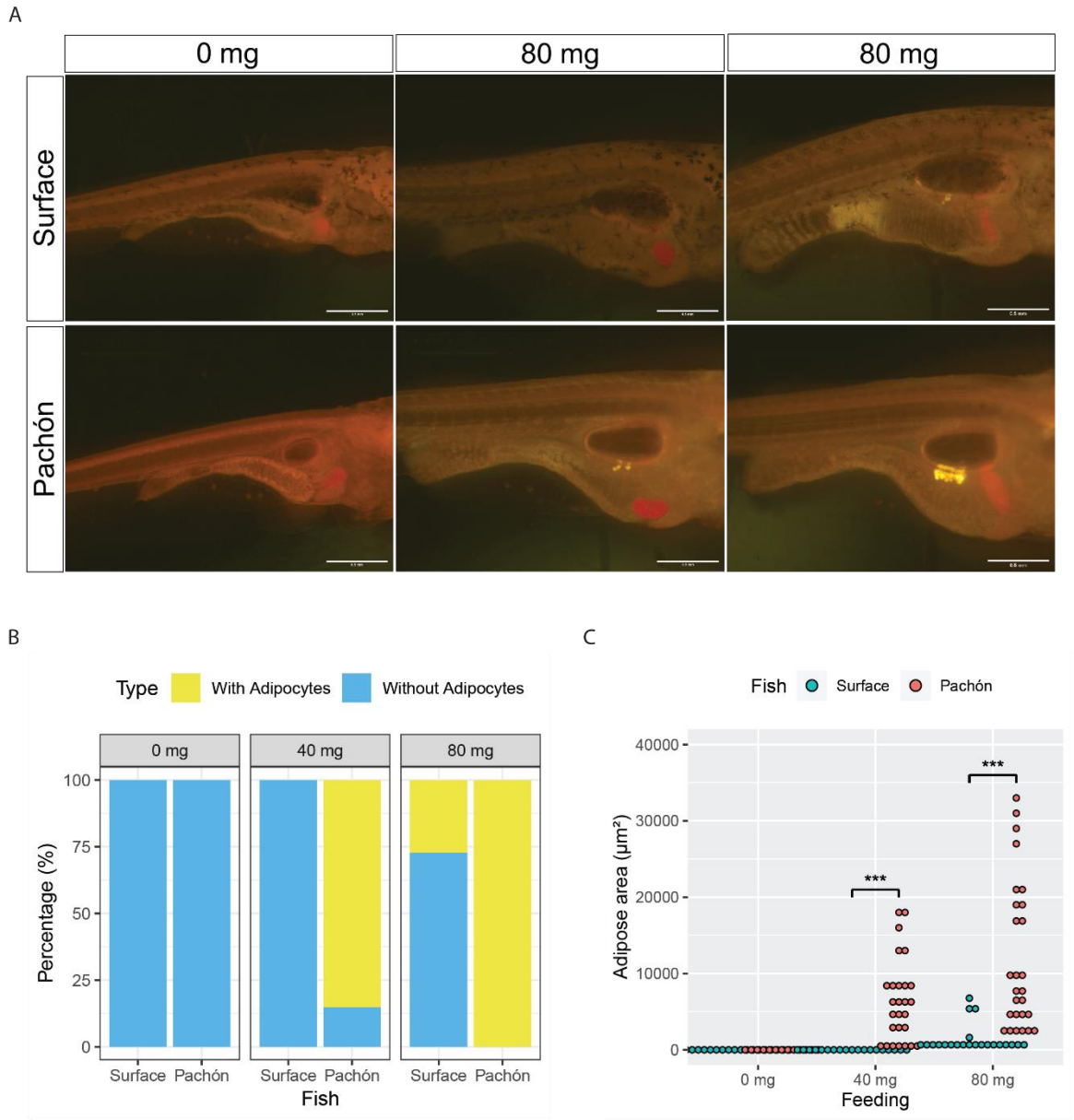

Figure 2.4 The effect of feeding amount on adipocyte development.

A) Nile red staining of adipocytes in surface fish and Pachón cavefish under different feeding conditions at 9 dpf. 40 mg and 80 mg indicate the wet weight of live artemia per feeding. The gold area under swim bladder marks adipose tissue. B) The percentage of fish with and without adipocyte development at 9 dpf under various feeding conditions. Yellow color shows the percentage of fish with adipocytes, blue indicates the percentage of fish without adipocytes. C) The size of adipose tissue comparison between surface and Pachón cavefish under different feeding conditions. Samples sizes were 18 surface fish and 13 Pachón cavefish for non-feeding groups; 19 surface fish and 27 Pachón cavefish for 40 mg

Artemia feeding groups; 22 surface fish and 27 Pachón cavefish for 80 mg Artemia feeding groups. Significant differences were calculated with Wilcoxon test and shown as ** ($p \leqslant 0.01$) or ***($p \leqslant 0.001$). Scale bar in A) is 500 µm.

2.3.5 The genetic architecture of adipogenesis in Astyanax

With similar appetite (Alie et al. 2018), Pachón cavefish larvae have similar development in general, but they have earlier and faster adipogenesis than surface fish. Therefore, these traits are genetically controlled.

To reveal the genetic basis of accelerated adipogenesis in Pachón cavefish, I performed multiple crosses and measured onset of adipogenesis and adipose tissue area in the resulting progenies. First, I interrogated the onset of adipogenesis in different fish populations at 9 dpf. I found that surface have not begun their adipogenesis and 23 out of 30 (77%) Pachón cavefish have adipocytes at 9 dpf. Moreover, 12 out of 28 (43%) F1, the first generation of hybrid between surface fish and Pachón cavefish, have developed adipocytes at 9 dpf, indicating the onset of adipogenesis is a dominant phenotype (Fig 2.5A). Meanwhile, 32 out of 136 (24%) F2, the progeny from a single pair F1, shown adipocytes. It implies the early onset of adipogenesis in Pachón cavefish is controlled by several genes instead of large number of genes. Moreover, it also indicates there is at least one dominant gene involved in controlling the onset of adipogenesis. Therefore, the early adipogenesis in Pachón cavefish is a promising trait to map.

Moreover, I also compared the distribution of fish adipose tissue area at 12 dpf. Most surface fish have small adipose tissue (median: 2860 μm^2) 12dpf (Fig 2.5 B), but Pachón cavefish have much bigger adipose tissue (median: 42700 μm^2) (Fig 2.5C). Meanwhile, F1 hybrid fish have intermediate size of adipose tissue (median: 18100 μm^2) (Fig 2.5D), indicating some dominant genes are contributing to adipose tissue expansion. However, F2 hybrid fish show similar adipose tissue area (median: 3230 μm^2) compared to surface fish and none of those F2 showed the similar adipose tissue size as the Pachón cavefish parent, indicating the area of adipose tissue is a polygenic trait (Fig 2.5E). It

would provide insights to reveal the genetic basis of earlier adipogenesis in Pachón cavefish compared to surface fish by using quantitative trait loci (QTL) analysis.

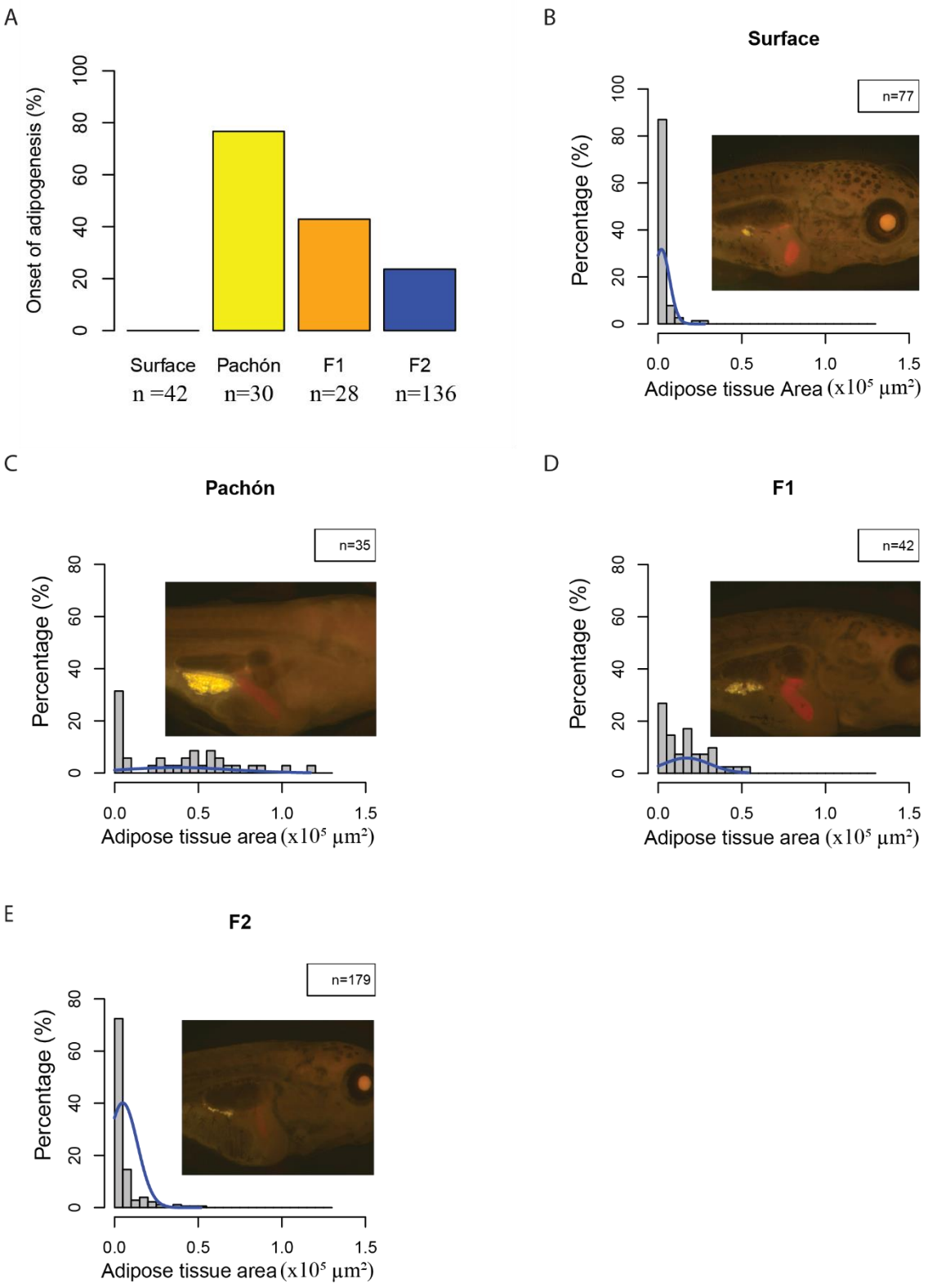

Figure 2.5 Genetic architecture of onset of adipogenesis and area of adipose tissue in Pachón cavefish.

A) At 9 dpf, no surface fish showed adipogenesis, but 77% of Pachón cavefish have already developed adipose tissue. 43% of F1 and 24% F2 hybrids showed onset of adipogenesis. Samples sizes are indicated in the panel. B) The distribution of adipose tissue area of surface fish at 12 dpf. C) The distribution of adipose tissue area of adipose tissue area of Pachón cavefish at 12 dpf. D) The distribution of adipose tissue area of adipose tissue area of Surface x Pachón F1 at 12 dpf. E) The distribution of adipose tissue area of adipose tissue area of Surface x Pachón F2 at 12 dpf. From B) to E), each image is a representative one for the fish population.

2.4 Discussion

To survive in the nutrient deprived cave environments, cavefish populations have evolved several strategies to save energy expenditure. One strategy in cavefish populations of *A. mexicanus* is to increase overall body fat level as energy reservoirs to deal with starvation periods (Hüppop, 2001). To my knowledge, no detailed regional analysis of the fat deposition has been performed in this species. In this study, I have focused on visceral adipose tissue (the fat tissue surrounding the visceral organs) owing to its importance in energy storage and its association with various medical pathologies (Shuster et al., 2012). While it is not a comprehensive analysis of visceral fat depots, the results show that cavefish acquire higher visceral fat depots when fed ad libitum or on a restricted diet in the laboratory mainly due to hypertrophy of the adipocytes in adults. However, Pachón cavefish also showed adipocyte hyperplasia when they are young compared to surface fish. Therefore, hypertrophy of the adipocytes substantially contributes to the overall increase in fat mass, Pachón cavefish also showed adipocyte hyperplasia. I also observed that Molino cavefish also display hypertrophy, though this increase in visceral fat is less pronounced than in Pachón and Tinaja, suggesting that the Molino populations rely on different strategies to acquire starvation resistance.

It has been shown that cavefish populations of Tinaja and Molino, but not Pachón, display hyperphagia presumably as a strategy to gain body fat (Aspiras et al., 2015). This hypothesis is in line with their food supply in these caves. Specifically, Tinaja and Molino caves receive substantial flooding during the rainy season as evidenced by large amount of debris throughout the cave and watermarks at the walls (Elliot, 2018). Under such circumstances, hyperphagia could serve as a strategy to binge eat when food is available to gain the necessary reserves for the following dry season. This is in contrast to the Pachón cave, which is located 120 m above local base level of the nearby river and as such is not

subjected to regular flooding events (Keene, 2015). Under these circumstances, an appetite-independent strategy may be more applicable. Hence, appetite-independent mechanisms should exist in Pachón cavefish to gain high body fat. Here, I show that both Pachón and Tinaja cavefish had higher visceral fat content after consuming the same amount of food as surface fish. It is likely because cavefish have lower energy requirements than surface fish. For example, cavefish save up to 15% of their energy simply by excluding the metabolic cost of making and maintaining eyes (Krishnan and Rohner, 2017; Moran et al., 2015). Also, cavefish do not have a fully functional circadian clock which allows them to save an additional 27% of energy (Moran et al., 2014). In addition to these physiological and behavioral changes, the Pachón cavefish populations display early developmental differences in their visceral fat development that could help them to gain the necessary fat depots faster. Interestingly, this developmental difference is not present in cavefish populations that display hyperphagia, such as Tinaja and Molino, suggesting this as an auxiliary mechanism in the absence of hyperphagia. While I controlled for differences in food consumption in the experiments, it is possible that the observed difference is due to a better usage of the food in the Pachón cavefish. In this respect, it is worth mentioning that a companion study provides evidence that the Pachón cavefish possess a more efficient digestive system which could allow them to extract more nutrition from their food (Riddle et al., 2018b) (See Table 1 for a summary of various metabolic phenotypes displayed by cavefish). This is in line with the observation that visceral fat development is food dependent. Taken together, I found accelerated adipogenesis in Pachón cavefish compared to other fish populations.

It is very interesting to find that Pachón cavefish has the unique capability to have earlier adipogenesis than surface fish. However, the underlying mechanism is still unknown. It would provide insights to study the following perspectives. First, studying the proliferation and differentiation of mesenchymal stem cells and adipocyte precursor cells

near the adipogenesis onset region would be insightful. It allows me to test whether Pachón cavefish have more adipocyte precursor cells or higher differentiation rate than surface fish. Second, using QTL-mapping to reveal the genetics basis of earlier adipogenesis in Pachón cavefish would be exciting. Given a single pair of surface fish and Pachón cavefish can easily generate hundreds of hybrid progenies and it is convenient to quantify traits about adipogenesis, it is feasible to collect F2 hybrids between surface fish and Pachón cavefish to do QTL-mapping. Third, it would be interesting to test whether Pachón cavefish have higher lipid absorption in the gut than surface fish. If it is true, it is worth to interrogate how the absorbed dietary lipids promote adipogenesis in Pachón cavefish. What lipid species can promote adipogenesis? How do the absorbed dietary lipids signal to the adipocyte precursor cells? How do the adipocyte precursor cells respond to the lipids? How does it initiate the precursor cell differentiation?

Table 1. Summary of various known metabolic phenotypes shown by Pachón, Tinaja and Molino cave populations.

Metabolic phenotype	Description	*Trait loci*	Pachón	Tinaja	Molino	Key references
Metabolic rate	Measured as a function of oxygen consumption	*Unknown*	Low metabolic rate	Not tested	Not tested	(Moran et al., 2015)
Insulin resistance	Measurement of phospho-AKT levels as a read out of insulin sensitivity	*INSRA P211L*	Yes	Yes	No	(Riddle et al., 2018a)
Hyperphagia	Measured as increased amount of food intake	*MC4R G145S*	No	Yes	Yes	(Aspiras et al., 2015)
Hyperglycemia	Increased blood glucose	*INSRA P211L*	Yes	Yes	Yes	(Riddle et al., 2018a)
Increased fat storage	Measurement of total triglyceride and visceral fat	*INSRA P211L,*	Yes	Yes	No	(Aspiras et al., 2015, Hüppop, 1988), Chapter II
		MC4R G145S				
Starvation resistance	Measured by loss of weight upon prolonged starvation	*MC4R G145S*	Yes	Yes	Yes	(Aspiras et al., 2015)
Circadian rhythm	Measurement of per1 and per2 gene expression in light and dark periods	*per1, per2*	Reduced rhythmicity	Not tested	Not tested	(Beale et al., 2013)
Churning motility in post-larval stomach	Pattern of food transit through the gut	*Unknown*	Increased churning	Not tested	Not tested	Riddle et al. (2018b)

Early adipogenesis	**Time of appearance of fat/adipose cells**	***Unknown***	**Yes**	**No**	**No**	**Chapter II**
Hypertrophic adipocytes	**Enlarged fat cells**	***Unknown***	**Yes**	**Yes**	**Yes**	**Chapter II**
Insulin resistance	**Measurement of phospho-AKT levels as a read out of insulin sensitivity**	***INSRA* P211L**	**Yes**	**Yes**	**No**	**(Riddle et al., 2018a)**

2.5 Limitations of study

Although this is the first study to carefully characterize and report accelerated adipogenesis in Pachón cavefish, this has provided a developmental mechanism for Pachón cavefish to gain high body fat. However, it has not revealed the underlying molecular mechanism for accelerated adipogenesis in Pachón cavefish. Given feeding is necessary for adipogenesis and high quantity food promotes adipocyte development, it is logical that macronutrient composition in the diet will play a role in adipogenesis. It will be intriguing to reveal the contributions of the different macronutrients and how they accelerate adipogenesis in Pachón cavefish compared to surface fish. Furthermore, it would be interesting to test whether there are some genetic factors which interact with those macronutrients.

2.6 Future directions

Since some studies have shown that dietary lipid promotes lipogenesis in Zebrafish (den Broeder et al., 2017), it is maybe similar in *Astyanax mexicanus* populations. It is important to investigate whether Pachón cavefish have higher lipid absorption efficiency than surface fish. Although Riddle et., al found that live food stayed in Pachón cavefish gut longer than surface fish and the digestive track of Pachón cavefish showed bi-directional churning motility in the stomach region (Riddle et al., 2018b), direct evidence that Pachón cavefish have higher nutrition absorption efficiency than surface fish is still lacking. Therefore, it would be interesting to interrogate whether fatty acid transporters have higher expression level in Pachón cavefish gut compared to surface fish. Additionally, it is also critical to test whether there are nonsynonymous mutations in the fatty acid transporters which make Pachón cavefish gut more efficient to absorb dietary lipids than surface fish.

Body fat of animals is also determined by genetic factors. Genome-wide association study (GWAS) in human populations showed that there are 77 significant loci associated with body fat percentage and 98 independent associations with body fat distribution (Hubel et al., 2019; Rask-Andersen et al., 2019). Although the results of GWAS are various because sample sizes of those studies were not identical, some genes are over-represented in association with obesity, including fat mass and obesity-associated protein (*fto*), *mc4r*, and transcription factor AP-2 beta (*tfap2b*) (Rask-Andersen et al., 2019; Riveros-McKay et al., 2019). It would be interesting to use GWAS or quantitative trait locus mapping (QTL-mapping) to pinpoint the loci for high body fat and accelerated adipogenesis in Pachón cavefish. Comparison between loci from fish and human might reveal whether different vertebrates use conserved or different strategies to accumulate high body fat.

Using scRNA-seq techniques, studies have identified cell types in mouse adipose tissue through their marker genes (Merrick et al., 2019; Schwalie et al., 2018). It maybe meaningful to examine the cell types of adipose tissue of 10 dpf using scRNA-seq to compare cell types and numbers between Pachón cavefish and surface fish. With this information, it will be possible to ask whether Pachón cavefish have more pre-adipocytes than surface fish or less adipogenesis-repressor cells. In addition, bromodeoxyuridine (BrdU) assays will reveal whether Pachón cavefish have faster cell division than surface fish. Together, testing these possibilities will provide insights into how Pachón cavefish have accelerated adipogenesis.

Chapter 3. Increased lipogenesis in the liver of Pachón cavefish

3.1 Introduction

Food availability can vary greatly throughout the year. To adapt to periods of dearth, most animals will store excess energy in the form of fat when food is available and utilize fat stores when food is lacking. Such fat gains can be impressive. Brown bears have been documented to gain up to 180 kg of weight, most of it as fat, in the few summer months before hibernation (Kingsley et al., 1983), and migrating birds can build up fat stores that make up 50% of their bodyweight before going on migration (Blem, 1976). Other extreme examples can be found in cave animals which rely on food chains that originate outside of the caves and are highly seasonal such as floods or bat droppings (Mitchell et al., 1977). One well studied example is the teleost species, *Astyanax mexicanus*. Previous studies have shown that cavefish populations of this species can gain substantially higher amounts of total body fat and visceral fat compared to the surface forms of the same species (Aspiras et al., 2015; Hüppop, 2001; Xiong et al., 2018). Some cavefish populations (e.g., Tinaja) achieve this fat gain through hyperphagia caused by nonsynonymous mutations in *mc4r* (Aspiras et al., 2015). Notably, the same mutations cause hyperphagia in humans as well (Aspiras et al., 2015). However, not all cavefish populations carry these mutations or display increased appetite. For example, cavefish from the Pachón population carry the wildtype allele of *mc4r* and display comparable appetites to surface fish (Alie et al., 2018; Aspiras et al., 2015). Several strategies have been proposed to explain how Pachón gain high body fat. Pachón develop visceral adipocytes earlier than surface fish (Xiong et al., 2018), their guts have shown to have higher digestion/absorption efficiency than surface fish (Riddle et al., 2018b), and Pachón skeletal muscles are insulin resistant which has been proposed to be an adaption to the

nutrient-limited environment (Riddle et al., 2018b). However, whether there are specific cellular changes to their lipid metabolism remains unknown.

Lipogenesis is the metabolic process of lipid synthesis. It includes fatty acid biosynthesis and triglyceride production (Kersten, 2001; Wang et al., 2015). Lipogenesis occurs mainly in the liver and adipose tissue (Numa and Yamashita, 1974). The synthesized triglycerides in the liver will be transported out of the liver by very low-density lipoprotein (VLDL) and stored in the adipose tissue (Fisher and Ginsberg, 2002; Yang et al., 1996). To understand whether lipogenesis is altered in cavefish, I studied the cellular mechanisms of fat accumulation in *Astyanax mexicanus*. I found that Pachón cavefish display a massive upregulation of lipogenesis gene expression in the liver after feeding (up to 100-fold), compared to surface fish. I found that this is accompanied by an upregulation of a master regulator of triglyceride synthesis, the nuclear receptor and transcription factor Pparγ. Moreover, I found increased levels of activators of Pparγ and identified nonsense mutations in a direct repressor of Pparγ in independently derived cavefish populations, supporting the notion that higher activity of lipogenesis through Pparγ underlies the increased adipogenesis in cavefish.

3.2 Material and methods

3.2.1 Experimental animals

All fish populations were housed in the lab as previously described (see section 2.2.1).

3.2.2 Total body fat measurement

Each fish populations (Surface fish, Pachón cavefish, and Tinaja cavefish), I used 5 one-year-old female fish with similar size. I euthanized the fish with 500 mg/mL MS-222. Given the ovary is a lipid-rich organ and I was only interested in the body fat of the fish, I dissected the ovary out. Then I used the remained fish body to measure the body fat composition. The EchoMRI™ analyzer was used to quantify fish body composition. EchoMRI™ machine employs a nuclear magnetic resonance method for measuring the masses of fat, lean tissues, and water in tissues and organisms (Kovner et al., 2010). Replicates were measured and averaged as the readout for each sample. Fat mass normalized to total body weight was indicated as body fat content.

3.2.3 H & E staining

The method was the same as 2.2.3. Briefly, each fish populations (Surface fish, Pachón cavefish, and Tinaja cavefish), I used 5 one-year-old female fish with similar size. I euthanized the fish with 500 mg/mL MS-222 and dissect the head and trunk of those fish samples individually. The head sample included the fish from snout to the end of operculum. The trunk was the body region from the beginning of the annal fin to 0.5 cm

after that line. Then, I fixed them in 4% paraformaldehyde (pfa) at 4 ℃ for 24 hours for fish trunk and 48 hours for fish head respectively. After sample fixation, Histology core facility help me do the tissue sectioning and H & E staining with fish head and trunk. Then, I used a VS120 virtual slide microscope (Olympus) to image the slides and analyzed with ImageJ. For fish head, representative area in the eye orbit with complete cell membrane was outlined and enlarged to be visualized. For fish trunk, the area of fat (white area) and total trunk section area (whole section) were measured respectively. Then, the relative fat area is defined as area of fat normalized to total trunk section area.

3.2.4 Total lipid content quantification

The Folch method (Flynn et al. 2009) was used to measure lipid content. In brief, I determined dry weight by drying tissue at 60 °C for 48 hours in 5 mL Eppendorf tubes (pre-weighted: W0), then measured the total weight of dried tissue and tube: W1, and calculated tissue dry weight: W1-W0. The whole tissue/organ was then homogenized with homogenizer (Benchmark Scientific, D1036) into powder, 1 mL chloroform and methanol mixed solution (2:1 = v/v) was added, then samples were washed with 200 μL 0.9% NaCl. Homogenates were vortexed and centrifuged at 2,000 x g for 30 min. The lower layer (containing liquid) was transferred to pre-weighted aluminum weigh dish (VWR, 25433-016). The liquid was dried in the hood completely (over 12h). Then, the mass of aluminum weigh dish containing lipids were determined using a Mettler Toledo (XS105 Dual range) balance. I calculated total lipid content of a tissue using following formula: Total lipid content = total lipids (mg) / tissue dry weight (mg) * 100%. Each fish populations, I used 5 one-year-old female fish with similar size.

3.2.5 Nile red staining

For adult fish head Nile red staining: the fish heads were dissected and washed in PBS three times to get rid of the blood. Then the heads were immersed in 1 μg/mL Nile red working solution at 4 degree for 7 days. The stained samples were washed with PBS and were ready for imaging. For fish larvae Nile red staining: the fish larvae were washed with PBS and immersed in 1 μg/mL Nile red working solution at room temperature for 30 mins. The stained larvae were washed with PBS and euthanized with 500 mg/L MS-222 before imaging. Images were obtained using a M205 C (Leica) microscope with an DFC7000 T (Leica) camera under GFP channel and analyzed with ImageJ. Briefly, wand tool in ImageJ was used to define the edge of adipose tissue and the area was measured using "Measure" under the "Analyze" menu.

3.2.6 RNA-seq analysis

I used four-month-old fish for this experiment because at this stage the livers are big enough to be dissected for ribonucleic acid (RNA) harvest and the fish are not sexually mature, which can affect lipid metabolism heavily. Fish were housed individually for the experiment. Each fish was fed 10mg Gemma twice per day for at least one week to allow the fish acclimate to the new environment. Once the fish were used to the new feeding regime, they were all fasted after one feeding (10mg Gemma per fish) for 4 days. These fish were termed as the fasted group. Half of the fish (3 surface and 3 Pachón cavefish) were refed 10mg Gemma after 4 days fasting and were termed the refed group. Fasted fish and refed fish (3 hour after feeding) were dissected quickly. Liver samples were collected, rinsed with cold PBS, and snap-frozen in liquid nitrogen. Total RNA was extracted using Trizol reagent (Ambion). Then library construction and sequencing were done by

molecular biology facility. Libraries were prepared according to manufacturer's instructions using the TruSeq Stranded mRNA Prep Kit (Illumina). The resulting libraries were purified using the Agencourt AMPure XP system (Beckman Coulter) then quantified using a Bioanalyzer (Agilent Technologies) and a Qubit fluorometer (Life Technologies). Libraries were re-quantified, normalized, pooled and sequenced on an Illumina HiSeq 2500 using v4 High Output chemistry, single read 50bp, RTA v1.18.64, and bcl2fastq2 v2.20 for demultiplexing and FASTQ file generation. The bioinformatics analyses were done by computational biology core. Both surface fish and Pachón cavefish reads were aligned to surface fish genome (Astyanax_mexicanus-2.0) via STAR aligner (v2.6.1c), under Ensembl 91 gene model. TPM gene expression values were generated using RSEM (v1.3.0). Pairwise differential expression analysis was performed using R package edgeR for different fish under different conditions. GO term enrichments were done based on upregulated DE genes in refed Pachón cavefish using Metascape (Zhou et al., 2019).

3.2.7 RT-qPCR

To confirm expression pattern of genes involved in lipogenesis, I did reverse transcription quantitative polymerase chain reaction (RT-qPCR). The complementary deoxyribonucleic acid (cDNA) was made from 1 μg total RNA (from previous step) with high-capacity RNA-to-cDNA kit (applied biosystems, 4387406) and treated with DNase. (Promega, M6101) Then, qPCR was conducted on a QuantStudio 6 Flex Real-Time PCR System with SYBR green detection. (Quantabio, 101414-288)). Amplification specificity for each real-time PCR reaction was confirmed by analysis of the dissociation curves. Determined C_t values were then exploited for further analysis, with the *rpl13a* gene as the reference. Each sample measurement was made in triplicate. Primer sequences for

acaca were acaca_F 5'- CGCAGTGCCCATCTACGTG -3' and acaca_R 5'- TGTTTGGGTCGCAGACAGC -3'. For *aclya*, the primer sequences were aclya_F 5'- GGGCACCACAGTTTTTCCAA -3' and aclya_R 5'- CTGTCCGTGTGCCTGACTGA -3'. For *fasn*, the primer sequences were fasn_F 5'- GGGCACCACAGTTTTTCCAA -3' and fasn_R 5'- CTGTCCGTGTGCCTGACTGA -3'. For *rpl13a*, primers were rpl13a_F 5'- GTTGGCATCAACGGATTTGG -3' and rpl13a_R 5'- CCAGGTCAATGAAGGGGTCA -3'.

3.2.8 Antibody generation

The protein sequence of Pparγ was used to blast against Astyanax genomes (Astyana_mexicanus-1.0.2 and Astyanax_mexicanus-2.0) to evaluate the peptide similarity of Pparγ and other proteins in the genomes. I chose 227-564aa of Pparγ as antigen for its relatively high specificity. This 338aa protein fragment was then expressed in Escherichia coli and used to immunize two rabbits for antibody production by GeneScript. ELISA titer > 1:128,000 and target protein fragment binding validation by western blot and cell line overexpression.

3.2.9 Western blot

For western blot, I used four-months-old juvenile fish. The feeding regime was the same as those fish for RNA-seq. Fish liver samples were dissected quickly, rinsed with cold PBS, and snap-frozen in liquid nitrogen. Western blotting was performed using standard protocols. Briefly, liver tissues were lysed in radioimmunoprecipitation assay buffer (RIPA buffer) and total protein concentrations were determined by MicroBCA protein assay kit (Thermo Scientific, 23235) according to the manufacturer's instructions

and infinite 200 PRO microplate reader (Tecan). For each sample, 10 ug total protein were loaded to each well to run SDS-PAGE gel, protein transfer from gel to polyvinylidene fluoride (pvdf) membrane, blocking, and antibody incubation. Imaging was carried out with Odyssey CLx system (LI-COR). The band intensity was calculated with FIJI.

3.2.10 HEK293T cell line overexpression

The surface fish and Pachón cavefish *pparγ* coding regions were cloned from cDNA, then they were inserted into pDestTol2 vector under the control of the hsp70 promoter (from zebrafish) respectively. 7.5 μg FuGene (E2311) and 2.5 μg plasmid were transfected into HEK293T cells on glass bottom microwell plates (MetTek, P35G-1.5-14-C). 24 hours later, 41 °C heat shock for 1 hour was performed. 48 hours after transfection, cells were fixed with 4% pfa for 20 min at room temperature (RT). Cells were permeabilized with PBST (0.1% Triton X-100) for 30 minutes at RT. Blocking was performed with Universal Blocking Reagent (BioGenex, HK085-5K) for 1 hour at RT. A series of anti-Pparγ antibody dilutions were used to incubate cells for 2 hours at RT. After PBST (0.1% Triton X-100) wash, cells were incubated with Alexa Fluor® 568 goat anti-rabbit (Invitrogen, A-11011) and DAPI (Sigma-Aldrich, D9542) for 1 hour at RT. After PBS wash, cells were imaged with Axiovert 200M microscope. The representative images in the figures were those samples treated with the appropriate anti-Pparγ antibody dilution.

3.2.11 Immunofluorescence staining

Liver tissues were fixed with 4% pfa for 16 hours at 4 ℃. Then liver sections (10 μm) were done through cryostat sectioning. Slides were treated with phosphate-buffered saline (PBS) to get rid of optimal cutting temperature compound (OTC compound) and

permeabilized with 0.1% phosphate-buffered saline Triton (PBST) for 45 min. Blocking was performed at room temperature for 1 hour. Samples were treated with TrueBlack® Lipofuscin Autofluorescence Quencher (Biotium, 23007) before addition of primary antibody. Then, primary antibody incubation was carried out at 4 °C overnight. Secondary antibodies and DAPI (Sigma-Aldrich, D9542) incubation were done at room temperature for 3 hours. The antibodies in this study include anti-Pparγ (see antibody generation), anti-E-Cadherin (BD Transduction Laboratories, 610182), goat anti-rabbit (Invitrogen, A32733), and donkey anti-mouse (Invitrogen, A31570). Images were taken with Leica TCS SP8 X microscope and analyzed with ImageJ.

3.2.12 Pparγ ChIP-seq

Livers from eight juvenile fish (4-month-old) were pooled together and snap frozen. Then the frozen tissues were grinded into powder, followed by 1% pfa (diluted from 16% pfa, Thermo Fisher, PI28906) fixation for 10 min at room temperature. The cross link was quenched with 0.125 M glycine. Chromatin shearing was performed by using a Bioruptor sonication system with following parameters: 30 seconds on and 30 seconds off per cycle, 10 cycles in total. DNA fragments were collected and purified with MAGnify™ Chromatin Immunoprecipitation System (ThermoFisher, 492024) according to the kit instruction. Purified DNA (~10 ng) for each sample was taken as input to construct the library. Libraries were prepared by molecular biology core. They used the KAPA HTP Library Prep Kit (Roche, Cat No. KK8234) with 15 cycles of PCR and used 1:125 dilution of NEXTflex DNA barcodes (Perkin Elmer, Cat No. NOVA-514104) to construct libraries. The resulting libraries were purified using the Agencourt AMPure XP system (Beckman Coulter) then quantified using a Bioanalyzer (Agilent Technologies) and a Qubit fluorometer (Life Technologies). Post amplification size selection was performed

on all libraries using a PippinHT (Sage Science). High throughput sequencing was performed on the Illumina NextSeq platform. Then, computation biology core helped me do the bioinformatics analysis. Both surface fish and Pachón cavefish reads were aligned to surface fish genome (Astyanax_mexicanus-2.0). Genome browser track files in bigwig format were generated using R (version 4.0.0) packages GenomicRanges (version 1.40) (Lawrence et al., 2013) and rtracklayer (version 1.48) (Lawrence et al., 2009). Signals were normalized to reads per million (RPM). Peaks were called using MACS2 (version 2.1.2) (Zhang et al., 2008) for individual and merged replicates, respectively (q-value cutoff of 0.01). Next, IDR (https://github.com/nboley/idr, version 2.0.4.2) was used to keep those peaks that occurred consistently in both replicates. I further filtered peaks using fold enrichment and q-value cutoffs at summit position (fold enrichment ≥ 5 and q-value ≤ 1E-20). I took the summit position of the filtered peaks and used R package ChIPseeker (version 1.24.0) (Yu et al., 2015) to annotate the peaks to genomic features, including promoters (± 3 Kb from transcription start site, TSS), exons, introns, downstream (within 3 Kb downstream of transcription end site), and distal intergenic regions. Astyanax genome annotation was obtained from Ensembl 98 (Yates et al., 2020). I combined and merged filtered peaks for Pachón and surface using bedtools (version 2.29) (Quinlan and Hall, 2010). For each merged peak, the new summit was assigned as the median of all overlapping peaks. Then the merged peaks were resized to 401 bp by extending 200 bp upstream and downstream of the new summits. The resized peaks were treated as the meta-peak list. I used FIMO (version 5.3.0) (Grant et al., 2011) to scan the occurrences (p-value cutoff : 1e-5) of mouse Pparγ motifs (MA0065.2 in JASPAR 2020 database (Fornes et al., 2020) in 10351 meta-peaks falling into promoter regions (defined as ±3 Kb from transcription start site). To test motif enrichment, I randomly placed these meta-peaks in the promoter regions of all protein coding genes and performed FIMO scan using the same parameters. This shuffle process was repeated 1000 times.

3.2.13 Pparγ inhibitor treatment

The 5dpf fish larvae of surface fish and Pachón cavefish were placed in a plastic cup with a mesh on the bottom (hole size=200 μm), then the cup with fish was placed in 3L tank. Fish larvae were fed with 40 mg Artemia twice per day (morning feeding and afternoon feeding) from 5dpf to 10dpf. In the afternoon, the fish larvae were treated with 0.2% DMSO (Corning, 25-950-CQC) or 40 μM GW-9662 (Enzy life sciences, BML-GR234-0050) for 3 hours each day. Then the fish larvae with cup were transferred back to 3L tank with fresh water. When the larvae were 11dpf, we only fed them in the moring, collected the larvae at noon, performed Nile red staining, euthanized larvae, and imaged them using a M205 C (Leica) microscope with an DFC7000 T (Leica) camera under GFP channel and analyzed with ImageJ. Briefly, wand tool in ImageJ was used to define the edge of adipose tissue and the area was measured using "Measure" under the "Analyze" menu.

3.2.14 Gene per2 genotyping

The cDNA was generated with the same method as 3.2.7 for all four fish populations (surface, Pachón, Tinaja, and Molino). Then the following primers and thermocycling conditions were used to amplify fragments of *per2* gene for each fish populations.

Primers used to capture alternative splicing in Pachón and Tinaja (5'-3'):

Forward: CATCACTGTGACGCTCTCTCATCATCCAG

Reverse: CTCAACCAGGGATGAACCTCAGCC

PCR conditions: Denaturing 95 ℃, 30 sec - Annealing 57 ℃, 30 sec - Extension 72 ℃, 45 sec, 35 cycles

Primers used for Molino genomic DNA confirmation of 7bp duplication (5'-3'):

Forward: CTAGGCAGTAATGATCACCTGATGAG

Reverse: GACTTGCCTGGAGCCTTTCTGGTC

PCR conditions: Denaturing 95 ℃, 30 sec - Annealing 56 ℃, 30 sec - Extension 72 ℃, 60 sec, 35 cycles

3.3 Results

3.3.1 Cavefish display increased body fat levels throughout the body

Previous studies have shown that cavefish populations, compared to surface fish, display higher total triglycerides and visceral fat when fed ad libitum (Aspiras et al., 2015; Hüppop, 2001; Xiong et al., 2018). To confirm these findings and more easily quantify total body fat in fish, I used EchoMRI to quantify body fat percentage. Consistent with previous total triglycerides measurements (Aspiras et al., 2015), fish from both the Pachón and Tinaja populations showed higher body fat than surface fish (Figure 3.1.1A). To better visualize fat distribution throughout the body, I dissected adult fish into various sections and used Hematoxylin and Eosin (H&E) staining of head and trunk of adult fish. I observed that Tinaja and Pachón cavefish store fat in the entire eye socket (Figure 3.1.1B) and have markedly more adipocytes in the ventral part and lateral sides of the trunk than surface fish (Figure 3.1.1C). In the dorsal part of the trunk, I observed only slightly more adipocytes in cavefish compared to surface fish (Figure 3.1.1C). In total, the relative adipose area in the transverse trunk section of cavefish was significantly higher than that of surface fish (Figure 3.1.1D). Additionally, I extracted total lipids using Folch method to quantify lipid content (Folch et al., 1957) from head and dorsal and ventral parts of the trunk (Figure 3.1.1E). I found Tinaja and Pachón cavefish had higher lipid content in the head, in the dorsal trunk section and ventral trunk sections compared to surface fish (Figure 3.1.1E).

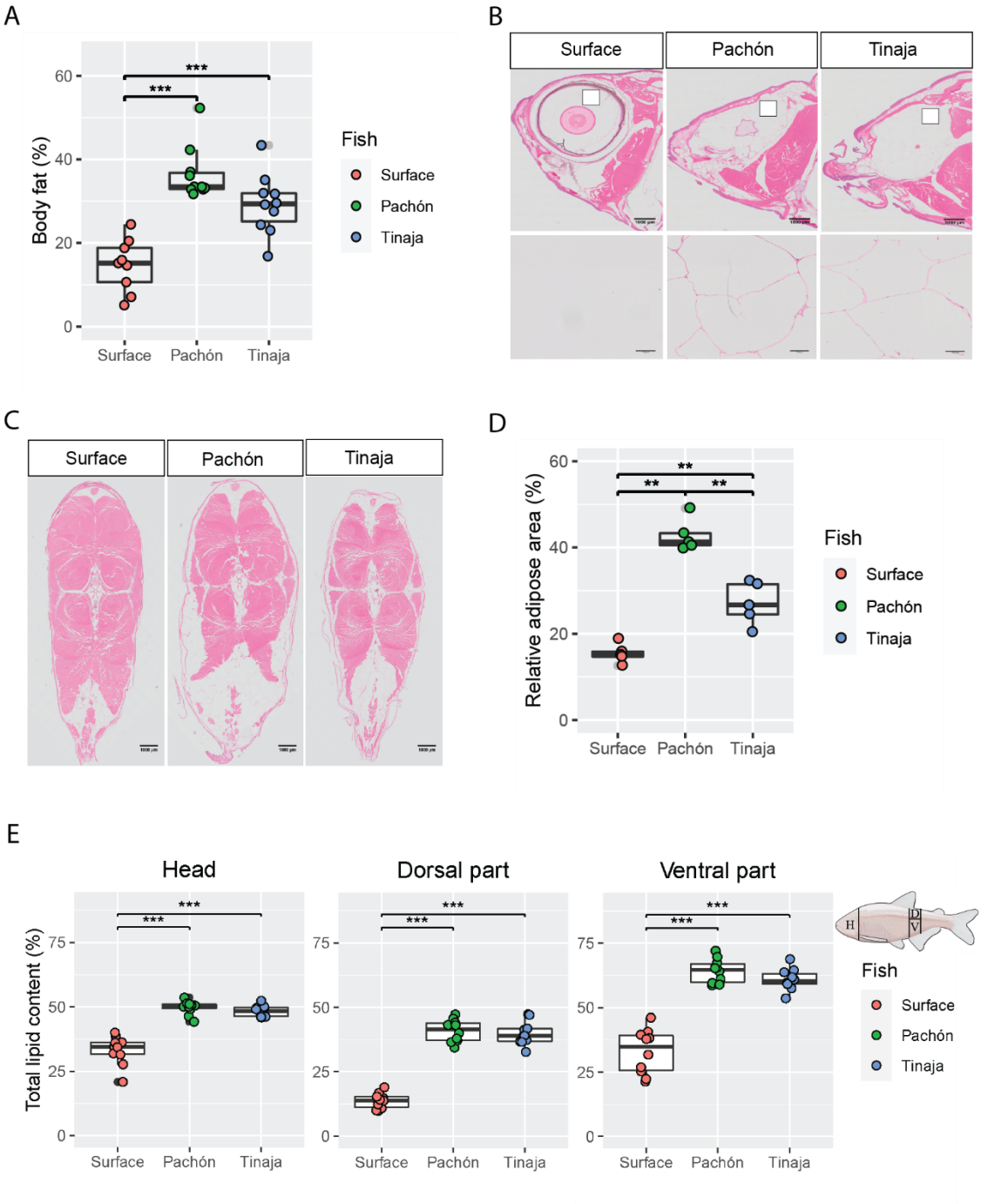

Figure 3.1.1. Cavefish display more body fat in various areas of the body compared to surface fish.

A) Total body fat comparison (fat mass/total body weight) between surface fish, Pachón, and Tinaja cavefish using EchoMRI (n=9,10,10 respectivelhy). B) H&E staining of fish head sections of the three fish populations. The sagittal sections were performed across the

eye area of the head, the upper panel showing the entire section and the lower panel showing the region indicated with a white box in the upper panel, revealing that in cavefish the eye socket is filled with adipocytes. (n=5 per population, scale bar =1000 μm in the upper panel, scale bar=100 μm in the bottom panel). C) H&E staining of fish trunk sections close to the anal fin of the three fish populations (n=5 per population, scale bar =1000 μm). D) Quantification of fat area to the whole section area in surface fish, Pachón, and Tinaja cavefish using "Convert to Mask" in ImageJ. (n=5 per population). E) Cartoon highlighting sampling areas for total lipid content quantification. (H = head, D = dorsal part, V = ventral part, black lines indicate the boundaries of sampling). Total lipid content (%) in surface fish, Pachón, and Tinaja cavefish (n=10 per population) using the Folch method. Significances calculated with Wilcoxon test, **p <0.01.

Given the liver is also an important organ for lipid metabolism and hepatic fat accumulation indicates the healthy state of organisms, I aimed to test whether there is any difference in hepatic fat amount between different fish populations. However, I found there is no obvious difference in hepatic triglyceride and total liver lipid between adult surface fish and cavefish populations (Figure 3.1.2), indicating cavefish did not over accumulate lipid in the liver of one year old fish on the lab feeding regime.

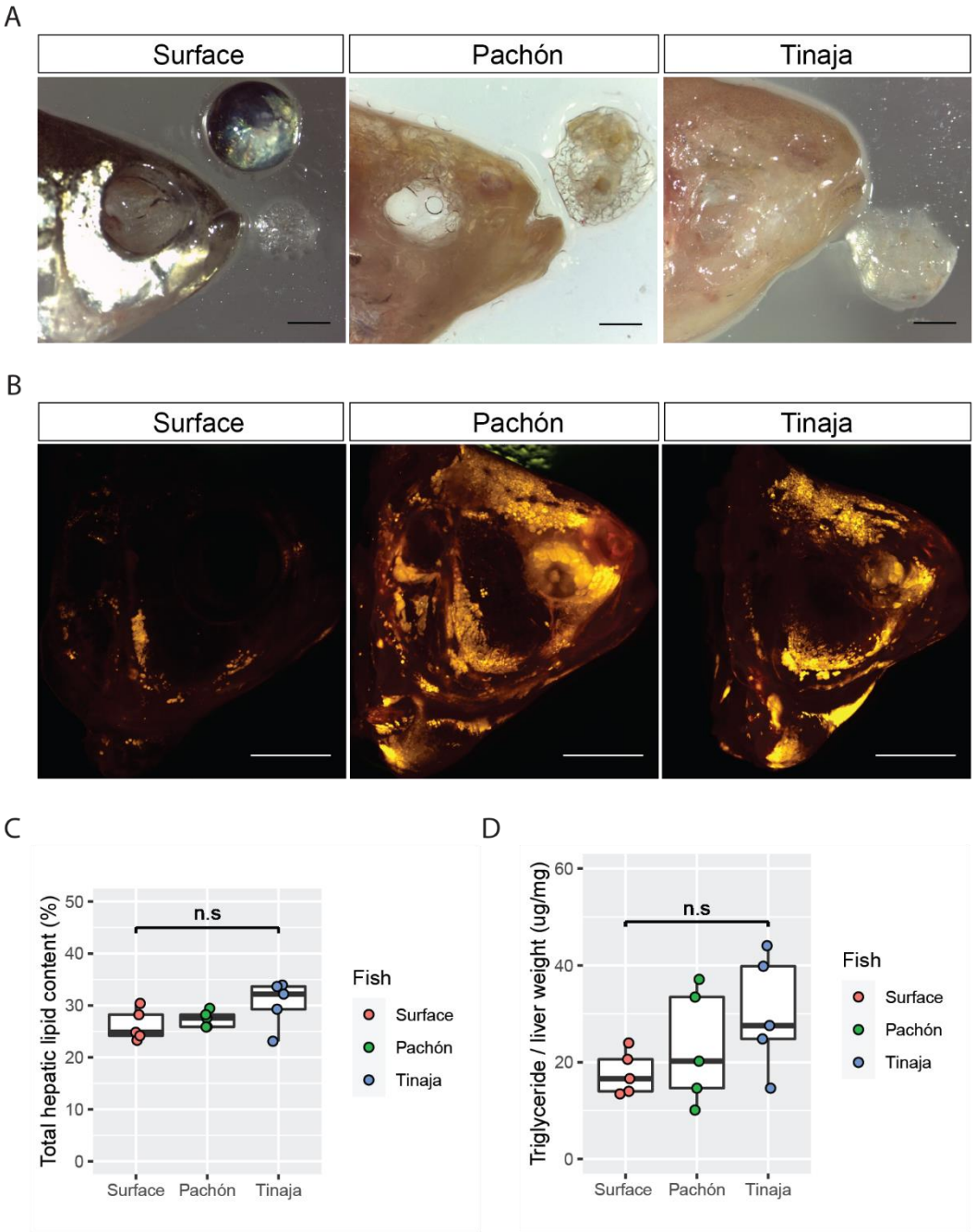

Figure 3.1.2. Fat comparison between surface fish and cavefish.

A) Fat comparison between surface fish and cavefish (scale bar=2 mm). B) Nile red staining of adult fish head, the golden-yellow area indicates lipid distribution in the fish head (scale bar=2 mm). C)Total lipid content (total lipid normalized to dried tissue weight) in the liver of surface fish and cavefish populations. D) Hepatic triglyceride (hepatic triglyceride normalized to fresh liver weight) comparison between surface fish and

cavefish populations (n=5 per population). Wilcoxon test was used to determine p value and n.s indicates not significant ($p>0.05$).

3.3.2 Cavefish had higher lipogenesis in the liver than surface fish

Given the dramatical differences in body fat content between cavefish and surface fish populations throughout different tissue parts, I hypothesized that cavefish display higher postprandial lipid anabolism than surface fish. This should be particularly pronounced in Pachón cavefish as they are known to have similar appetites as surface fish (Alie et al., 2018; Aspiras et al., 2015). To study the transcriptional response to feeding, I first fasted juvenile Pachón cavefish and surface fish for 4 days to allow lipid anabolism to reduce to similar base level. Then I refed the different morphs the same amount of food (10 mg Gemma) and performed bulk RNA-seq of the livers of fish from both the fasted and the refed conditions (Figure 3.2.1A). I identified around 16,000 genes (Transcripts Per Kilobase Million (TPM) > 1) to be expressed, of which ~2300 were differentially expressed (DE) between the refed Pachón and surface fish samples (Figure 3.2.1B, C).

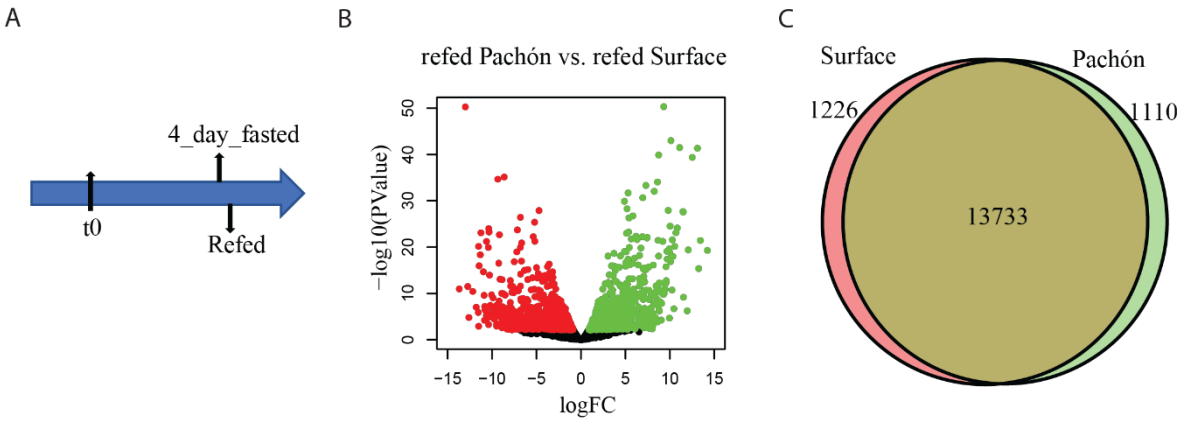

Figure 3.2.1. Transcriptome comparison between refed surface and refed Pachón cavefish liver samples.

A) Scheme of the experimental design for the RNA-seq analysis of Pachón and surface fish (n=3 per population and condition). B) Volcano plot shows the transcriptome profile comparison between refed surface and refed Pachón cavefish. Each dot indicates one transcript. The red and green dots show the down-regulated and up-regulated transcripts in refed Pachón cavefish compared to surface fish respectively. Black dots represent transcripts with similar expression level between the two fish populations. B) Venn diagram of the transcript number comparison between refed surface and refed Pachón cavefish. From left to right: down-regulated, unchanged, and up-regulated transcripts in refed Pachón cavefish compared to surface fish respectively.

I performed GO-term enrichment analysis of the DE genes and identified a number of metabolic pathways, including carbon metabolism, pyruvate metabolism, lipid metabolism, to be overrepresented in the cavefish samples (Figure 3.2.2A). Specifically, fatty acid biosynthesis and triglyceride biosynthesis, which directly contribute to body fat accumulation, are also enriched in the cavefish samples (Figure 3.2.2A). To further dissect these pathways, I focused on key genes of these pathways (i.e., *aclya, acaca, fasn, scd, elovl6, gpam, dgat1b, dgat2, lpin1, acsl4a, oxsm, olah*) (Figure 3.2.2B). Interestingly, these genes showed similar expression level at the fasted state between surface fish and Pachón cavefish, but much higher expression levels in refed Pachón cavefish compared to refed surface fish (Figure 3.2.2B). These results point towards an enhanced ability to perform lipogenesis in cavefish after feeding. I confirmed these results by focusing on three key fatty acid biosynthesis genes (ATP citrate lyase (*acly*), acetyl-CoA carboxylase 1 (*acaca*), and fatty acid synthase (*fasn*)) using qRT-PCR. All three genes did respond to feeding by 10 to 1000-fold increase of expression in Pachón cavefish compared to surface fish (Figure 3.2.2C), suggesting that Pachón cavefish have a much higher ability to synthesize fatty acids after feeding than surface fish do.

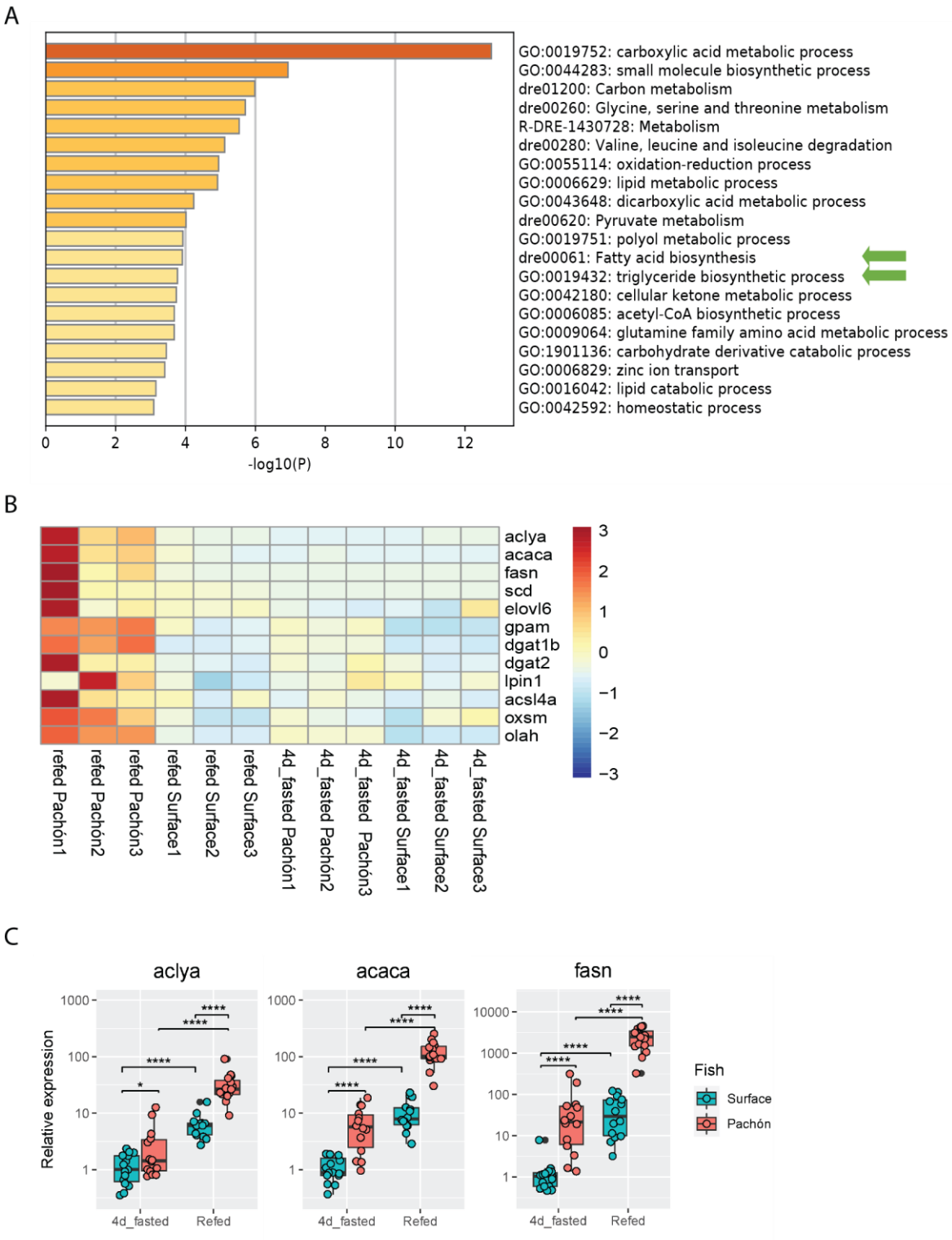

Figure 3.2.2. Lipogenesis is upregulated in the liver of Pachón cavefish compared to surface fish.

A) GO-term analysis of upregulated genes in refed Pachón livers compared to refed surfaced fish livers. Green arrows indicate the key lipid anabolic pathways, fatty acid

biosynthesis and triglyceride biosynthesis process. B) Heatmap of lipogenesis genes in fasted and refed surface fish and Pachón cavefish. C) Relative expression level (RT-qPCR) of fatty acid biosynthesis genes in livers of fasted (4d_fasted: 4 day fasted) and refed (3 hours after refeeding) surface fish and Pachón cavefish (n=12, Wilcoxon test were used to determine p-value: * $p<0.05$; ** $p<0.01$; ***$p<0.001$; ****$p<0.0001$).

To test whether the higher lipogenesis capability is also applied to other cavefish populations, I extended the analysis of lipogenesis gene expression to Tinaja and Molino cavefish. Like Pachón cavefish, Tinaja and Molino cavefish also upregulated to a much higher extent after refeeding compared to surface fish (Figure 3.2.3A), indicating all three cavefish populations have higher lipogenesis capability in the liver compared to surface fish.

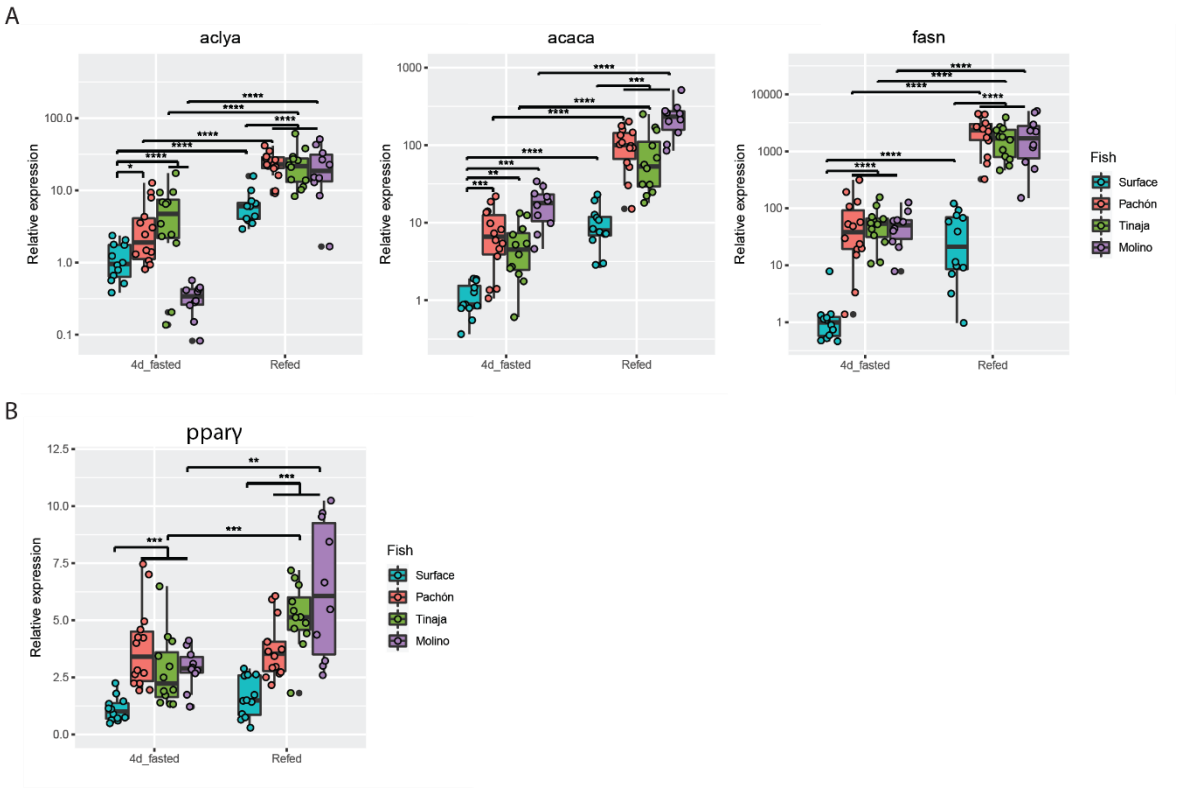

Figure 3.2.3 RNA expression level of lipogenesis genes.

A) RNA relative expression level of lipogenesis genes (*aclya*, *acaca*, and *fasn*) in the livers of four fish populations (Surface, Pachón, Tinaja, and Molino) after starvation followed by refeeding (n=12 per sample). B) RNA relative expression level of *pparγ* in four fish populations at starvation (4 day starved) and refed state (n=12 per sample).

To better understand the temporal dynamics of gene expression and how long the upregulation of lipogenesis genes lasts in Pachón cavefish, I performed a time course study of lipogenesis genes expression. I measured transcription levels of the key fatty acid biosynthesis genes (*acly*, *acaca*, *fasn*) and triglyceride biosynthesis genes (*scd*, *elovl6*, *gpam*, and *dgat2*) using qRT-PCR of liver tissues of surface fish and Pachón cavefish at different time points after paired feeding. I found higher expression of these lipogenesis genes in cavefish samples compared to surface fish up to 24 hours after feeding, with the highest expression at the 6-hour time point (Figure 3.2.4A, B). The gene expression differences were no longer detected at the 5-day time point. This indicates the upregulation of lipogenesis can last more than 24 hours (but less than 5 days) after feeding the same amount of food in Pachón cavefish compared to surface fish.

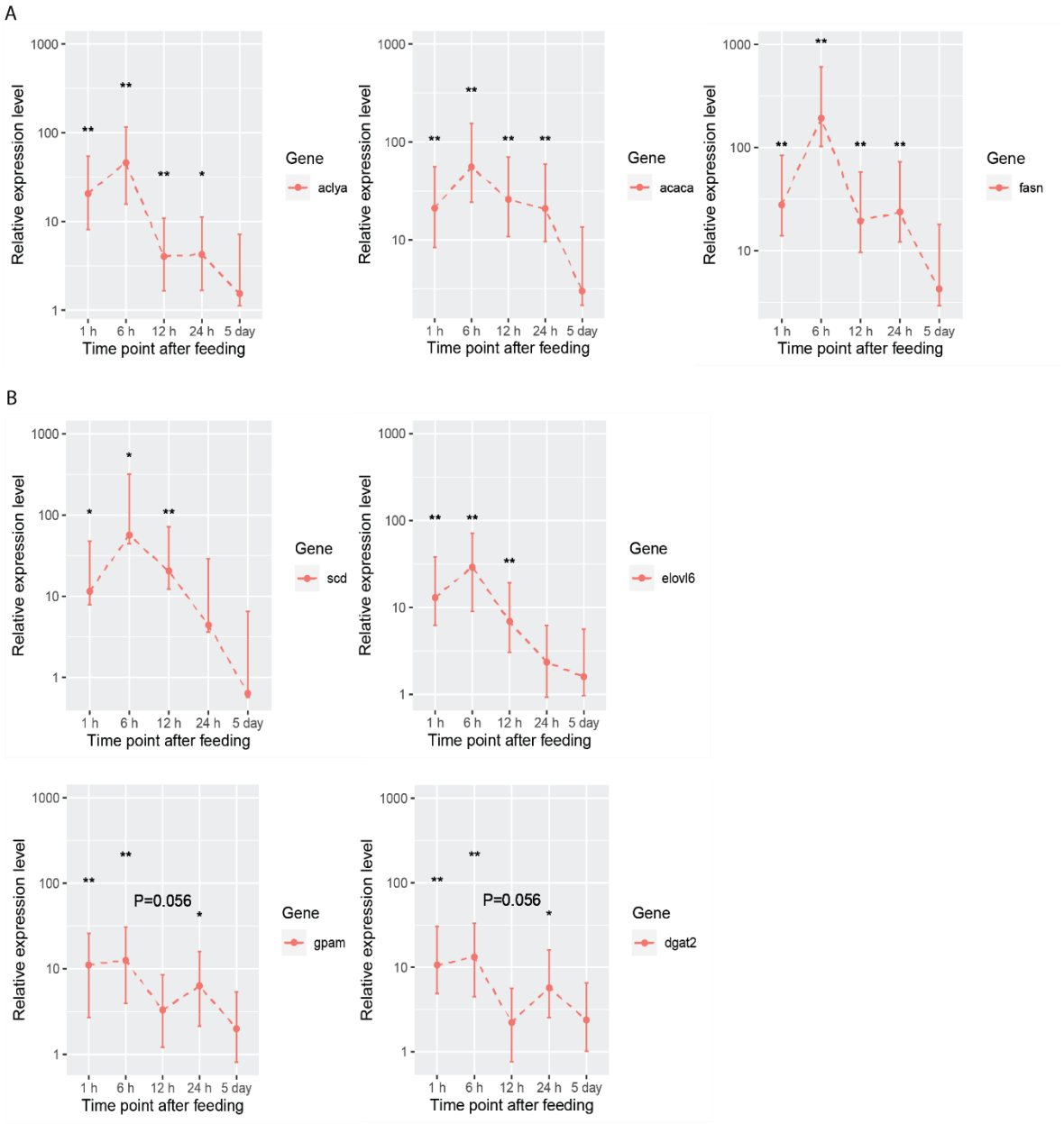

Figure 3.2.4. Lipogenesis gene expression dynamics after feeding.

A) Relative expression level (Pachón compared to surface) change of fatty acid biosynthesis genes (*aclya*, *acaca*, and *fasn*) at different time points (1 hour, 6 hours, 12 hours, 24 hours, and 5 days) after feeding in the liver of surface fish and Pachón cavefish. B) Expression change of triglyceride biosynthesis genes (*scd1*, *elovl6*, *gpam*, and *dgat2*) at different time points (1 hour, 6 hours, 12 hours, 24 hours, and 5 days) after paired feeding in the liver of surface fish and Pachón cavefish. Wilcoxon test was used to determine p-value, * $p<0.05$; ** $p<0.01$.

To find further evidence of increased lipogenesis in cavefish, I monounsaturated fatty acids, a key step in the conversion of fatty acids to triglycerides (Ntambi and Miyazaki, 2004; Wang et al., 2015). The products are monounsaturated fatty acids (MUFAs), mainly including oleate (C18:1) and palmitoleate (C16:1) (Enoch et al., 1976; Ntambi et al., 2002) and the desaturase gene, *scd*, catalyzes this process. Therefore, the expression level of *scd* gene and the amount of MUFAs reflect the level of lipogenesis. I checked mRNA expression of *scd* and found its expression enhanced in Pachón cavefish liver samples compared to surface fish after feeding (Figure 3.2.5A). Then, using available lipidomics data (Medley et al., 2020), I compared the abundance of MUFAs in cavefish. Indeed, I found that both oleic acid and palmitoleic acid were present in higher levels in refed Pachón cavefish livers compared to surface fish samples (Figure 3.2.5B). Another indicator of lipogenesis is the fatty acid desaturation index, the ratio of product (C16:1n-7 and C18:1n-9) to precursor (C16:0 and C18:0) fatty acids (Chong et al., 2008; Harding et al., 2015; Klawitter et al., 2014). Similarly, refed Pachón cavefish have a higher desaturation index for palmitoleic acid and oleic acid (Figure 3.2.5C). Taken together, this data strongly suggests that Pachón cavefish have enhanced lipogenesis in the liver.

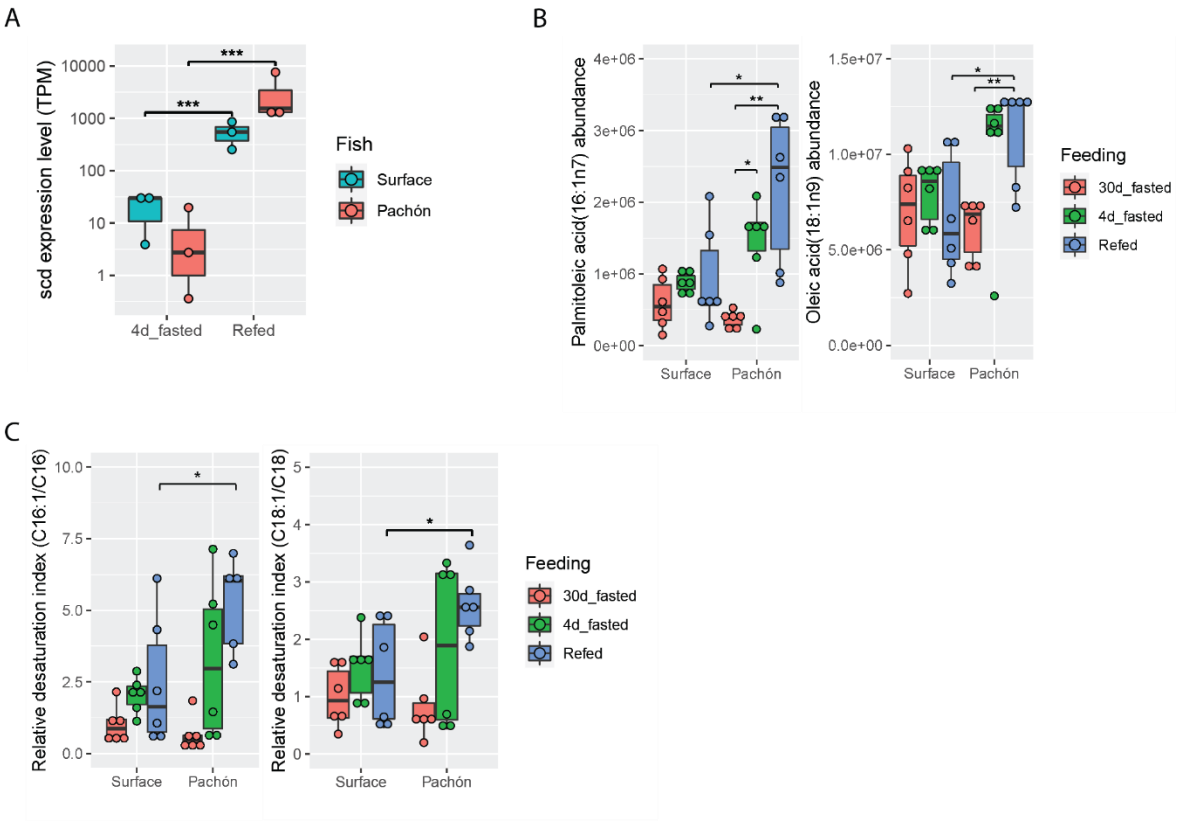

Figure 3.2.5. Desaturation of fatty acids indicates higher lipogenesis in Pachón cavefish liver than surface fish.

A) Expression of *scd* in livers of fasted and refed surface fish and Pachón cavefish (n=3), TPM: transcript per million. B) Fatty acids profiles of two monounsaturated fatty acids (n=6) data from (Medley et al., 2020). C) Refed Pachón cavefish livers have a higher desaturation index (C16:1n7/C16, and C18:1n9/C18) than surface fish (n=6) data from (Medley et al., 2020). Wilcoxon test was used to determine p-value, *p<0.05; **p<0.01; ***p<0.001.

3.3.3 Pparγ, a lipid metabolism regulator, was upregulated in cavefish

To identify upstream regulators underlying the upregulation of DNL gene expression, I checked expression of transcription factors known to regulate lipogenesis in the RNA-seq data. I found no significant difference in expression of the genes coding for the transcription factors, Srebp1, Chrebp (mlxipl), Lxr (nr1h3), and Usf (usf1 and usf2) between the surface and Pachón samples (Figure 3.3.1).

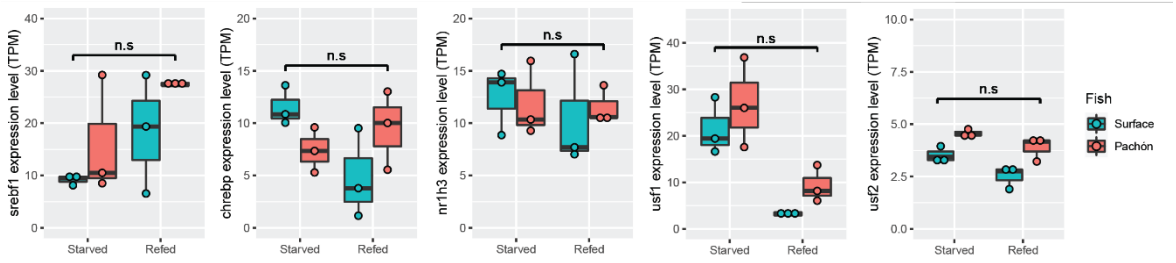

Figure 3.3.1. The expression levels of lipogenesis transcription factors.

RNA expression level of genes coding for known lipogenesis transcription factors in surface and Pachón cavefish livers. These transcription factors include Srebf1(Srebp1), Chrebp, Nr1h3, Usf1, and Usf2. TPM means transcripts per million reads. Cyan color indicates surface fish and red color represents Pachón cavefish. Fasted and refed indicate the feeding state of the fish sample (n=3 per sample, Wilcoxon test was used to determine p value; n.s indicate not significance).

However, I noticed that gene *pparγ*, a transcription factor known to regulate adipogenesis and lipogenesis (Ahmadian et al., 2013; Lee et al., 2012; Sharma and Staels, 2007; Tontonoz and Spiegelman, 2008) to be significantly upregulated in Pachón cavefish samples at both the fasted and the refed state (Figure 3.3.3A). Moreover, the *pparγ* gene responds to feeding to a much higher extend in Pachón liver than surface fish (49.40% vs. 21.18%, Figure 3.3.3A). To test whether the differences in gene expression translate to the protein level, I generated an antibody for Pparγ and validated its specificity. To determine its specificity, I co-transfected either surface fish or Pachón cavefish *pparγ* along with GFP in HEK293T cell lines and immunostained the cells. Given there are 3 amino acids difference in Pparγ peptides between surface fish or Pachón cavefish, I did the transfection for both sequences. Pparγ antibody localized only in the nuclei of cells that were positive for GFP as the transfection control, suggesting specificity of the antibody. (Figure 3.3.2A).

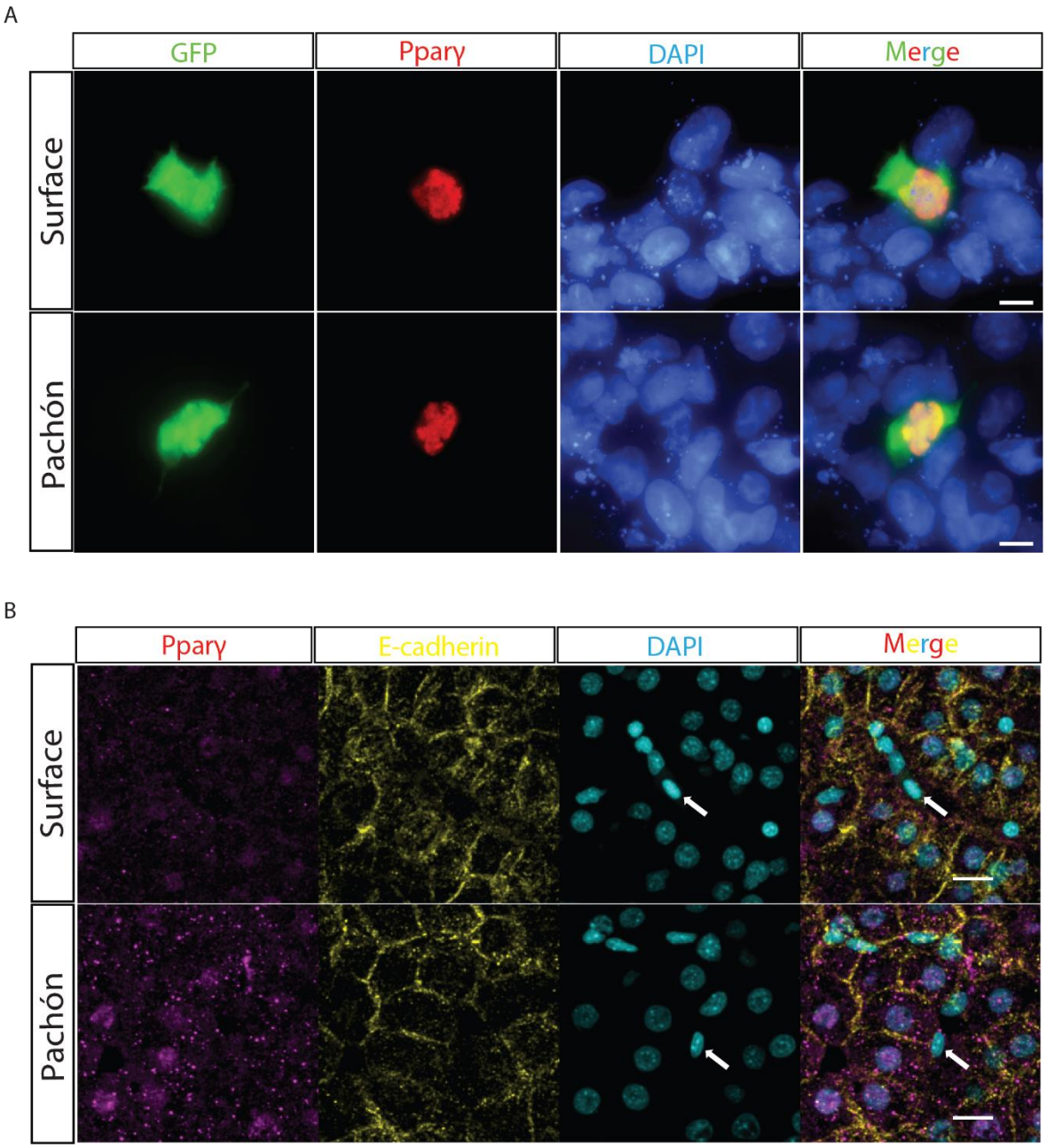

Figure 3.3.2. Anti-Pparγ antibody detects surface and Pachón Pparγ.

A) Transient co-transfection of expression plasmids encoding for either surface fish Pparγ (top panel) or cavefish Pparγ (bottom panel) with GFP in HEK293T cell lines. GFP (green channel) is expressed in the cytoplasm. Pparγ in surface fish or in Pachón cavefish (red channel) localizes in the nucleus. DNA was stained with DAPI (blue channel). The merge channel shows the superposition of each channel. Scale bar =10 μm. B) Immunostaining of Pparγ (magenta), E-cadherin (yellow), and DAPI (turquoise) in liver sections of surface fish and Pachón cavefish. The white arrows indicate blood cells. Scale bar =10 μm.

I next used the antibody to quantify Pparγ protein levels in *Astyanax mexicanus*. I found higher levels of Pparγ in the liver of Pachón cavefish compared to surface fish (Figure 3.3.3B). To visualize cellular distribution of Pparγ, I performed immuno-fluorescence staining on fish liver sections. I found that Pparγ was mainly expressed in the nucleus and again found visibly higher levels in Pachón cavefish hepatocytes compared to surface fish liver cells (Figure 3.3.3D, E). Meanwhile, given the fact Pparγ did not express in blood cells in mammals, I did not detect any Pparγ antibody binding in the nucleus of blood cells within the liver tissue (Figure 3.3.2B), further indicating the specificity of the antibody. Together, these results show that *pparγ* is upregulated at the mRNA and protein levels in the liver of Pachón cavefish compared to surface fish.

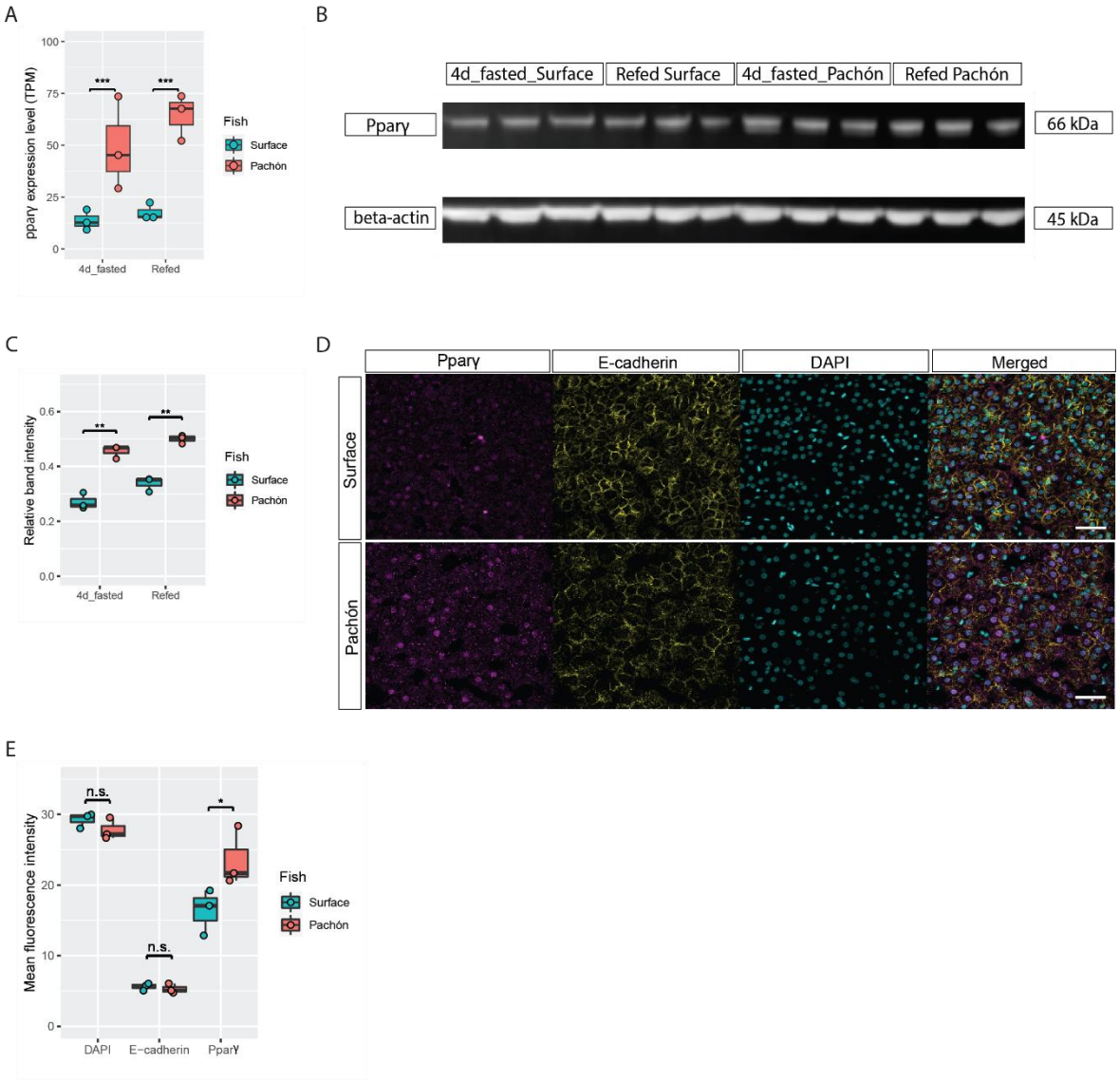

Figure 3.3.3. Pparγ is upregulated in cavefish livers.

A) *pparγ* mRNA expression level comparison between surface fish and Pachón cavefish under two feeding conditions: 4 day fasted and refed. TPM indicates transcript per million reads (n=3). B) Western blots of Pparγ in the liver of surface fish and Pachón cavefish with beta-actin as loading control (n=3). C) Quantification of western blot band intensity after normalizing to beta-actin control) (n=3). D) Immunofluorescence staining for Pparγ, E-cadherin, and DAPI in liver sections of surface fish and Pachón cavefish. Representative picture from each per fish populations (n=34). Scale bar =100 μm. E) Quantification of mean fluorescent intensity of Pparγ staining (n=3, 4 for surface fish and Pachón cavefish liver respectively). 187-317 hepatocytes were randomly selected from each fish liver

sample for intensity measurement. The intensity of DAPI and E-cadherin indicated the quantification of nucleus and cell membrane staining. Wilcoxon test was used to determine p-value, **p<0.01, ***p<0.001

3.3.4 Genome-wide analysis revealed Pparγ binding with target genes

To study whether the increase in transcription factor level translates into higher binding on the DNA level, I performed Chromosome immunoprecipitation sequencing (ChIP-Seq) for Pparγ in two livers of surface fish and Pachón cavefish, respectively. Pearson correlations between replicates showed high correlation, indicating the high quality of the library and reliability of the data (Figure 3.4.1A). I used IDR to keep peaks that occurred consistently in both replicates and identified 5371 high-confidence peaks (q value<=0.01) located within 3kb of the predicted transcription start sites for the surface fish samples and 8960 peaks for the Pachón cavefish samples (Figure 3.4.1B). Using those shared peaks associated genes (within 3kb distance), I did the GO term analysis and found those genes are involved in general biological processes, including cellular process, ion transport, cell differentiation, transcription etc (Figure 3.4.1C).

A

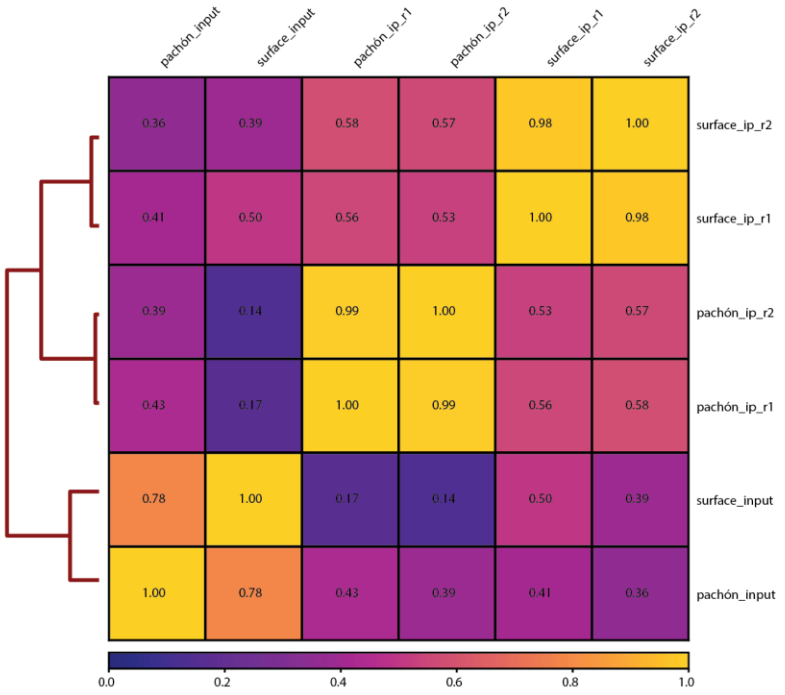
pachón_input
surface_input
pachón_ip_r1
pachón_ip_r2
surface_ip_r1
surface_ip_r2
0.36 0.39 0.58 0.57 0.98 1.00 surface_ip_r2
0.41 0.50 0.56 0.53 1.00 0.98 surface_ip_r1
0.39 0.14 0.99 1.00 0.53 0.57 pachón_ip_r2
0.43 0.17 1.00 0.99 0.56 0.58 pachón_ip_r1
0.78 1.00 0.17 0.14 0.50 0.39 surface_input
1.00 0.78 0.43 0.39 0.41 0.36 pachón_input
0.0 0.2 0.4 0.6 0.8 1.0

B

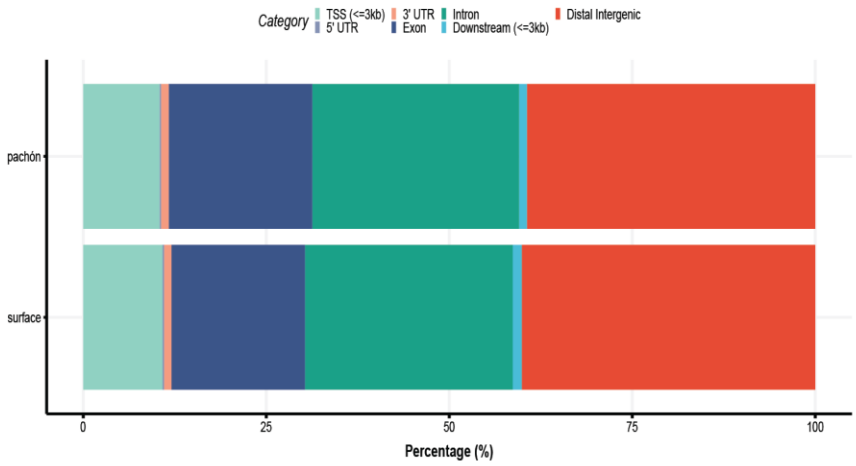
Category
TSS (<=3kb)
5' UTR
3' UTR
Exon
Intron
Downstream (<=3kb)
Distal Intergenic
pachón
surface
0
25
50
75
100
Percentage (%)

C

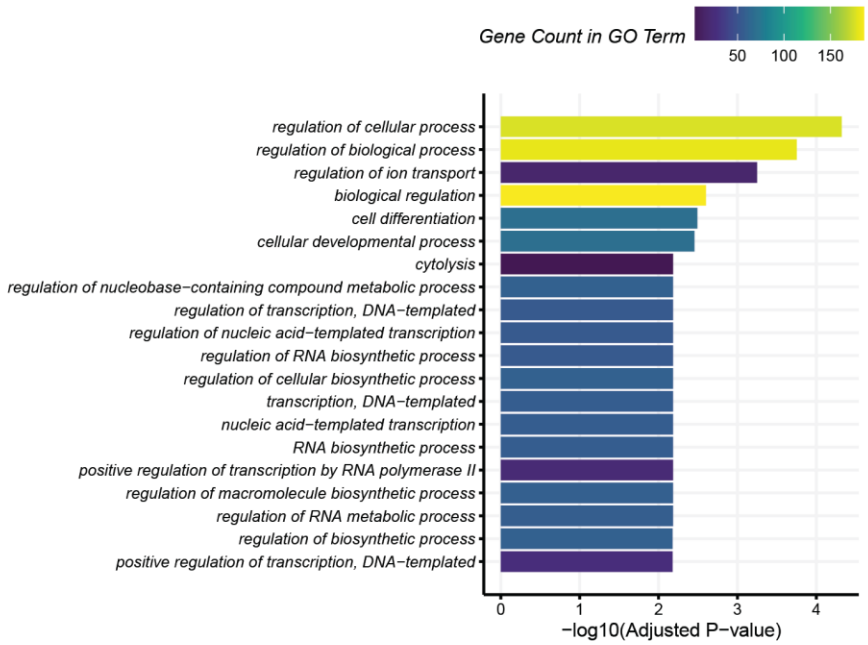
Gene Count in GO Term
50 100 150
regulation of cellular process
regulation of biological process
regulation of ion transport
biological regulation
cell differentiation
cellular developmental process
cytolysis
regulation of nucleobase−containing compound metabolic process
regulation of transcription, DNA−templated
regulation of nucleic acid−templated transcription
regulation of RNA biosynthetic process
regulation of cellular biosynthetic process
transcription, DNA−templated
nucleic acid−templated transcription
RNA biosynthetic process
positive regulation of transcription by RNA polymerase II
regulation of macromolecule biosynthetic process
regulation of RNA metabolic process
regulation of biosynthetic process
positive regulation of transcription, DNA−templated
0 1 2 3 4
−log10(Adjusted P−value)

Figure 3.4.1. Pparγ ChIP-Seq sample correlation, genome distribution, and GO term analysis.

A) Pearson Correlation Coefficient Sample Heatmap highlighting strong correlation between biological replicates. The correlation plot is based on the log2 read counts of bins across the genome that are generated using the R package GenomicAlignments with fixed bin size (n=10000). B) Predicted genome distribution of the peaks identified in Pparγ ChIP-Seq using the Ensembl annotation of the *Astyanax mexicanus* surface fish genome in Pachón (top) and surface fish (bottom) liver samples. For further analysis we focused on peaks near predicted transcriptional start site (TSS) (<=3kb). C) GO term analysis of genes with canonical Pparγ binding peaks near TSS (<=3kb).

Among those peaks, 3980 of them were shared between two fish populations (Fig 3.4.2A). To test if these peaks contain an enrichment for predicted Pparγ binding sites, I searched all 10251 peaks for the presence of the mouse Pparγ::Rxra motif using FIMO scan. I identified the predicted mouse Pparγ::Rxra motif in 576 (5.56%) peaks, compared to a maximum of 268 (2.59%) motifs when randomly placing the same peaks in the TSS regions of all protein coding genes (repeated 1000 times), suggesting an enrichment of potential Pparγ binding sites in the dataset (Fisher's exact test, $p < 1e\text{-}16$). In addition to more genomic binding in Pachón liver samples, I also found these peaks to be higher with significantly more reads than in the surface fish samples (Figure 3.4.2B). Notably, I identified genomic binding in known Pparγ target genes involved in lipid storage (e.g., mgat1a, cd36; Figure 3.4.2C) (Feng et al., 2000; Lee et al., 2012; Zhou et al., 2008). These results are in line with the findings of higher levels of Pparγ in Pachón liver cells potentially driving expression of Pparγ target genes to a higher extend than in surface fish cells, providing an important data set of Pparγ genome binding sites for future studies.

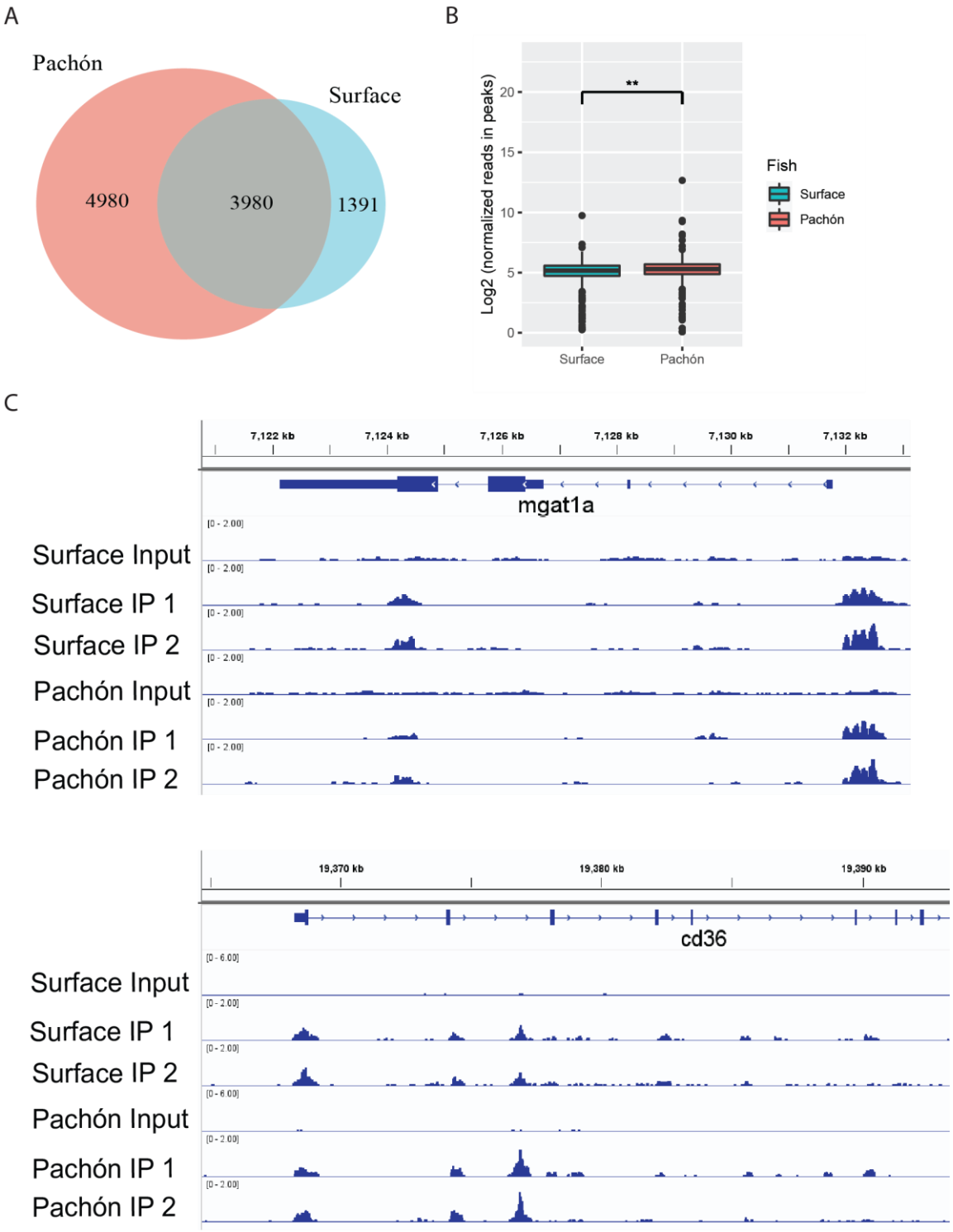

Figure 3.4.2. Genome-wide Pparγ binding sites analysis.

A) Venn diagram of Pparγ ChIP-seq peaks within 3kb of predicted transcription start sites in surface and Pachón cavefish livers. B) Comparison of Pparγ ChIP-seq peak height (in log2 normalized read number) between surface fish and Pachón cavefish (576 peaks with Pparγ canonical binding sites. Wilcoxon test, ** $p<0.01$). C) Examples of Pparγ ChIP-seq peaks on known lipogenesis target genes (*mgat1a*, *cd36*).

3.3.5 The pharmacological manipulation of Pparγ

Given *pparγ* is a key regulator of lipid homeostasis and robustly differentially expressed between surface fish and Pachón cavefish at RNA (Figure 3.3.3A) and protein levels (Figure 3.3.3C, E), it stood out as a top candidate for variation in fat accumulation in *Astyanax*. We next performed pharmacological experiments to test whether upregulation of *pparγ* in cavefish contributes to higher fat accumulation than surface fish. GW 9662 is a potent and selective *pparγ* antagonist, which has been used in human cell lines to inhibit *pparγ* (Seargent et al., 2004; Zizzo and Cohen, 2015). Consistent with the positive correlation between *pparγ* expression level and body fat level, administration of 40 μM GW 9662 reduced the adipose tissue area significantly compared to control groups (DMSO treatment) in both fish populations at larvae stage (surface fish median size from 4000 μm^2 to 2000 μm^2; Pachón cavefish median size from 28000 μm^2 to 18000 μm^2), indicating *pparγ* promotes fat accumulation in *Astyanax* (Figure 3.5A, C). However, it also significantly prevented the adipogenesis onset in surface fish but not Pachón cavefish (Figure 3.5B). Specifically, the adipogenesis onset in surface fish dropped from 45.65% to 12.33%, it only reduced from 100% to 97.83% in Pachón cavefish (Figure 3.5B). It is likely because surface fish are more sensitive to *pparγ* inhibitor than Pachón cavefish since the former have lower *pparγ* expression level than the latter.

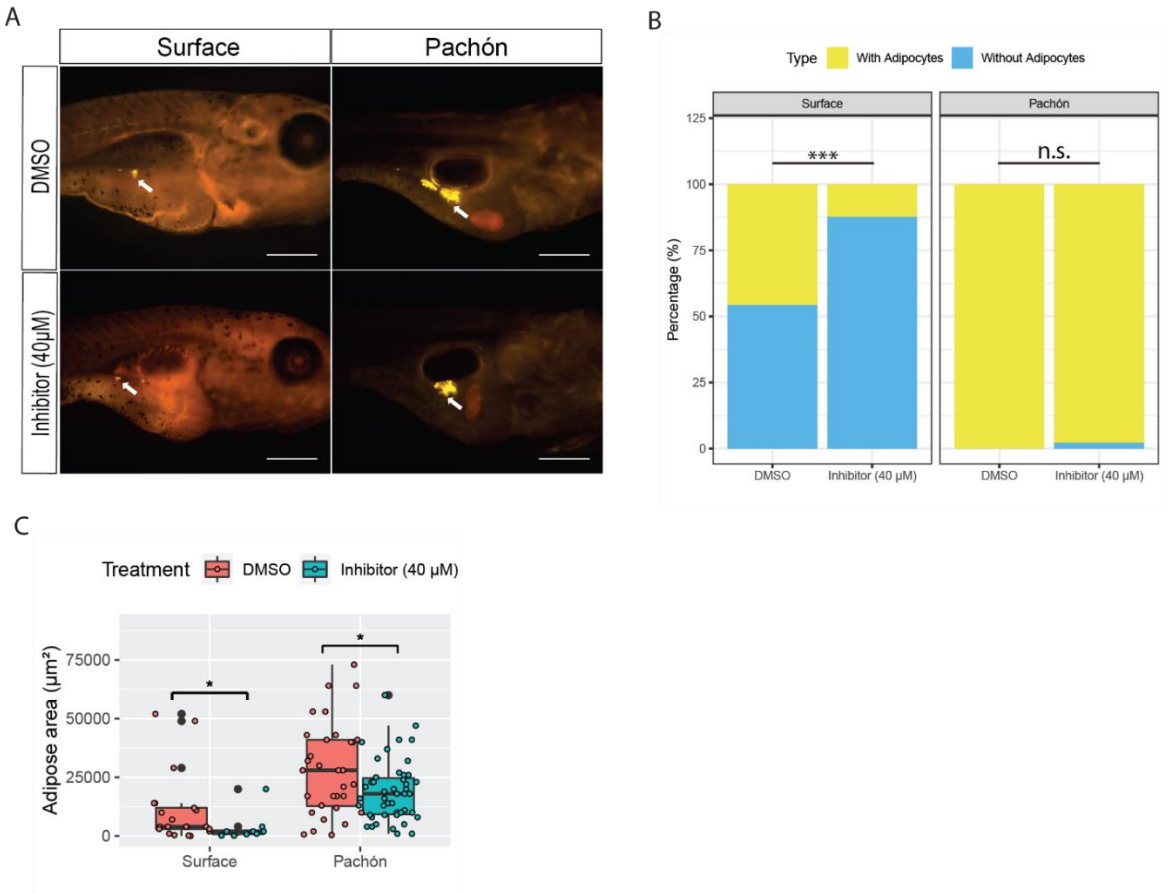

Figure 3.5. Pharmacological manipulation of Pparγ in *Astyanax*.

A) Representative images of Nile red staining of Surface fish and Pachón cavefish at 11dpf raised under control condition (0.2% DMSO) and Pparγ inhibitor, GW9662 (40 μM). Wright arrows indicate the locations of adipose tissue. Scale bar=500μm. B) The onset of adipogenesis comparison between surface fish and Pachón cavefish at 11dpf raised under control condition and Pparγ inhibitor. Samples sizes for surface fish were: 21 with adipocytes and 25 without adipocytes under DMSO treatment; 9 with adipocytes and 64 without adipocytes under inhibitor treatment. Sample sizes for Pachón cavefish were: 32 with adipocytes and 0 without adipocytes under DMSO treatment; 45 with adipocytes and 1 without adipocytes under inhibitor treatment. Significance was calculated with Chi-squre test: n.s. $p>0.05$; ***$p<0.001$. C) The adipose tissue area comparison between surface fish and Pachón cavefish at 11dpf raised under control condition and Pparγ inhibitor). Sample sizes were 21, 9, 32, 45 respectively for boxplot from left to right. Significance was calculated with Wilcoxon test: *$p<0.05$.

3.3.6 The mutations of per2, a suppressor of Pparγ

I next interrogated whether there are any regulators of *pparγ* gene, interestingly, I identified a genomic mutation in a known suppressor of Pparγ. Previously, it has been reported that Period circadian clock 2 (Per2) suppresses Pparγ-mediated transcription by direct binding to its C-terminal domain (Grimaldi et al., 2010). Analyzing the RNA-Seq liver data, I found that in Pachón liver samples the *per2* transcript is alternatively spliced leading to a skipping of Exon 21 (Figure 3.6.1A). The final transcript then contains a premature stop codon in Exon 22, which is predicted to lead to a truncation of 160 amino acids from Per2 C-terminus (Figure 3.6.1A). I validated the splice variant using Sanger sequencing from cDNA generated from fresh liver tissue and found the alternatively spliced transcript to make up the majority, if not all, of the cDNA molecules (Figure 3.6.1A). Interestingly, I found the same splice variant to be the predominant variant also in liver samples of Tinaja cavefish, but not in Molino cavefish (Figure 3.6 A). When I sequenced the amplicon of Molino *per2* transcript, I identified a different non-sense mutation further upstream of the Pachón and Tinaja variant. Molino carry a 7 bp deletion in Exon 13 of *per2*, leading to a premature stop codon in Exon 13 and a loss of 855 amino acids from Per2 (Figure 3.6A). Furthermore, I also investigated whether the alternative splicing of *per2* gene is liver specific or common to multiple tissues. I further extracted the total RNA from fin, brain, adipose, heart, and muscle. Then, we amplified *per2* cDNA and sequenced them. I found that the alternative splicing in *per2* gene is common to all those tissues (Figure 3.6B). The presence of two independent non-sense mutations in *per2* in three independently derived cavefish populations may imply a putative role in cave adaptation. While future experiments will be needed to show if these mutations affect binding of Pparγ, it is tempting to speculate that these mutations may attenuate the inhibition effect of Per2 on Ppar*γ,* which in combination with higher levels of activators would lead to higher transcriptional activity of Ppar*γ*.

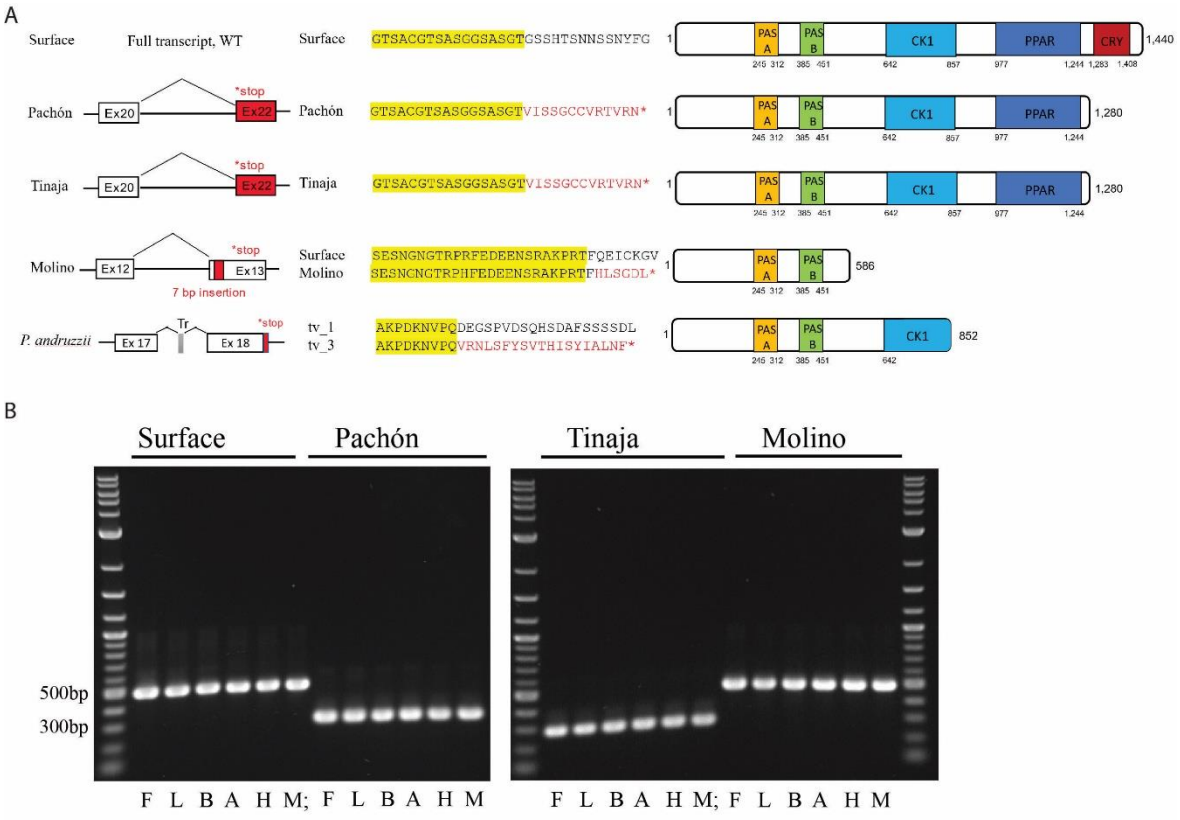

Figure 3.6. Mutations of per2 in *Astyanax*.

A) Schematic depiction of the splice variant of *per2* leading to a skipping of Exon 21 and a premature stop codon in Exon 22 in Pachón and Tinaja cavefish. The 7bp nucleotide insertion in Molino *per2* Exon 13 leads to a premature stop codon. The dominant transcript of *per2* in *Phreatichthys andruzzii* (Somalian cavefish). The filled dark grey box (Tr), 225bp nucleotides, shows the location of transposon-derived sequences, which is incorporated into the transcript. 25 bp nucleotides in the intron 18 inserted into the transcript generate a premature stop codon. In the middle, the panel shows the amino acids near the stop codon. The yellow highlighted part shows the consensus peptides, the black amino acids show the reference sequence, the red indicates the alternative spliced transcript. The red star symbol indicates the stop codon location. In Somalian cavefish, tv_1 means the transcript variant 1 and tv_3 indicates the transcript variant 3, which is the dominant and most abundant transcript. On the right side, it indicates the schematic graphic protein of Per2 in Mexican cavefish and Somalian cavefish. PPAR: homology to

predicted Pparγ binding domain. CRY: homology to Cry1 interacting region. PAS: homology to Per-Arnt-Sim domain; CK1: homology to casein kinase binding domain. Numbers indicate the amino acid number from N-terminal (left) to C-terminal (right). B) The gel images of *per2* cDNA amplicon bands in various tissues of *Astyanax* populations. The abbreviations include F:fin; L:liver; B:brain; A:adipose; H:heart; M:muscle.

3.4 Discussion

My goal was to interrogate the cellular mechanisms which contribute to high body fat accumulation in cavefish. First, I confirmed previous results showing that cavefish populations can store more fat than surface fish (Aspiras et al., 2015; Xiong et al., 2018). This study extends previous analyses by showing that cavefish store body fat in a variety of tissues and locations in the body with certain areas more prone to body fat than others. For example, there are even mor fat (fat in eye orbit and subcutaneous fat) in the head of cavefish compared to surface. However, I did not find the cavefish to develop a fatty liver, which is contrast to previous findings (Aspiras et al., 2015). This can either be due to differences in the diet of the fish used for the study, or the age of the fish used. I analyzed relatively young adult fish (~1 year), while previous studies have used older fish. Studying the effect of those factors, including age and diets, on lipid metabolism could provide important insights into how cavefish deal with the accumulation of liver fat, which in humans causes nonalcoholic fatty liver disease (Rinella, 2015; Vernon et al., 2011). Furthermore, I developed a fast, reliable and cheap method of quantifying total body fat in fish using EchoMRI, which will open the door for high-throughput genetic analysis (i.e., QTL analysis) of fat accumulation in future studies.

Using transcriptomic analysis, I showed a massive upregulation of lipogenesis enzyme genes in the liver of Pachón cavefish compared to surface fish. My qPCR results further show that other cavefish populations, including Tinaja and Molino, have higher lipogenesis gene expression compared to surface fish, indicating all three cavefish populations have higher lipogenesis gene expression in the liver than surface fish. Moreover, the lipidomic profiling demonstrated enhanced lipogenesis level at the metabolite level in Pachón cavefish liver. This both argues for an increased ability of cavefish to synthesize triglycerides from fatty acids through de novo lipogenesis. The food

consumed by fish in the lab is high in protein (~60%), arguing for a high turnover through de novo lipogenesis, which is in line with the observed upregulation of genes involved in fatty acid synthesis (*acly*, *acaca*, and *fasn*). However, the food also contains a significant amount of fat (~ 15%), which makes it likely that some of the triglyceride biosynthesis occurs through absorption and esterification of fatty acids from the dietary fat. Follow-up experiments with different diets, will be needed to fully disentangle this.

Furthermore, I found Pparγ, a transcription factor mediating lipid metabolism, to be significantly upregulated in the liver of Pachón cavefish compared to surface fish. Pparγ, upon ligand activation, induces many target genes involved in lipogenesis and adipogenesis (Ahmadian et al., 2013; Lee et al., 2012; Schadinger et al., 2005; Sharma and Staels, 2007; Tontonoz and Spiegelman, 2008), making it an excellent candidate transcription factor to explain the upregulation of some of the lipogenesis genes in cavefish. While Pparγ has been shown to be upregulated in obese rodent models and human patients (Lee et al., 2012; Pettinelli and Videla, 2011; Wolf Greenstein et al., 2017; Yu et al., 2003), a role of Pparγ in a species naturally adapted to food scarcity has not been reported before. Notably, I found the upregulation of Pparγ to be present already in juvenile fish (before sexual maturation) and in specific response to the feeding event, further suggesting that it has an adaptive rather than pathological role. As Pparγ plays important roles in adipogenesis, it is likely that the role of Pparγ goes beyond the increased expression of lipogenesis genes, but that Pparγ is also involved in increased adipogenesis in cavefish, potentially buffering the effect of lipotoxic lipid species (Medina-Gomez et al., 2007). Notably, I found evidence for increased genomic binding of Pparγ using ChIP-Seq analysis. However, there are some limitations of this analysis. While I have validated the specificity of the antibody in vitro, I cannot fully exclude that some of the peaks are due to unspecific binding. I did identify a highly significant enrichment for the mouse Pparγ::Rxra motif in peaks near predicted transcription start sites, but further functional

analysis will be needed to test if the same motif is used in fish. To sum up, my analysis sets an important foundation for ChIP-Seq analysis of transcription factors in non-traditional research systems.

Moreover, I also used pharmacological manipulation to test whether the upregulation of *pparγ* contributes to fat accumulation in *Astyanax* mexicanus. Consistent with my hypothesis, the administration of Pparγ inhibitor, GW 9662, indeed slowed down the expansion of the adipose tissue in both surface fish and Pachón cavefish. Moreover, the inhibitor even dramatically postponed the onset of adipogenesis in surface fish but not in Pachón cavefish at 11 dpf. That's likely because surface fish have lower Pparγ protein level in the liver than Pachón cavefish. When both fish were treated with Pparγ inhibitor of same concentration, Pparγ in surface fish would be inhibited to a higher extent than that of Pachón cavefish. However, the inhibitor immersion of fish larvae only partly demonstrated the functionality of Pparγ in *Astyanax*. That's because Pparγ inhibitor not only affect lipogenesis but also adipocyte development, both of which directly affect the adipose tissue growth. Therefore, to specifically test the upregulation of *pparγ* in the liver contributes to fat accumulation in *Astyanax* mexicanus, genetic manipulations would be better options than drug treatment. For example, using liver-specific overexpression *pparγ* transgenic fish to test the sufficiency and liver-specific knock-out fish to test the necessity would be helpful. However, given the long generation time (around 1 year) of *Astyanax* mexicanus, it would be very difficult for me to finish it during my graduate program.

Importantly, I identified genomic mutations in one of its known repressors. Previous work has shown that PER2 represses Pparγ directly and knock-down of *Per2* leads to an increased activation of adipogenesis genes in vitro (Grimaldi et al., 2010). These findings are in line with the observed phenotypes in the cavefish. While in Molino the *per2* mutation is predicted to delete the Pparγ binding domain, in Pachón and Tinaja the nonsense mutation is located 36 amino acids downstream of the predicted Pparγ

binding domain, potentially leaving the binding domain intact (Figure 3.5.2). Whether the mutation affects Pparγ directly or has a destabilizing effect on the protein remains to be shown.

The finding of *per2* nonsense mutations in cavefish populations is interesting in terms of previous observations of association between this gene and circadian rhythms in cavefish. In studies of circadian rhythm in *Astyanax mexicanus,* it was found that the ability to entrain a circadian rhythm is not completely lost in cavefish, but that there are differences in altitude and timing of the rhythm (Beale et al., 2013; Mack et al., 2020). It has been speculated that this could be in part due to increased basal expression levels of *per2* (Beale et al., 2013; Froland Steindal et al., 2018). My results add to these findings, potentially suggesting that Per2 is not fully functional even though its transcript is upregulated. To what extend the splice variant is present in other tissues such as the fin or embryos used for the previous studies needs to be investigated.

Circadian rhythm proteins changes are a hallmark of cavefish evolution. Interestingly, in the Somalian cavefish, *Phreatichthys andruzzi*, *per2* is found to have a nonsense mutation, which is like the mutations I found in *Astyanax* (Ceinos et al., 2018) (Figure 3.5.2). A similar mutation in the same gene in a distantly related, convergent case of cave adaptation is an important sign of a role for this gene in adaptation. In this respect it may be worth noting that icefish have also lost *per2* (Kim et al., 2019). This is further emphasized by the fact that I found mutations in *per2* in three independently derived cavefish populations (Bradic et al., 2012), making *per2* a major target of evolution and highlighting important connections between circadian rhythm and metabolism (Moran et al., 2014).

3.5 Limitations of study

This study showed Pachón cavefish stored much more body fat at multiple locations in the body and have higher lipogenesis capability in the liver than surface fish. Then, it proposed the upregulation of Pparγ contributed to the high lipogenesis in Pachón cavefish. However, the causation between increased Pparγ expression and high lipogenesis is only partly established in Astyanax. Moreover, functional studies of *per2* mutations in cavefish populations are also missing.

3.6 Future directions

Studies have shown that Pparγ contributes to hepatic fat accumulation in mice, the upregulation of Pparγ likely contributes to high lipogenesis in Pachón cavefish. The cause-and-effect relationship between them needs to be validated. Hence, pharmacological and genetic manipulation should provide insights on the role of Pparγ in lipid metabolism and fat accumulation in the liver of Pachón cavefish.

Pharmacological manipulation can be achieved through either immersion of fish in drug solution or IP injection to deliver drugs to fish. The specific inhibitors of Pparγ include GW9666, T0070907, and SR202, whereas the common agonists contain pioglitazone hydrochloride, rosiglitazone maleate, and edaglitazone (Gross and Staels, 2007; Seargent et al., 2004). If my hypothesis is correct, inhibiting Pparγ in Pachón cavefish will reduce lipogenesis and fat accumulation more than in surface fish, because Pachón cavefish have higher Pparγ expression level in the liver, and it should be more sensitive to inhibition effect. In contrast, stimulating Pparγ with agonists in Pachón cavefish will increase lipogenesis and lipid accumulation more than in surface fish.

Genetic manipulation is another strategy to test whether enhanced Pparγ expression is the cause. Overexpression of Pparγ in surface fish liver can be done using promoter sequences of liver specific-expressed genes (i.e., fatty acid binding protein 10a (fabp10a)) (Evason et al., 2015; Her et al., 2003a; Her et al., 2003b). Theoretically, it will lead to surface fish increasing lipogenesis in the liver and to hepatic fat accumulation. Liver-specific knock-down of Pparγ in Pachón cavefish would also be informative. It may result in reduction of lipogenesis capability in the liver of Pachón cavefish, making it thinner than WT Pachón cavefish.

Apart from liver, adipose tissue is another vital organ for lipid homeostasis. However, it is still unknown whether there is any difference in lipid metabolism in the

adipose tissue between surface fish and cavefish populations. Hence, it is necessary to compare lipid metabolism in adipose tissue between them. Specifically, insights from testing whether cavefish have higher lipid anabolism and/or lower lipid catabolism than surface fish in the adipose tissue would be useful. Moreover, since adipose tissue is an important endocrine organ, which affect lipid metabolism heavily. It is worth comparing some proteins, including leptin and TNF-α, between surface fish and cavefish, because they are secreted by adipose tissue and related with obesity. (Hotamisligil et al., 1993; Myers et al., 2010; Paracchini et al., 2005; Tzanavari et al., 2010).

Chapter 4. Conclusion and future directions

4.1 Key conclusions

My goal was to uncover the underlying mechanisms, through which make cavefish achieve higher body fat compared to surface fish. I investigated the question from two perspectives: adipocyte development and lipogenesis in the liver. For the adipocyte development project, first, I found all three cavefish populations (Pachón, Tinaja, and Molino) had higher body fat and showed adipocyte hypertrophy in adult compared to surface fish. Pachón and Tinaja cavefish accumulated more visceral fat than surface fish under paired feeding, indicating appetite-independent mechanisms exist. Furthermore, I found Pachón cavefish develop visceral adipocyte earlier than surface fish, Tinaja showed similar adipogenesis pattern as surface fish, but Molino had delayed adipogenesis compared to surface fish. Moreover, adipogenesis is feeding dependent and more feeding can accelerate adipogenesis in fish populations. Taken together, adipocyte hypertrophy in adult cavefish populations and accelerated adipogenesis in Pachón cavefish contribute to high body fat.

For the lipogenesis comparison project, first, I extended the body fat comparison to different body locations and I found Pachón and Tinaja stored more fat in the orbit cavity and trunk area (subcutaneous fat). Then, I interrogated the lipogenesis gene expression profile in the liver of surface fish and Pachón cavefish. The results showed that lipogenesis genes were dramatically upregulated in the liver of Pachón cavefish compared to that of surface fish. Parallelly, some MUFAs, metabolites of lipogenesis, were much higher in the liver of fed Pachón cavefish than that of surface fish, indicating higher lipogenesis. Moreover, I found a regulator of lipid metabolism, Pparγ, was upregulated in Pachón

cavefish liver compared to surface fish. The activators of Pparγ, some PUFAs, showed higher level in the liver of Pachón cavefish than surface fish. Additionally, a suppressor gene of Pparγ, *per2*, showed mutations. Both increased level of activators and mutated suppressor may lead to higher transcriptional capability of Pparγ. To sum up, enhanced Pparγ leads to higher lipogenesis and high body fat in Pachón cavefish compared to surface fish.

4.2 Future Directions

The teleost fish, *Astyanax mexicanus*, is becoming an important model to study biological questions in the context of evolution. In the past 20 years, an increasing number of studies revealed the underpinnings of lost traits as well as gained phenotypes in the cavefish populations compared to surface fish. These traits include loss of pigmentations, eyes, sleep, heart regeneration capability, and gain of enhanced sensory capability, high blood glucose level, and high body fat (Jeffery, 2020). Since some metabolic traits resemble human diseases, this fish species is emerging as a biomedical model to study human diseases. Here, I propose *Astyanax mexicanus* can be used as an additional model to study obesity. Since it provides natural mutants to study obesity with surface fish as the WT. Moreover, many key organs in human also exist in fish and some vital genes involved in lipid metabolism are conserved between human and fish (Seth et al., 2013).

In mammals, adipocytes have multiple origins, including mesenchymal progenitors of mesodermal origin and hematopoietic stem cells from the bone marrow (Crossno et al., 2006; Majka et al., 2011). However, spatial and temporal of adipogenesis dynamics in mammals are not very clear. Since I have found accelerated adipogenesis in Pachón cavefish compared to surface fish, I propose to use *Astyanax mexicanus* to address this question. The fish larvae are transparent when they begin to develop adipocytes, which

facilitates the observation of adipocytes. Furthermore, it will be helpful to make a transgenic line, which can be used to label and trace adipocytes. This can be achieved by driving reporter gene (i.e., GFP) with adiponectin promoter sequence, which is exclusively expressed in adipocytes (Uhrig-Schmidt et al., 2014).

To fully understand how cavefish gain high body fat compared to surface fish, comparison study of lipid catabolism is also necessary. Because the fat storage is determined by the balance between fat synthesis and degradation. Given some studies showed cavefish populations consumed less oxygen than surface fish (Bilandzija et al., 2020; Moran et al., 2014; Salin et al., 2010), it is worthwhile to test whether cavefish populations have lower fatty acid oxidation than surface fish. If it is the case for all cavefish populations, how do they make it? Do they have lower expression levels of genes involved in fatty acid oxidation or do they have some mutations in those genes? If it is only true for some specific cavefish populations, how do they achieve it while others cannot?

Obesity, which is defined as body mass index (BMI) over 30, has become more common globally (Afshin et al., 2017). Almost 11% of global human population are obese and it is much more serious in the developed countries (Collaboration, 2016). Obesity is usually associated with other medical problems, including inflammation, type 2 diabetes (T2D), hypertension, heart stroke, and even cancer (Gonzalez-Muniesa et al., 2017; Williams et al., 2015). In nature, some animals (i.e., polar bear, cavefish) can gain high body fat, yet they are still healthy (without obvious accompanied syndromes) (Peuss et al., 2020). Studying those organisms, which can maintain good health while being obese, may bring therapeutic implications for human obesity.

Appendix

Table 2. Summary of various known metabolic phenotypes shown by *Astyanax* cave populations.

Metabolic phenotype	Description	*Trait loci*	Pachón	Tinaja	Molino	Key references
Metabolic rate	Measured as a function of oxygen consumption	*Unknown*	Low metabolic rate	Not tested	Not tested	(Moran et al., 2015)
Insulin resistance	Measurement of phospho-AKT levels as a read out of insulin sensitivity	*INSRA P211L*	Yes	Yes	No	(Riddle et al., 2018a)
Hyperphagia	Measured as increased amount of food intake	*MC4R G145S*	No	Yes	Yes	(Aspiras et al., 2015)
Hyperglycemia	Increased blood glucose	*INSRA P211L*	Yes	Yes	Yes	(Riddle et al., 2018a)
Increased fat storage	Measurement of total triglyceride and visceral fat	*INSRA P211L,* *MC4R G145S*	Yes	Yes	No	(Aspiras et al., 2015, Hüppop, 1988), Chapter II
Starvation resistance	Measured by loss of weight upon prolonged starvation	*MC4R G145S*	Yes	Yes	Yes	(Aspiras et al., 2015)
Circadian rhythm	Measurement of per1 and per2 gene expression in light and dark periods	*per1, per2*	Reduced rhythmicity	Not tested	Not tested	(Beale et al., 2013)

Churning motility in post-larval stomach	**Pattern of food transit through the gut**	***Unknown***	**Increased churning**	**Not tested**	**Not tested**	**Riddle et al. (2018b)**
Early adipogenesis	**Time of appearance of fat/adipose cells**	***Unknown***	**Yes**	**No**	**No**	**Chapter II**
Hypertrophic adipocytes	**Enlarged fat cells**	***Unknown***	**Yes**	**Yes**	**Yes**	**Chapter II**
Insulin resistance	**Measurement of phospho-AKT levels as a read out of insulin sensitivity**	***INSRA* P211L**	**Yes**	**Yes**	**No**	**(Riddle et al., 2018a)**
Upregulation of lipogenesis	**Upregulated *pparγ* leads to increase lipogenesis in the liver**	***pparγ***	**Yes**	**Yes**	**Yes**	**Chapter III**

References

Abumrad, N, Harmon, C, Ibrahimi, A (1998) Membrane transport of long-chain fatty acids: evidence for a facilitated process. J Lipid Res *39*, 2309-2318.

Abumrad, NA, Davidson, NO (2012) Role of the gut in lipid homeostasis. Physiological reviews *92*, 1061-1085.

Afshin, A, Reitsma, MB, Murray, CJL (2017) Health Effects of Overweight and Obesity in 195 Countries. N Engl J Med *377*, 1496-1497.

Ahmadian, M, Suh, JM, Hah, N, Liddle, C, Atkins, AR, Downes, M, Evans, RM (2013) PPARgamma signaling and metabolism: the good, the bad and the future. Nat Med *19*, 557-566.

Alie, A, Devos, L, Torres-Paz, J, Prunier, L, Boulet, F, Blin, M, Elipot, Y, Retaux, S (2018) Developmental evolution of the forebrain in cavefish, from natural variations in neuropeptides to behavior. eLife *7*.

Arrese, EL, Soulages, JL (2010) Insect fat body: energy, metabolism, and regulation. Annual review of entomology *55*, 207-225.

Aspiras, AC, Rohner, N, Martineau, B, Borowsky, RL, Tabin, CJ (2015) Melanocortin 4 receptor mutations contribute to the adaptation of cavefish to nutrient-poor conditions. Proc Natl Acad Sci U S A *112*, 9668-9673.

Barak, Y, Nelson, MC, Ong, ES, Jones, YZ, Ruiz-Lozano, P, Chien, KR, Koder, A, Evans, RM (1999) PPAR gamma is required for placental, cardiac, and adipose tissue development. Mol Cell *4*, 585-595.

Bartz, R, Li, WH, Venables, B, Zehmer, JK, Roth, MR, Welti, R, Anderson, RG, Liu, P, Chapman, KD (2007) Lipidomics reveals that adiposomes store ether lipids and mediate phospholipid traffic. J Lipid Res *48*, 837-847.

Beale, A, Guibal, C, Tamai, TK, Klotz, L, Cowen, S, Peyric, E, Reynoso, VH, Yamamoto, Y, Whitmore, D (2013) Circadian rhythms in Mexican blind cavefish Astyanax mexicanus in the lab and in the field. Nat Commun *4*, 2769.

Berry, DC, Stenesen, D, Zeve, D, Graff, JM (2013) The developmental origins of adipose tissue. Development *140*, 3939-3949.

Beuchat, CA (1990) Body size, medullary thickness, and urine concentrating ability in mammals. Am J Physiol *258*, R298-308.

Bilandzija, H, Hollifield, B, Steck, M, Meng, G, Ng, M, Koch, AD, Gracan, R, Cetkovic, H, Porter, ML, Renner, KJ, Jeffery, W (2020) Phenotypic plasticity as a mechanism of cave colonization and adaptation. eLife *9*.

Bishop, CM, Spivey, RJ, Hawkes, LA, Batbayar, N, Chua, B, Frappell, PB, Milsom, WK, Natsagdorj, T, Newman, SH, Scott, GR, Takekawa, JY, Wikelski, M, Butler, PJ (2015) The roller coaster flight strategy of bar-headed geese conserves energy during Himalayan migrations. Science *347*, 250-254.

Bouchama, A, Knochel, JP (2002) Heat stroke. N Engl J Med *346*, 1978-1988.

Bouret, SG, Simerly, RB (2006) Developmental programming of hypothalamic feeding circuits. Clinical genetics *70*, 295-301.

Bowers, RR, Kim, JW, Otto, TC, Lane, MD (2006) Stable stem cell commitment to the adipocyte lineage by inhibition of DNA methylation: role of the BMP-4 gene. Proc Natl Acad Sci U S A *103*, 13022-13027.

Bradic, M, Beerli, P, Garcia-de Leon, FJ, Esquivel-Bobadilla, S, Borowsky, RL (2012) Gene flow and population structure in the Mexican blind cavefish complex (Astyanax mexicanus). BMC Evol Biol *12*, 9.

Bradic, M, Teotonio, H, Borowsky, RL (2013) The population genomics of repeated evolution in the blind cavefish Astyanax mexicanus. Mol Biol Evol *30*, 2383-2400.

Brock, TJ, Browse, J, Watts, JL (2007) Fatty acid desaturation and the regulation of adiposity in Caenorhabditis elegans. Genetics *176*, 865-875.

Burdi, AR, Poissonnet, CM, Garn, SM, Lavelle, M, Sabet, MD, Bridges, P (1985) Adipose tissue growth patterns during human gestation: a histometric comparison of buccal and gluteal fat depots. International journal of obesity *9*, 247-256.

Caldwell, JP (1999) Animal adaptations. Deserts, 24-27.

Caro, JF, Kolaczynski, JW, Nyce, MR, Ohannesian, JP, Opentanova, I, Goldman, WH, Lynn, RB, Zhang, PL, Sinha, MK, Considine, RV (1996) Decreased cerebrospinal-fluid/serum leptin ratio in obesity: a possible mechanism for leptin resistance. Lancet *348*, 159-161.

Ceinos, RM, Frigato, E, Pagano, C, Frohlich, N, Negrini, P, Cavallari, N, Vallone, D, Fuselli, S, Bertolucci, C, Foulkes, NS (2018) Mutations in blind cavefish target the light-regulated circadian clock gene, period 2. Sci Rep *8*, 8754.

Chippindale, AK, Chu, TJF, Rose, MR (1996) Complex Trade-Offs and the Evolution of Starvation Resistance in Drosophila Melanogaster. Evolution; international journal of organic evolution *50*, 753-766.

Choe, SS, Huh, JY, Hwang, IJ, Kim, JI, Kim, JB (2016) Adipose Tissue Remodeling: Its Role in Energy Metabolism and Metabolic Disorders. Front Endocrinol (Lausanne) *7*, 30.

Chong, MF, Hodson, L, Bickerton, AS, Roberts, R, Neville, M, Karpe, F, Frayn, KN, Fielding, BA (2008) Parallel activation of de novo lipogenesis and stearoyl-CoA desaturase activity after 3 d of high-carbohydrate feeding. Am J Clin Nutr *87*, 817-823.

Clement, K, Vaisse, C, Lahlou, N, Cabrol, S, Pelloux, V, Cassuto, D, Gourmelen, M, Dina, C, Chambaz, J, Lacorte, JM, Basdevant, A, Bougneres, P, Lebouc, Y, Froguel, P, Guy-Grand, B (1998) A mutation in the human leptin receptor gene causes obesity and pituitary dysfunction. Nature *392*, 398-401.

Coghill, LM, Darrin Hulsey, C, Chaves-Campos, J, Garcia de Leon, FJ, Johnson, SG (2014) Next generation phylogeography of cave and surface Astyanax mexicanus. Molecular phylogenetics and evolution *79*, 368-374.

Collaboration, NCDRF (2016) Trends in adult body-mass index in 200 countries from 1975 to 2014: a pooled analysis of 1698 population-based measurement studies with 19.2 million participants. Lancet *387*, 1377-1396.

Coppola, A, Marfella, R, Coppola, L, Tagliamonte, E, Fontana, D, Liguori, E, Cirillo, T, Cafiero, M, Natale, S, Astarita, C (2009) Effect of weight loss on coronary circulation and adiponectin levels in obese women. International journal of cardiology *134*, 414-416.

Crawford, DL, Powers, DA (1989) Molecular basis of evolutionary adaptation at the lactate dehydrogenase-B locus in the fish Fundulus heteroclitus. Proc Natl Acad Sci U S A *86*, 9365-9369.

Crossno, JT, Jr., Majka, SM, Grazia, T, Gill, RG, Klemm, DJ (2006) Rosiglitazone promotes development of a novel adipocyte population from bone marrow-derived circulating progenitor cells. J Clin Invest *116*, 3220-3228.

Dawson, TJ, Webster, KN, Maloney, SK (2014) The fur of mammals in exposed environments; do crypsis and thermal needs necessarily conflict? The polar bear and marsupial koala compared. J Comp Physiol B *184*, 273-284.

den Broeder, MJ, Moester, MJB, Kamstra, JH, Cenijn, PH, Davidoiu, V, Kamminga, LM, Ariese, F, de Boer, JF, Legler, J (2017) Altered Adipogenesis in Zebrafish Larvae Following High Fat Diet and Chemical Exposure Is Visualised by Stimulated Raman Scattering Microscopy. Int J Mol Sci *18*.

DiMichele, L, Paynter, KT, Powers, DA (1991) Evidence of lactate dehydrogenase-B allozyme effects in the teleost, Fundulus heteroclitus. Science *253*, 898-900.

DiMichele, L, Powers, DA (1982) Physiological basis for swimming endurance differences between LDH-B genotypes of Fundulus heteroclitus. Science *216*, 1014-1016.

Duboue, ER, Keene, AC, Borowsky, RL (2011) Evolutionary convergence on sleep loss in cavefish populations. Curr Biol *21*, 671-676.

Duncan, RE, Ahmadian, M, Jaworski, K, Sarkadi-Nagy, E, Sul, HS (2007) Regulation of lipolysis in adipocytes. Annu Rev Nutr *27*, 79-101.

Elipot, Y, Legendre, L, Pere, S, Sohm, F, Retaux, S (2014) Astyanax transgenesis and husbandry: how cavefish enters the laboratory. Zebrafish *11*, 291-299.

Elliot, WR (2018) Astyanax Caves of Mexico: Cavefishes of Tamaulipas, San Luís Potosí, and Guerrero. Association for Mexican Cave Studies Bulletin 26.

Elliott, JP, Drackley, JK, Beaulieu, AD, Aldrich, CG, Merchen, NR (1999) Effects of saturation and esterification of fat sources on site and extent of digestion in steers: digestion of fatty acids, triglycerides, and energy. J Anim Sci *77*, 1919-1929.

Enoch, HG, Catala, A, Strittmatter, P (1976) Mechanism of rat liver microsomal stearyl-CoA desaturase. Studies of the substrate specificity, enzyme-substrate interactions, and the function of lipid. J Biol Chem *251*, 5095-5103.

Evason, KJ, Francisco, MT, Juric, V, Balakrishnan, S, Lopez Pazmino Mdel, P, Gordan, JD, Kakar, S, Spitsbergen, J, Goga, A, Stainier, DY (2015) Identification of Chemical

Inhibitors of beta-Catenin-Driven Liver Tumorigenesis in Zebrafish. PLoS Genet *11*, e1005305.

Fahy, E, Subramaniam, S, Murphy, RC, Nishijima, M, Raetz, CR, Shimizu, T, Spener, F, van Meer, G, Wakelam, MJ, Dennis, EA (2009) Update of the LIPID MAPS comprehensive classification system for lipids. J Lipid Res *50 Suppl*, S9-14.

Fain, JN, Madan, AK, Hiler, ML, Cheema, P, Bahouth, SW (2004) Comparison of the release of adipokines by adipose tissue, adipose tissue matrix, and adipocytes from visceral and subcutaneous abdominal adipose tissues of obese humans. Endocrinology *145*, 2273-2282.

Feldhamer, GAD, Lee C.; Vessey, Stephen H.; Merritt, Joseph F.; Krajewski, Carey (2007) Environmental Adaptations. Mammalogy: Adaptation, Diversity, Ecology, 176–190. .

Feng, J, Han, J, Pearce, SF, Silverstein, RL, Gotto, AM, Jr., Hajjar, DP, Nicholson, AC (2000) Induction of CD36 expression by oxidized LDL and IL-4 by a common signaling pathway dependent on protein kinase C and PPAR-gamma. J Lipid Res *41*, 688-696.

Fisher, EA, Ginsberg, HN (2002) Complexity in the secretory pathway: the assembly and secretion of apolipoprotein B-containing lipoproteins. J Biol Chem *277*, 17377-17380.

Flynn, EJ, 3rd, Trent, CM, Rawls, JF (2009) Ontogeny and nutritional control of adipogenesis in zebrafish (Danio rerio). J Lipid Res *50*, 1641-1652.

Fornes, O, Castro-Mondragon, JA, Khan, A, van der Lee, R, Zhang, X, Richmond, PA, Modi, BP, Correard, S, Gheorghe, M, Baranasic, D, Santana-Garcia, W, Tan, G, Cheneby, J, Ballester, B, Parcy, F, Sandelin, A, Lenhard, B, Wasserman, WW, Mathelier, A (2020) JASPAR 2020: update of the open-access database of transcription factor binding profiles. Nucleic Acids Res *48*, D87-D92.

Fox, K, Peters, D, Armstrong, N, Sharpe, P, Bell, M (1993) Abdominal fat deposition in 11-year-old children. Int J Obes Relat Metab Disord *17*, 11-16.

Frank, CL (1988) Diet Selection by a Heteromyid Rodent: Role of Net Metabolic Water Production. Ecology *69*, 1943-1951.

Froland Steindal, IA, Beale, AD, Yamamoto, Y, Whitmore, D (2018) Development of the Astyanax mexicanus circadian clock and non-visual light responses. Developmental biology *441*, 345-354.

Fujimoto, T, Parton, RG (2011) Not just fat: the structure and function of the lipid droplet. Cold Spring Harbor perspectives in biology *3*.

Ghaben, AL, Scherer, PE (2019) Adipogenesis and metabolic health. Nat Rev Mol Cell Biol *20*, 242-258.

Gondret, F, Ferre, P, Dugail, I (2001) ADD-1/SREBP-1 is a major determinant of tissue differential lipogenic capacity in mammalian and avian species. J Lipid Res *42*, 106-113.

Gonzalez-Muniesa, P, Martinez-Gonzalez, MA, Hu, FB, Despres, JP, Matsuzawa, Y, Loos, RJF, Moreno, LA, Bray, GA, Martinez, JA (2017) Obesity. Nature reviews Disease primers *3*, 17034.

Goodman, BE (2010) Insights into digestion and absorption of major nutrients in humans. Advances in physiology education *34*, 44-53.

Grant, CE, Bailey, TL, Noble, WS (2011) FIMO: scanning for occurrences of a given motif. Bioinformatics *27*, 1017-1018.

Greenspan, P, Mayer, EP, Fowler, SD (1985) Nile red: a selective fluorescent stain for intracellular lipid droplets. J Cell Biol *100*, 965-973.

Gregoire, FM, Smas, CM, Sul, HS (1998) Understanding adipocyte differentiation. Physiological reviews *78*, 783-809.

Grimaldi, B, Bellet, MM, Katada, S, Astarita, G, Hirayama, J, Amin, RH, Granneman, JG, Piomelli, D, Leff, T, Sassone-Corsi, P (2010) PER2 controls lipid metabolism by direct regulation of PPARgamma. Cell Metab *12*, 509-520.

Gross, B, Staels, B (2007) PPAR agonists: multimodal drugs for the treatment of type-2 diabetes. Best practice & research Clinical endocrinology & metabolism *21*, 687-710.

Gross, JB, Borowsky, R, Tabin, CJ (2009) A novel role for Mc1r in the parallel evolution of depigmentation in independent populations of the cavefish Astyanax mexicanus. PLoS Genet *5*, e1000326.

Gupta, T, Mullins, MC (2010) Dissection of organs from the adult zebrafish. Journal of visualized experiments : JoVE.

Harding, SV, Bateman, KP, Kennedy, BP, Rideout, TC, Jones, PJ (2015) Desaturation index versus isotopically measured de novo lipogenesis as an indicator of acute systemic lipogenesis. BMC Res Notes *8*, 49.

Harrison, DE, Archer, JR, Astle, CM (1984) Effects of food restriction on aging: separation of food intake and adiposity. Proc Natl Acad Sci U S A *81*, 1835-1838.

Hawkes, LA, Balachandran, S, Batbayar, N, Butler, PJ, Chua, B, Douglas, DC, Frappell, PB, Hou, Y, Milsom, WK, Newman, SH, Prosser, DJ, Sathiyaselvam, P, Scott, GR, Takekawa, JY, Natsagdorj, T, Wikelski, M, Witt, MJ, Yan, B, Bishop, CM (2013) The paradox of extreme high-altitude migration in bar-headed geese Anser indicus. Proceedings Biological sciences *280*, 20122114.

Her, GM, Chiang, CC, Chen, WY, Wu, JL (2003a) In vivo studies of liver-type fatty acid binding protein (L-FABP) gene expression in liver of transgenic zebrafish (Danio rerio). FEBS Lett *538*, 125-133.

Her, GM, Yeh, YH, Wu, JL (2003b) 435-bp liver regulatory sequence in the liver fatty acid binding protein (L-FABP) gene is sufficient to modulate liver regional expression in transgenic zebrafish. Developmental dynamics : an official publication of the American Association of Anatomists *227*, 347-356.

Herman, A, Brandvain, Y, Weagley, J, Jeffery, WR, Keene, AC, Kono, TJY, Bilandzija, H, Borowsky, R, Espinasa, L, O'Quin, K, Ornelas-Garcia, CP, Yoshizawa, M, Carlson, B, Maldonado, E, Gross, JB, Cartwright, RA, Rohner, N, Warren, WC, McGaugh, SE (2018) The role of gene flow in rapid and repeated evolution of cave-related traits in Mexican tetra, Astyanax mexicanus. Mol Ecol *27*, 4397-4416.

Hinds, DS (1973) Acclimatization of thermoregulation in the desert cottontail, Sylvilagus audubonii. Journal of mammalogy *54*, 708-728.

Horikawa, M, Nomura, T, Hashimoto, T, Sakamoto, K (2008) Elongation and desaturation of fatty acids are critical in growth, lipid metabolism and ontogeny of Caenorhabditis elegans. J Biochem *144*, 149-158.

Horton, JD, Bashmakov, Y, Shimomura, I, Shimano, H (1998) Regulation of sterol regulatory element binding proteins in livers of fasted and refed mice. Proc Natl Acad Sci U S A *95*, 5987-5992.

Horton, JD, Shah, NA, Warrington, JA, Anderson, NN, Park, SW, Brown, MS, Goldstein, JL (2003) Combined analysis of oligonucleotide microarray data from transgenic and knockout mice identifies direct SREBP target genes. Proc Natl Acad Sci U S A *100*, 12027-12032.

Hotamisligil, GS, Shargill, NS, Spiegelman, BM (1993) Adipose expression of tumor necrosis factor-alpha: direct role in obesity-linked insulin resistance. Science *259*, 87-91.

Houten, SM, Violante, S, Ventura, FV, Wanders, RJ (2016) The Biochemistry and Physiology of Mitochondrial Fatty Acid beta-Oxidation and Its Genetic Disorders. Annual review of physiology *78*, 23-44.

Huang, H, Song, TJ, Li, X, Hu, L, He, Q, Liu, M, Lane, MD, Tang, QQ (2009) BMP signaling pathway is required for commitment of C3H10T1/2 pluripotent stem cells to the adipocyte lineage. Proc Natl Acad Sci U S A *106*, 12670-12675.

Hubel, C, Gaspar, HA, Coleman, JRI, Finucane, H, Purves, KL, Hanscombe, KB, Prokopenko, I, investigators, M, Graff, M, Ngwa, JS, Workalemahu, T, Eating Disorders Working Group of the Psychiatric Genomics, C, Major Depressive Disorder Working Group of the Psychiatric Genomics, C, Schizophrenia Working Group of the Psychiatric Genomics, C, Tourette Syndrome/Obsessive-Compulsive Disorder Working Group of the Psychiatric Genomics, C, O'Reilly, PF, Bulik, CM, Breen, G (2019) Genomics of body fat percentage may contribute to sex bias in anorexia nervosa. American journal of medical genetics Part B, Neuropsychiatric genetics : the official publication of the International Society of Psychiatric Genetics *180*, 428-438.

Hüppop, K (2001) How do cave animals cope with food scarcity in caves? . In: Wilkens, H, Culver, DC and Humphreys, WF, Eds, Subterranean Ecosystems, Elsevier Press, Amsterdam *417-432*.

Iizuka, K, Bruick, RK, Liang, G, Horton, JD, Uyeda, K (2004) Deficiency of carbohydrate response element-binding protein (ChREBP) reduces lipogenesis as well as glycolysis. Proc Natl Acad Sci U S A *101*, 7281-7286.

Ingalls, AM, Dickie, MM, Snell, GD (1950) Obese, a new mutation in the house mouse. J Hered *41*, 317-318.

Ingle, DL, Bauman, DE, Garrigus, US (1972) Lipogenesis in the ruminant: in vivo site of fatty acid synthesis in sheep. J Nutr *102*, 617-623.

Iqbal, J, Hussain, MM (2009) Intestinal lipid absorption. Am J Physiol Endocrinol Metab *296*, E1183-1194.

Jaggard, JB, Stahl, BA, Lloyd, E, Prober, DA, Duboue, ER, Keene, AC (2018) Hypocretin underlies the evolution of sleep loss in the Mexican cavefish. eLife *7*.

Jeffery, WR (2020) Astyanax surface and cave fish morphs. EvoDevo *11*, 14.

Jeffery, WR, Strickler, AG, Yamamoto, Y (2003) To see or not to see: evolution of eye degeneration in mexican blind cavefish. Integr Comp Biol *43*, 531-541.

Jessen, TH, Weber, RE, Fermi, G, Tame, J, Braunitzer, G (1991) Adaptation of bird hemoglobins to high altitudes: demonstration of molecular mechanism by protein engineering. Proc Natl Acad Sci U S A *88*, 6519-6522.

Kadowaki, T, Yamauchi, T (2005) Adiponectin and adiponectin receptors. Endocr Rev *26*, 439-451.

Keene, A, Yoshizawa, M, McGaugh, S (2015) Biology and Evolution of the Mexican Cavefish. Academic Press.

Kerner, J, Hoppel, C (2000) Fatty acid import into mitochondria. Biochim Biophys Acta *1486*, 1-17.

Kershaw, EE, Flier, JS (2004) Adipose tissue as an endocrine organ. J Clin Endocrinol Metab *89*, 2548-2556.

Kersten, S (2001) Mechanisms of nutritional and hormonal regulation of lipogenesis. EMBO Rep *2*, 282-286.

Kersten, S, Seydoux, J, Peters, JM, Gonzalez, FJ, Desvergne, B, Wahli, W (1999) Peroxisome proliferator-activated receptor alpha mediates the adaptive response to fasting. J Clin Invest *103*, 1489-1498.

Kim, BM, Amores, A, Kang, S, Ahn, DH, Kim, JH, Kim, IC, Lee, JH, Lee, SG, Lee, H, Lee, J, Kim, HW, Desvignes, T, Batzel, P, Sydes, J, Titus, T, Wilson, CA, Catchen, JM, Warren, WC, Schartl, M, Detrich, HW, 3rd, Postlethwait, JH, Park, H (2019) Antarctic blackfin icefish genome reveals adaptations to extreme environments. Nature ecology & evolution *3*, 469-478.

Kingsley, MCS, Nagy, JA, Russell, RH (1983) Patterns of weight gain and loss for grizzly bears in northern Canada. Bears: Their Biology and Management *5: 174-178*.

Klawitter, J, Bek, S, Zakaria, M, Zeng, C, Hornberger, A, Gilbert, R, Shokati, T, Klawitter, J, Christians, U, Boernsen, KO (2014) Fatty acid desaturation index in human plasma: comparison of different analytical methodologies for the evaluation of diet effects. Anal Bioanal Chem *406*, 6399-6408.

Knittle, JL, Timmers, K, Ginsberg-Fellner, F, Brown, RE, Katz, DP (1979) The growth of adipose tissue in children and adolescents. Cross-sectional and longitudinal studies of adipose cell number and size. J Clin Invest *63*, 239-246.

Kolodziejczyk, AA, Kim, JK, Svensson, V, Marioni, JC, Teichmann, SA (2015) The technology and biology of single-cell RNA sequencing. Mol Cell *58*, 610-620.

Kovner, I, Taicher, GZ, Mitchell, AD (2010) Calibration and validation of EchoMRI whole body composition analysis based on chemical analysis of piglets, in comparison with the same for DXA. International journal of body composition research *8*, 17-29.

Kowalko, JE, Rohner, N, Linden, TA, Rompani, SB, Warren, WC, Borowsky, R, Tabin, CJ, Jeffery, WR, Yoshizawa, M (2013a) Convergence in feeding posture occurs through different genetic loci in independently evolved cave populations of Astyanax mexicanus. Proc Natl Acad Sci U S A *110*, 16933-16938.

Kowalko, JE, Rohner, N, Rompani, SB, Peterson, BK, Linden, TA, Yoshizawa, M, Kay, EH, Weber, J, Hoekstra, HE, Jeffery, WR, Borowsky, R, Tabin, CJ (2013b) Loss of schooling behavior in cavefish through sight-dependent and sight-independent mechanisms. Curr Biol *23*, 1874-1883.

Krishnan, J, Rohner, N (2017) Cavefish and the basis for eye loss. Philosophical transactions of the Royal Society of London Series B, Biological sciences *372*.

Kuroda, H, Tahara, Y, Saito, K, Ohnishi, N, Kubo, Y, Seo, Y, Otsuka, M, Fuse, Y, Ohura, Y, Hirao, A, Shibata, S (2012) Meal frequency patterns determine the phase of mouse peripheral circadian clocks. Sci Rep *2*, 711.

Langecker, TG (2000) The effects of continuous darkness on cave ecology and cavernicolous evolution In: Wilkens H, Culver DC, Humphreys WF, editors Ecosystems of the World 30 Subterranean Ecosystems Amsterdam: Elsevier Academic Press, 17-39.

Lawrence, M, Gentleman, R, Carey, V (2009) rtracklayer: an R package for interfacing with genome browsers. Bioinformatics *25*, 1841-1842.

Lawrence, M, Huber, W, Pages, H, Aboyoun, P, Carlson, M, Gentleman, R, Morgan, MT, Carey, VJ (2013) Software for computing and annotating genomic ranges. PLoS computational biology *9*, e1003118.

Leber, R, Zinser, E, Zellnig, G, Paltauf, F, Daum, G (1994) Characterization of lipid particles of the yeast, Saccharomyces cerevisiae. Yeast *10*, 1421-1428.

Lee, SS, Pineau, T, Drago, J, Lee, EJ, Owens, JW, Kroetz, DL, Fernandez-Salguero, PM, Westphal, H, Gonzalez, FJ (1995) Targeted disruption of the alpha isoform of the peroxisome proliferator-activated receptor gene in mice results in abolishment of the pleiotropic effects of peroxisome proliferators. Mol Cell Biol *15*, 3012-3022.

Lee, YJ, Ko, EH, Kim, JE, Kim, E, Lee, H, Choi, H, Yu, JH, Kim, HJ, Seong, JK, Kim, KS, Kim, JW (2012) Nuclear receptor PPARgamma-regulated monoacylglycerol O-acyltransferase 1 (MGAT1) expression is responsible for the lipid accumulation in diet-induced hepatic steatosis. Proc Natl Acad Sci U S A *109*, 13656-13661.

Lefterova, MI, Zhang, Y, Steger, DJ, Schupp, M, Schug, J, Cristancho, A, Feng, D, Zhuo, D, Stoeckert, CJ, Jr., Liu, XS, Lazar, MA (2008) PPARgamma and C/EBP factors orchestrate adipocyte biology via adjacent binding on a genome-wide scale. Genes Dev *22*, 2941-2952.

Leone, TC, Weinheimer, CJ, Kelly, DP (1999) A critical role for the peroxisome proliferator-activated receptor alpha (PPARalpha) in the cellular fasting response: the

PPARalpha-null mouse as a model of fatty acid oxidation disorders. Proc Natl Acad Sci U S A *96*, 7473-7478.

Liang, G, Yang, J, Horton, JD, Hammer, RE, Goldstein, JL, Brown, MS (2002) Diminished hepatic response to fasting/refeeding and liver X receptor agonists in mice with selective deficiency of sterol regulatory element-binding protein-1c. J Biol Chem *277*, 9520-9528.

Lihn, AS, Pedersen, SB, Richelsen, B (2005) Adiponectin: action, regulation and association to insulin sensitivity. Obes Rev *6*, 13-21.

Liu, XZ, Li, SL, Jing, H, Liang, YH, Hua, ZQ, Lu, GY (2001) Avian haemoglobins and structural basis of high affinity for oxygen: structure of bar-headed goose aquomet haemoglobin. Acta crystallographica Section D, Biological crystallography *57*, 775-783.

Mack, KL, Jaggard, JB, Persons, JL, Passow, CN, Stanhope, BA, Ferrufino, E, Tsuchiya, D, Smith, SE, Slaughter, BD, Kowalko, J, Rohner, N, Keene, AC, McGaugh, SE (2020) Repeated evolution of circadian clock dysregulation in cavefish populations. bioRxiv *2020.01.14.906628*.

Majka, SM, Barak, Y, Klemm, DJ (2011) Concise review: adipocyte origins: weighing the possibilities. Stem cells *29*, 1034-1040.

McGarry, JD, Mannaerts, GP, Foster, DW (1977) A possible role for malonyl-CoA in the regulation of hepatic fatty acid oxidation and ketogenesis. J Clin Invest *60*, 265-270.

Medina-Gomez, G, Gray, SL, Yetukuri, L, Shimomura, K, Virtue, S, Campbell, M, Curtis, RK, Jimenez-Linan, M, Blount, M, Yeo, GS, Lopez, M, Seppanen-Laakso, T, Ashcroft, FM, Oresic, M, Vidal-Puig, A (2007) PPAR gamma 2 prevents lipotoxicity by controlling adipose tissue expandability and peripheral lipid metabolism. PLoS Genet *3*, e64.

Medley, JK, Persons, J, Peuss, R, Olsen, L, Xiong, S, Rohner, N (2020) Untargeted Metabolomics of the Cavefish Astyanax mexicanus Reveals the Basis of Metabolic Strategies in Adaptation to Extreme Conditions. bioRxiv *2020.10.27.358077*.

Meir, JU, York, JM, Chua, BA, Jardine, W, Hawkes, LA, Milsom, WK (2019) Reduced metabolism supports hypoxic flight in the high-flying bar-headed goose (Anser indicus). eLife *8*.

Merrick, D, Sakers, A, Irgebay, Z, Okada, C, Calvert, C, Morley, MP, Percec, I, Seale, P (2019) Identification of a mesenchymal progenitor cell hierarchy in adipose tissue. Science *364*.

Minchin, JE, Rawls, JF (2017a) In vivo imaging and quantification of regional adiposity in zebrafish. Methods in cell biology *138*, 3-27.

Minchin, JEN, Rawls, JF (2017b) A classification system for zebrafish adipose tissues. Disease models & mechanisms *10*, 797-809.

Mitchell, RW, Russell, WH, Elliott, WR (1977) Mexican eyeless characin fishes, genus Astyanax : environment, distribution, and evolution (Lubbock, Texas Tech Press).

Moran, D, Softley, R, Warrant, EJ (2014) Eyeless Mexican cavefish save energy by eliminating the circadian rhythm in metabolism. PLoS One *9*, e107877.

Moran, D, Softley, R, Warrant, EJ (2015) The energetic cost of vision and the evolution of eyeless Mexican cavefish. Science advances *1*, e1500363.

Mourot, J, Guy, G, Lagarrigue, S, Peiniau, P, Hermier, D (2000) Role of hepatic lipogenesis in the susceptibility to fatty liver in the goose (Anser anser). Comp Biochem Physiol B Biochem Mol Biol *126*, 81-87.

Munzberg, H, Bjornholm, M, Bates, SH, Myers, MG, Jr. (2005) Leptin receptor action and mechanisms of leptin resistance. Cell Mol Life Sci *62*, 642-652.

Muoio, DM, MacLean, PS, Lang, DB, Li, S, Houmard, JA, Way, JM, Winegar, DA, Corton, JC, Dohm, GL, Kraus, WE (2002) Fatty acid homeostasis and induction of lipid regulatory genes in skeletal muscles of peroxisome proliferator-activated receptor (PPAR) alpha knock-out mice. Evidence for compensatory regulation by PPAR delta. J Biol Chem *277*, 26089-26097.

Musilova, Z, Cortesi, F, Matschiner, M, Davies, WIL, Patel, JS, Stieb, SM, de Busserolles, F, Malmstrom, M, Torresen, OK, Brown, CJ, Mountford, JK, Hanel, R, Stenkamp, DL, Jakobsen, KS, Carleton, KL, Jentoft, S, Marshall, J, Salzburger, W (2019) Vision using multiple distinct rod opsins in deep-sea fishes. Science *364*, 588-592.

Myers, MG, Cowley, MA, Munzberg, H (2008) Mechanisms of leptin action and leptin resistance. Annual review of physiology *70*, 537-556.

Myers, MG, Jr., Leibel, RL, Seeley, RJ, Schwartz, MW (2010) Obesity and leptin resistance: distinguishing cause from effect. Trends Endocrinol Metab *21*, 643-651.

Nafikov, RA, Beitz, DC (2007) Carbohydrate and lipid metabolism in farm animals. J Nutr *137*, 702-705.

Neels, JG, Grimaldi, PA (2014) Physiological functions of peroxisome proliferator-activated receptor beta. Physiological reviews *94*, 795-858.

Ntambi, JM, Miyazaki, M (2004) Regulation of stearoyl-CoA desaturases and role in metabolism. Prog Lipid Res *43*, 91-104.

Ntambi, JM, Miyazaki, M, Stoehr, JP, Lan, H, Kendziorski, CM, Yandell, BS, Song, Y, Cohen, P, Friedman, JM, Attie, AD (2002) Loss of stearoyl-CoA desaturase-1 function protects mice against adiposity. Proc Natl Acad Sci U S A *99*, 11482-11486.

Numa, S, Yamashita, S (1974) Regulation of lipogenesis in animal tissues. Curr Top Cell Regul *8*, 197-246.

Oh, DK, Ciaraldi, T, Henry, RR (2007) Adiponectin in health and disease. Diabetes Obes Metab *9*, 282-289.

Pan, X, Hussain, MM (2012) Gut triglyceride production. Biochim Biophys Acta *1821*, 727-735.

Paracchini, V, Pedotti, P, Taioli, E (2005) Genetics of leptin and obesity: a HuGE review. American journal of epidemiology *162*, 101-114.

Parichy, DM, Elizondo, MR, Mills, MG, Gordon, TN, Engeszer, RE (2009) Normal table of postembryonic zebrafish development: staging by externally visible anatomy of the living fish. Developmental dynamics : an official publication of the American Association of Anatomists *238*, 2975-3015.

Perutz, MF (1983) Species adaptation in a protein molecule. Mol Biol Evol *1*, 1-28.

Pettinelli, P, Videla, LA (2011) Up-regulation of PPAR-gamma mRNA expression in the liver of obese patients: an additional reinforcing lipogenic mechanism to SREBP-1c induction. J Clin Endocrinol Metab *96*, 1424-1430.

Peuss, R, Box, AC, Chen, S, Wang, Y, Tsuchiya, D, Persons, JL, Kenzior, A, Maldonado, E, Krishnan, J, Scharsack, JP, Slaughter, BD, Rohner, N (2020) Adaptation to low parasite abundance affects immune investment and immunopathological responses of cavefish. Nature ecology & evolution *4*, 1416-1430.

Pierce, VA, Crawford, DL (1997) Phylogenetic analysis of glycolytic enzyme expression. Science *276*, 256-259.

Poissonnet, CM, Burdi, AR, Bookstein, FL (1983) Growth and development of human adipose tissue during early gestation. Early human development *8*, 1-11.

Poissonnet, CM, Burdi, AR, Garn, SM (1984) The chronology of adipose tissue appearance and distribution in the human fetus. Early human development *10*, 1-11.

Protas, M, Conrad, M, Gross, JB, Tabin, C, Borowsky, R (2007) Regressive evolution in the Mexican cave tetra, Astyanax mexicanus. Curr Biol *17*, 452-454.

Protas, M, Tabansky, I, Conrad, M, Gross, JB, Vidal, O, Tabin, CJ, Borowsky, R (2008) Multi-trait evolution in a cave fish, Astyanax mexicanus. Evol Dev *10*, 196-209.

Protas, ME, Hersey, C, Kochanek, D, Zhou, Y, Wilkens, H, Jeffery, WR, Zon, LI, Borowsky, R, Tabin, CJ (2006) Genetic analysis of cavefish reveals molecular convergence in the evolution of albinism. Nat Genet *38*, 107-111.

Quinlan, AR, Hall, IM (2010) BEDTools: a flexible suite of utilities for comparing genomic features. Bioinformatics *26*, 841-842.

Rask-Andersen, M, Karlsson, T, Ek, WE, Johansson, A (2019) Genome-wide association study of body fat distribution identifies adiposity loci and sex-specific genetic effects. Nat Commun *10*, 339.

Riddle, MR, Aspiras, AC, Gaudenz, K, Peuss, R, Sung, JY, Martineau, B, Peavey, M, Box, AC, Tabin, JA, McGaugh, S, Borowsky, R, Tabin, CJ, Rohner, N (2018a) Insulin resistance in cavefish as an adaptation to a nutrient-limited environment. Nature *555*, 647-651.

Riddle, MR, Boesmans, W, Caballero, O, Kazwiny, Y, Tabin, CJ (2018b) Morphogenesis and motility of the Astyanax mexicanus gastrointestinal tract. Developmental biology *441*, 285-296.

Rinella, ME (2015) Nonalcoholic fatty liver disease: a systematic review. Jama *313*, 2263-2273.

Riveros-McKay, F, Mistry, V, Bounds, R, Hendricks, A, Keogh, JM, Thomas, H, Henning, E, Corbin, LJ, Understanding Society Scientific, G, O'Rahilly, S, Zeggini, E, Wheeler, E, Barroso, I, Farooqi, IS (2019) Genetic architecture of human thinness compared to severe obesity. PLoS Genet *15*, e1007603.

Rosen, ED, Hsu, CH, Wang, X, Sakai, S, Freeman, MW, Gonzalez, FJ, Spiegelman, BM (2002) C/EBPalpha induces adipogenesis through PPARgamma: a unified pathway. Genes Dev *16*, 22-26.

Rosen, ED, Sarraf, P, Troy, AE, Bradwin, G, Moore, K, Milstone, DS, Spiegelman, BM, Mortensen, RM (1999) PPAR gamma is required for the differentiation of adipose tissue in vivo and in vitro. Mol Cell *4*, 611-617.

Russo, L, Lumeng, CN (2018) Properties and functions of adipose tissue macrophages in obesity. Immunology *155*, 407-417.

Sadoglu, P (1957) Mendelian inheritance in hybrids between the Mexican blind fish and their overground ancestors. Verh Dtsch Zool Ges *1957*.

Salin, K, Voituron, Y, Mourin, J, Hervant, F (2010) Cave colonization without fasting capacities: an example with the fish Astyanax fasciatus mexicanus. Comp Biochem Physiol A Mol Integr Physiol *156*, 451-457.

Schadinger, SE, Bucher, NL, Schreiber, BM, Farmer, SR (2005) PPARgamma2 regulates lipogenesis and lipid accumulation in steatotic hepatocytes. Am J Physiol Endocrinol Metab *288*, E1195-1205.

Schaffer, JE, Lodish, HF (1994) Expression cloning and characterization of a novel adipocyte long chain fatty acid transport protein. Cell *79*, 427-436.

Schulte, PM, Glemet, HC, Fiebig, AA, Powers, DA (2000) Adaptive variation in lactate dehydrogenase-B gene expression: role of a stress-responsive regulatory element. Proc Natl Acad Sci U S A *97*, 6597-6602.

Schwalie, PC, Dong, H, Zachara, M, Russeil, J, Alpern, D, Akchiche, N, Caprara, C, Sun, W, Schlaudraff, KU, Soldati, G, Wolfrum, C, Deplancke, B (2018) A stromal cell population that inhibits adipogenesis in mammalian fat depots. Nature *559*, 103-108.

Schwartz, JP, Jungas, RL (1971) Studies on the hormone-sensitive lipase of adipose tissue. J Lipid Res *12*, 553-562.

Scott, GR, Milsom, WK (2007) Control of breathing and adaptation to high altitude in the bar-headed goose. Am J Physiol Regul Integr Comp Physiol *293*, R379-391.

Seargent, JM, Yates, EA, Gill, JH (2004) GW9662, a potent antagonist of PPARgamma, inhibits growth of breast tumour cells and promotes the anticancer effects of the PPARgamma agonist rosiglitazone, independently of PPARgamma activation. Br J Pharmacol *143*, 933-937.

Seth, A, Stemple, DL, Barroso, I (2013) The emerging use of zebrafish to model metabolic disease. Disease models & mechanisms *6*, 1080-1088.

Sharma, AM, Staels, B (2007) Review: Peroxisome proliferator-activated receptor gamma and adipose tissue--understanding obesity-related changes in regulation of lipid and glucose metabolism. J Clin Endocrinol Metab *92*, 386-395.

Shimizu, H, Inoue, K, Mori, M (2007) The leptin-dependent and -independent melanocortin signaling system: regulation of feeding and energy expenditure. J Endocrinol *193*, 1-9.

Shimobayashi, MS, S.; Frei, I. C.; Wölnerhanssen, B. K.; Weissenberger, D.; Dietz, N.; Thomas, A.; Ritz, D.; Meyer-Gerspach, A. C.; Maier, T.; Hay, N.; Peterli , R.; Rohner, N.; Hall, M. N.; (2019) Diet-induced loss of adipose Hexokinase 2 triggers hyperglycemia. bioRxiv *https://doi.org/10.1101/2019.12.28.887794*.

Shuster, A, Patlas, M, Pinthus, JH, Mourtzakis, M (2012) The clinical importance of visceral adiposity: a critical review of methods for visceral adipose tissue analysis. The British journal of radiology *85*, 1-10.

Siegel, MJ, Hildebolt, CF, Bae, KT, Hong, C, White, NH (2007) Total and intraabdominal fat distribution in preadolescents and adolescents: measurement with MR imaging. Radiology *242*, 846-856.

Skurk, T, Alberti-Huber, C, Herder, C, Hauner, H (2007) Relationship between adipocyte size and adipokine expression and secretion. J Clin Endocrinol Metab *92*, 1023-1033.

Soni, KG, Lehner, R, Metalnikov, P, O'Donnell, P, Semache, M, Gao, W, Ashman, K, Pshezhetsky, AV, Mitchell, GA (2004) Carboxylesterase 3 (EC 3.1.1.1) is a major adipocyte lipase. J Biol Chem *279*, 40683-40689.

Spalding, KL, Arner, E, Westermark, PO, Bernard, S, Buchholz, BA, Bergmann, O, Blomqvist, L, Hoffstedt, J, Naslund, E, Britton, T, Concha, H, Hassan, M, Ryden, M, Frisen, J, Arner, P (2008) Dynamics of fat cell turnover in humans. Nature *453*, 783-787.

Staples, JF (2016) Metabolic Flexibility: Hibernation, Torpor, and Estivation. Comprehensive Physiology *6*, 737-771.

Stockdale, WT, Lemieux, ME, Killen, AC, Zhao, J, Hu, Z, Riepsaame, J, Hamilton, N, Kudoh, T, Riley, PR, van Aerle, R, Yamamoto, Y, Mommersteeg, MTM (2018) Heart Regeneration in the Mexican Cavefish. Cell Rep *25*, 1997-2007 e1997.

Strauss, EW (1966) Electron microscopic study of intestinal fat absorption in vitro from mixed micelles containing linolenic acid, monoolein, and bile salt. J Lipid Res *7*, 307-323.

Stremmel, W (1988) Uptake of fatty acids by jejunal mucosal cells is mediated by a fatty acid binding membrane protein. J Clin Invest *82*, 2001-2010.

Stremmel, W, Lotz, G, Strohmeyer, G, Berk, PD (1985) Identification, isolation, and partial characterization of a fatty acid binding protein from rat jejunal microvillous membranes. J Clin Invest *75*, 1068-1076.

Sun, K, Kusminski, CM, Scherer, PE (2011) Adipose tissue remodeling and obesity. J Clin Invest *121*, 2094-2101.

Tang, F, Barbacioru, C, Wang, Y, Nordman, E, Lee, C, Xu, N, Wang, X, Bodeau, J, Tuch, BB, Siddiqui, A, Lao, K, Surani, MA (2009) mRNA-Seq whole-transcriptome analysis of a single cell. Nat Methods *6*, 377-382.

Tartaglia, LA, Dembski, M, Weng, X, Deng, N, Culpepper, J, Devos, R, Richards, GJ, Campfield, LA, Clark, FT, Deeds, J, Muir, C, Sanker, S, Moriarty, A, Moore, KJ, Smutko, JS, Mays, GG, Wool, EA, Monroe, CA, Tepper, RI (1995) Identification and expression cloning of a leptin receptor, OB-R. Cell *83*, 1263-1271.

Tian, J, Goldstein, JL, Brown, MS (2016) Insulin induction of SREBP-1c in rodent liver requires LXRalpha-C/EBPbeta complex. Proc Natl Acad Sci U S A *113*, 8182-8187.

Tomas, E, Tsao, TS, Saha, AK, Murrey, HE, Zhang Cc, C, Itani, SI, Lodish, HF, Ruderman, NB (2002) Enhanced muscle fat oxidation and glucose transport by ACRP30 globular domain: acetyl-CoA carboxylase inhibition and AMP-activated protein kinase activation. Proc Natl Acad Sci U S A *99*, 16309-16313.

Tontonoz, P, Hu, E, Spiegelman, BM (1994) Stimulation of adipogenesis in fibroblasts by PPAR gamma 2, a lipid-activated transcription factor. Cell *79*, 1147-1156.

Tontonoz, P, Spiegelman, BM (2008) Fat and beyond: the diverse biology of PPARgamma. Annual review of biochemistry *77*, 289-312.

Tracy, RL, Walsberg, GE (2000) Prevalence of cutaneous evaporation in Merriam's kangaroo rat and its adaptive variation at the subspecific level. J Exp Biol *203*, 773-781.

Tzanavari, T, Giannogonas, P, Karalis, KP (2010) TNF-alpha and obesity. Current directions in autoimmunity *11*, 145-156.

Uhrig-Schmidt, S, Geiger, M, Luippold, G, Birk, G, Mennerich, D, Neubauer, H, Grimm, D, Wolfrum, C, Kreuz, S (2014) Gene delivery to adipose tissue using transcriptionally targeted rAAV8 vectors. PLoS One *9*, e116288.

Ukkola, O, Santaniemi, M (2002) Adiponectin: a link between excess adiposity and associated comorbidities? J Mol Med (Berl) *80*, 696-702.

Urity, VB, Issaian, T, Braun, EJ, Dantzler, WH, Pannabecker, TL (2012) Architecture of kangaroo rat inner medulla: segmentation of descending thin limb of Henle's loop. Am J Physiol Regul Integr Comp Physiol *302*, R720-726.

Uspenskii, SM (1977) The Polar Bear. Moscow: Nauka.

Vaisse, C, Clement, K, Guy-Grand, B, Froguel, P (1998) A frameshift mutation in human MC4R is associated with a dominant form of obesity. Nat Genet *20*, 113-114.

Vernon, G, Baranova, A, Younossi, ZM (2011) Systematic review: the epidemiology and natural history of non-alcoholic fatty liver disease and non-alcoholic steatohepatitis in adults. Alimentary pharmacology & therapeutics *34*, 274-285.

Wang, EA, Israel, DI, Kelly, S, Luxenberg, DP (1993) Bone morphogenetic protein-2 causes commitment and differentiation in C3H10T1/2 and 3T3 cells. Growth factors *9*, 57-71.

Wang, W, Seale, P (2016) Control of brown and beige fat development. Nat Rev Mol Cell Biol *17*, 691-702.

Wang, Y, Viscarra, J, Kim, SJ, Sul, HS (2015) Transcriptional regulation of hepatic lipogenesis. Nat Rev Mol Cell Biol *16*, 678-689.

Wehrli, NE, Bural, G, Houseni, M, Alkhawaldeh, K, Alavi, A, Torigian, DA (2007) Determination of age-related changes in structure and function of skin, adipose tissue, and skeletal muscle with computed tomography, magnetic resonance imaging, and positron emission tomography. Seminars in nuclear medicine *37*, 195-205.

Wilkens, HC, D.C, Humphreys, W.F (2000) Subterranean Ecosystems (Ecosystems of the World). Elsevier.

Williams, EP, Mesidor, M, Winters, K, Dubbert, PM, Wyatt, SB (2015) Overweight and Obesity: Prevalence, Consequences, and Causes of a Growing Public Health Problem. Current obesity reports *4*, 363-370.

Wolf Greenstein, A, Majumdar, N, Yang, P, Subbaiah, PV, Kineman, RD, Cordoba-Chacon, J (2017) Hepatocyte-specific, PPARgamma-regulated mechanisms to promote steatosis in adult mice. J Endocrinol *232*, 107-121.

Xiong, S, Krishnan, J, Peuss, R, Rohner, N (2018) Early adipogenesis contributes to excess fat accumulation in cave populations of Astyanax mexicanus. Developmental biology *441*, 297-304.

Xu, X, So, JS, Park, JG, Lee, AH (2013) Transcriptional control of hepatic lipid metabolism by SREBP and ChREBP. Semin Liver Dis *33*, 301-311.

Yamashita, H, Takenoshita, M, Sakurai, M, Bruick, RK, Henzel, WJ, Shillinglaw, W, Arnot, D, Uyeda, K (2001) A glucose-responsive transcription factor that regulates carbohydrate metabolism in the liver. Proc Natl Acad Sci U S A *98*, 9116-9121.

Yamauchi, T, Kamon, J, Minokoshi, Y, Ito, Y, Waki, H, Uchida, S, Yamashita, S, Noda, M, Kita, S, Ueki, K, Eto, K, Akanuma, Y, Froguel, P, Foufelle, F, Ferre, P, Carling, D, Kimura, S, Nagai, R, Kahn, BB, Kadowaki, T (2002) Adiponectin stimulates glucose utilization and fatty-acid oxidation by activating AMP-activated protein kinase. Nat Med *8*, 1288-1295.

Yamauchi, T, Kamon, J, Waki, H, Terauchi, Y, Kubota, N, Hara, K, Mori, Y, Ide, T, Murakami, K, Tsuboyama-Kasaoka, N, Ezaki, O, Akanuma, Y, Gavrilova, O, Vinson, C, Reitman, ML, Kagechika, H, Shudo, K, Yoda, M, Nakano, Y, Tobe, K, Nagai, R, Kimura, S, Tomita, M, Froguel, P, Kadowaki, T (2001) The fat-derived hormone adiponectin reverses insulin resistance associated with both lipoatrophy and obesity. Nat Med *7*, 941-946.

Yan, H, Liang, C, Li, Z, Liu, Z, Miao, B, He, C, Sheng, L (2015) Impact of precipitation patterns on biomass and species richness of annuals in a dry steppe. PLoS One *10*, e0125300.

Yang, LY, Kuksis, A, Myher, JJ, Steiner, G (1996) Contribution of de novo fatty acid synthesis to very low density lipoprotein triacylglycerols: evidence from mass isotopomer

distribution analysis of fatty acids synthesized from [2H6]ethanol. J Lipid Res *37*, 262-274.

Yates, AD, Achuthan, P, Akanni, W, Allen, J, Allen, J, Alvarez-Jarreta, J, Amode, MR, Armean, IM, Azov, AG, Bennett, R, Bhai, J, Billis, K, Boddu, S, Marugan, JC, Cummins, C, Davidson, C, Dodiya, K, Fatima, R, Gall, A, Giron, CG, Gil, L, Grego, T, Haggerty, L, Haskell, E, Hourlier, T, Izuogu, OG, Janacek, SH, Juettemann, T, Kay, M, Lavidas, I, Le, T, Lemos, D, Martinez, JG, Maurel, T, McDowall, M, McMahon, A, Mohanan, S, Moore, B, Nuhn, M, Oheh, DN, Parker, A, Parton, A, Patricio, M, Sakthivel, MP, Abdul Salam, AI, Schmitt, BM, Schuilenburg, H, Sheppard, D, Sycheva, M, Szuba, M, Taylor, K, Thormann, A, Threadgold, G, Vullo, A, Walts, B, Winterbottom, A, Zadissa, A, Chakiachvili, M, Flint, B, Frankish, A, Hunt, SE, G, II, Kostadima, M, Langridge, N, Loveland, JE, Martin, FJ, Morales, J, Mudge, JM, Muffato, M, Perry, E, Ruffier, M, Trevanion, SJ, Cunningham, F, Howe, KL, Zerbino, DR, Flicek, P (2020) Ensembl 2020. Nucleic Acids Res *48*, D682-D688.

Yeo, GS, Farooqi, IS, Aminian, S, Halsall, DJ, Stanhope, RG, O'Rahilly, S (1998) A frameshift mutation in MC4R associated with dominantly inherited human obesity. Nat Genet *20*, 111-112.

Yoshizawa, M, Yamamoto, Y, O'Quin, KE, Jeffery, WR (2012) Evolution of an adaptive behavior and its sensory receptors promotes eye regression in blind cavefish. BMC Biol *10*, 108.

Yu, G, Wang, LG, He, QY (2015) ChIPseeker: an R/Bioconductor package for ChIP peak annotation, comparison and visualization. Bioinformatics *31*, 2382-2383.

Yu, S, Matsusue, K, Kashireddy, P, Cao, WQ, Yeldandi, V, Yeldandi, AV, Rao, MS, Gonzalez, FJ, Reddy, JK (2003) Adipocyte-specific gene expression and adipogenic steatosis in the mouse liver due to peroxisome proliferator-activated receptor gamma1 (PPARgamma1) overexpression. J Biol Chem *278*, 498-505.

Zechner, R, Strauss, JG, Haemmerle, G, Lass, A, Zimmermann, R (2005) Lipolysis: pathway under construction. Curr Opin Lipidol *16*, 333-340.

Zhang, Y, Liu, T, Meyer, CA, Eeckhoute, J, Johnson, DS, Bernstein, BE, Nusbaum, C, Myers, RM, Brown, M, Li, W, Liu, XS (2008) Model-based analysis of ChIP-Seq (MACS). Genome Biol *9*, R137.

Zhang, Y, Proenca, R, Maffei, M, Barone, M, Leopold, L, Friedman, JM (1994) Positional cloning of the mouse obese gene and its human homologue. Nature *372*, 425-432.

Zheng, G, Li, K, Wang, Y (2019) The Effects of High-Temperature Weather on Human Sleep Quality and Appetite. International journal of environmental research and public health *16*.

Zhou, J, Febbraio, M, Wada, T, Zhai, Y, Kuruba, R, He, J, Lee, JH, Khadem, S, Ren, S, Li, S, Silverstein, RL, Xie, W (2008) Hepatic fatty acid transporter Cd36 is a common target of LXR, PXR, and PPARgamma in promoting steatosis. Gastroenterology *134*, 556-567.

Zhou, Y, Zhou, B, Pache, L, Chang, M, Khodabakhshi, AH, Tanaseichuk, O, Benner, C, Chanda, SK (2019) Metascape provides a biologist-oriented resource for the analysis of systems-level datasets. Nat Commun *10*, 1523.

Zhu, N, Pankow, JS, Ballantyne, CM, Couper, D, Hoogeveen, RC, Pereira, M, Duncan, BB, Schmidt, MI (2010) High-molecular-weight adiponectin and the risk of type 2 diabetes in the ARIC study. J Clin Endocrinol Metab *95*, 5097-5104.

Zimmermann, R, Strauss, JG, Haemmerle, G, Schoiswohl, G, Birner-Gruenberger, R, Riederer, M, Lass, A, Neuberger, G, Eisenhaber, F, Hermetter, A, Zechner, R (2004) Fat mobilization in adipose tissue is promoted by adipose triglyceride lipase. Science *306*, 1383-1386.

Zizzo, G, Cohen, PL (2015) The PPAR-gamma antagonist GW9662 elicits differentiation of M2c-like cells and upregulation of the MerTK/Gas6 axis: a key role for PPAR-gamma in human macrophage polarization. Journal of inflammation *12*, 36.

Zwick, RK, Guerrero-Juarez, CF, Horsley, V, Plikus, MV (2018) Anatomical, Physiological, and Functional Diversity of Adipose Tissue. Cell Metab *27*, 68-83.